Energy, Mines and Resources Canada

Énergie, Mines et Ressources Canada

CANMET

Canada Centre for Mineral and Energy Technology

Centre canadien de la technologie des minéraux et de l'énergie

Mining Research Laboratories

Laboratoires de recherche minière

Canada

ASSESSMENT OF ERRORS IN AIRFLOW MEASURING INSTRUMENTS

J. BIGU ELLIOT LAKE LABORATORY

MRL 90-055 (TR)

Report in compliance with AECB Contract No. 3.124.1

This document is an unedited interim report prepared primarily for circulation and internal use purposes. It does not represent a final expression of the opinion of the Canada Centre for Mineral and Energy Technology (CANMET)

Ce document est un rapport provisoire non-révisé et rédigé principalement pour fin de diffusion et de documentation interne. Il ne constitue aucunement l'expression définitive de l'opinion du Centre canadien de la technologie des minéraux et de l'énergie (CANMET)

MICROMEDIA

134 pp

90-07127/

ASSESSMENT OF ERRORS IN AIRFLOW MEASURING INSTRUMENTS

J. Bigu*

ABSTRACT

Comprehensive tests on the behaviour of several air sampling pumps have been conducted. Extensive measurements of the pumps airflow rates under a variety of experimental conditions have been carried out using a number of airflow rate measuring devices. Pumps were tested using two types of filters commonly used in radon (and thoron) progeny air sampling, namely, glass fibre (GF) filters and Millipore filters. Furthermore, the effect of the length of plastic tubing used to connect the filter/filter holder system to the intake port of the sampling pump, and the effect of attaching a length of platic tubing to the exhaust port of the pump have been investigated. Attaching varying lengths of plastic tubing to both the intake or the exhaust ports of a sampling pump is a common practice in many experimental situations. The most interesting effect observed in the course of these investigations is the appearance of airflow rate resonance effects when the tubing length was varied from a few cm to about ~4.5 m. This investigation was partly prompted by previous experimental observations regarding 'abnormal' flowrate effects during the technical evaluation of an Instant Working Level Meter.

Key words: Sampling pumps; Airflow rate; Resonance.

*Research Scientist and Radiation/Respirable Dust/Ventilation Section Head, Elliot Lake Laboratory, CANMET, Energy, Mines and Resources Canada, Elliot Lake, Ontario, Canada. P5A 2J6

ÉVALUATION DES ERREURS ASSOCIÉES AUX INSTRUMENTS DE MESURE DU DÉBIT D'AIR

J. Bigu*

RÉSUMÉ

Des essais détaillés ont été réalisés avec plusieurs pompes d'échantillonnage de l'air. On a mesuré les débits d'air des pompes dans diverses conditions expérimentales en utilisant plusieurs appareils de mesure du débit d'air. Les pompes ont été essayées avec deux types de filtre couramment utilisés pour l'échantillonnage de l'air contenant des produits de filiation du radon (et du thoron), soit des filtres en fibre de verre et des filtres Millipore. On a également étudié l'effet de l'insertion d'un tube de plastique entre le système filtre/porte-filtre et l'orifice d'admission de la pompe d'échantillonnage, ainsi que l'effet de l'ajout d'un tube de plastique à l'orifice de sortie de la pompe. L'ajout de tubes de plastique de diverses longueurs aux orifices d'admission et de sortie d'une pompe d'échantillonnage constitue une pratique courante dans de nombreuses situations expérimentales. L'effet le plus intéressant observé lors de ces études a été l'apparition d'un phénomène de résonance du débit lorsque la longueur des tubes variait de quelques centimètres à environ 4,5 m. Ces études avaient été entreprises en partie après qu'on eût observé des débits "anormaux" lors de l'évaluation technique d'un moniteur de niveau opérationnel instantané.

Mots-clés: pompes d'échantillonnage; débit d'air; résonance.

*Chercheur et chef de la Section de recherche en radiation, ventilation et poussières respirables, Laboratoire d'Elliot Lake, CANMET, Énergie, Mines et Ressources Canada, Elliot Lake, Ontario, Canada. P5A 2J6

CONTENTS

	Page
ABSTRACT	i
RESUME	ii
INTRODUCTION	1
PRELIMINARY REMARKS	2
EXPERIMENTAL PROCEDURE	4
EXPERIMENTAL RESULTS AND DISCUSSION	7
A. Gilian Pump	8
B. SKC Pump	16
C. Alpha-1 Pump	20
D. Aquarium Pump	22
FURTHER TESTS	23
A. Relationship Between Pressure Differential and Airflow Rate	23
B. Effect of Ambient Temperature on the Relationship Between ΔP and Q	24
C. Measurement of Airflow Rate by Several Methods	24
MAIN CONCLUSIONS	25
ACKNOWLEDGEMENTS	27

TABLES

No.		
1.	Operation of the Gilian pump under unregulated airflow conditions	28
2.	Effect of temperature on pump flow rate and filter pressure differential	29
3.	Comparison of pump airflow rates measured by different airflow rate measuring devices	30

FIGURES

1.	Experimental arrangement used	32
2.	Airflow rate versus intake tubing length for the Gilian pump. No filter	33
3.	Airflow rate versus intake tubing length for the Gilian pump. No filter	34
4.	Airflow rate versus intake tubing length for the Gilian pump. No filter	35
5.	Airflow rate versus intake tubing length for the Gilian pump. No filter	36

6. Airflow rate versus exhaust tubing length for the Gilian pump. No filter 37

7. Airflow rate versus exhaust tubing length for the Gilian pump. No filter 38

8. Airflow rate versus exhaust tubing length for the Gilian pump. No filter 39

9. Airflow rate versus exhaust tubing length for the Gilian pump. No filter 40

10. Airflow rate versus exhaust tubing length for the Gilian pump. No filter 41

11. Airflow rate versus intake tubing length for the Gilian pump. Glass fibre filter 42

12. Airflow rate versus intake tubing length for the Gilian pump. Glass fibre filter 43

13. Pressure drop across the filter versus intake tubing length. Glass fibre filter 44

14. Airflow rate versus intake tubing length for the Gilian pump. Glass fibre filter 45

15. Airflow rate versus intake tubing length for the Gilian pump. Glass fibre filter 46

16. Airflow rate versus intake tubing length for the Gilian pump. Millipore filter 47

17. Airflow rate versus intake tubing length for the Gilian pump. Millipore filter 48

18. Airflow rate versus intake tubing length for the Gilian pump. Millipore filter 49

19. Airflow rate versus intake tubing length for the Gilian pump. Millipore filter 50

20. Airflow rate versus intake tubing length for the Gilian pump. Millipore filter 51

21. Pressure drop across the filter versus intake tubing length for the Gilian pump. Millipore filter 52

22. Airflow rate versus exhaust tubing length for the Gilian pump. Glass fibre filter 53

23. Airflow rate versus exhaust tubing length for the Gilian pump. Glass fibre filter 54

24. Airflow rate versus exhaust tubing length for the Gilian pump. Glass fibre filter 55

25. Airflow rate versus exhaust tubing length for the Gilian pump. Glass fibre filter 56

26. Pressure drop across the filter versus exhaust tubing length for the Gilian pump. Glass fibre filter 57

27. Airflow rate versus exhaust tubing length for the Gilian pump. Millipore filter 58

28. Airflow rate versus exhaust tubing length for the Gilian pump. Millipore filter 59

29. Airflow rate versus exhaust tubing length for the Gilian pump. Millipore filter 60

30. Airflow rate versus exhaust tubing length for the Gilian pump. Millipore filter 61

31. Airflow rate versus exhaust tubing length for the Gilian pump. Millipore filter 62

32. Airflow rate versus exhaust tubing length for the Gilian pump. Millipore filter 63

33. Pressure drop across the filter versus exhaust tubing length for the Gilian pump. Millipore filter 64

34. Pressure drop across the filter versus airflow rate for the Millipore filters (upper graphs), and glass fibre filters (lower graph). Gilian pump 65

35. Airflow rate versus time for the Gilian pump 66

36. Pressure drop across the filter versus time for the Gilian pump 67

37. Airflow rate versus number of glass fibre filters for the Gilian pump operating on the flow regulated mode 68

38. Airflow rate versus number of glass fibre filters for the Gilian pump, non-flow regulating mode 69

39. Airflow rate versus intake tubing length for the SKC pump. Glass fibre filter 70

40. Airflow rate versus intake tubing length for the SKC pump. Glass fibre filter 71

41. Airflow rate versus intake tubing length for the SKC pump. Glass fibre filter 72

42. Airflow rate versus intake tubing length for the SKC pump. Millipore filter 73

43. Airflow rate versus intake tubing length for the SKC pump. Millipore filter 74

44. Airflow rate versus intake tubing length for the SKC pump. Millipore filter 75

45. Airflow rate versus exhaust tubing length for the SKC pump. Glass fibre filter 76

46. Airflow rate versus exhaust tubing length for the SKC pump. Glass fibre filter 77

47. Airflow rate versus exhaust tubing length for the SKC pump. Glass fibre filter 78

48. Airflow rate versus exhaust tubing length for the SKC pump. Glass fibre filter 79

49. Pressure drop across the filter versus exhaust tubing length for the SKC pump. Glass fibre filter 80

50. Airflow rate versus exhaust tubing length for the SKC pump. Glass fibre filter 81

51. Pressure drop across the filter versus exhaust tubing length for the SKC pump. Glass fibre filters 82

52. Airflow rate versus exhaust tubing length for the SKC pump. Millipore filter 83

53. Airflow rate versus exhaust tubing length for the SKC pump. Millipore filter 84

54. Airflow rate versus exhaust tubing length for the SKC pump. Millipore filter 85

55. Pressure drop across the filter versus exhaust tubing length for the SKC pump. Millipore filter 86

56. Airflow rate versus exhaust tubing length for the SKC pump. Millipore filter 87

57. Airflow rate versus exhaust tubing length for the SKC pump. Millipore filter 88

58. Pressure drop across the filter versus exhaust tubing length for the SKC pump. Millipore filter 89

59. Pressure drop across the filter versus airflow rate for the Millipore filter (upper graph), and glass fibre filters (lower graphs) SKC pump 90

60. Airflow rate versus time for the SKC pump. Millipore filter 91

61. Pressure drop across the filter versus time for the SKC pump. Millipore filter 92

62. Airflow rate versus intake tubing length for the Alpha-1 pump. Glass fibre filter 93

63. Airflow rate versus intake tubing length for the Alpha-1 pump. Glass fibre filter 94

64. Airflow rate versus intake tubing length for the Alpha-1 pump. Glass fibre filter 95

65. Airflow rate versus intake tubing length for the Alpha-1 pump. Millipore filter 96

66. Airflow rate versus intake tubing length for the Alpha-1 pump. Millipore filter 97

67. Airflow rate versus intake tubing length for the Alpha-1 pump. Millipore filter 98

68. Airflow rate versus intake tubing length for the Alpha-1 pump. Millipore filter 99

69. Pressure drop across the filter versus intake tubing length for the Alpha-1 pump. Millipore filter 100

70. Airflow rate versus exhaust tubing length for the Alpha-1 pump. Glass fibre filter 101

71. Airflow rate versus exhaust tubing length for the Alpha-1 pump. Glass fibre filter 102

72. Airflow rate versus exhaust tubing length for the Alpha-1 pump. Glass fibre filter 103

73. Airflow rate versus exhaust tubing length for the Alpha-1 pump. Glass fibre filter 104

74. Pressure drop across the filter versus exhaust tubing length for the Alpha-1 pump. Glass fibre filter 105

75. Airflow rate versus exhaust tubing length for the Alpha-1 pump. Millipore filter 106

76. Airflow rate versus exhaust tubing length for the Alpha-1 pump. Millipore filter 107

77. Airflow rate versus exhaust tubing length for the Alpha-1 pump. Millipore filter 108

78. Airflow rate versus exhaust tubing length for the Alpha-1 pump. Millipore filter 109

79. Pressure drop across the filter versus exhaust tubing length for the Alpha-1 pump. Millipore filter 110

80. Airflow rate versus time for the Alpha-1 pump. Millipore filter ... 111

81. Pressure drop across the filter versus time for the Alpha-1 pump. Millipore filter 112

82. Airflow rate versus intake tubing length for the aquarium pump. No filter 113

83. Airflow rate versus intake tubing length for the aquarium pump. Millipore filter (lower graph), and glass fibre filter (upper graph) 114

84. Airflow rate versus intake tubing length (lower graph), and exhaust tubing length (upper graph) for the aquarium pump. No filter 115

85. Airflow rate versus exhaust tubing length for the aquarium pump. Millipore filter (lower graph), and glass fibre filter (upper graph) 116

86. Airflow rate versus time for the aquarium pump. No filter 117

87. Airflow rate versus time for the aquarium pump. Millipore filter .. 118

88. Pressure drop across the filter versus time for the aquarium pump. Millipore filter 119

89. Pressure drop across the filter versus pump intake airflow rate for all the pumps 120

90. Pressure drop across the filter versus the pump intake and exhaust airflow rates for all the pumps. Glass fibre filter 121

91. Pressure drop across the filter versus pump intake airflow rate for all the pumps. Millipore filter 122

92. Pressure drop across the filter versus the pump's intake and exhaust airflow rates for all the pumps. Millipore filter 123

93. Pressure drop across the filter versus airflow rate for all the pumps at two different temperatures: 21°C (upper graph) and -8°C (lower graph). Millipore filter. Measurements carried out with a mass flow meter 124

94. Pressure drop across the filter versus airflow rate for all the pumps at two different temperatures: 21°C (upper graph) amd -8°C (lower graph). Millipore filter. Measurements conducted with a dry gas test meter 125

INTRODUCTION

Characterization and quantification of airborne pollutants are two areas of utmost importance for assessing occupational health hazards at the work place as well as for estimating the potential health risks to which the general public at large is exposed, particularly in the highly polluted environments of today's urban areas.

Assessment of air quality, and the estimation of the potential health risks associated with the inhalation of air polluted environments are carried out by routine air sampling and air monitoring according to well established and accepted experimental procedures.

Air monitoring and air sampling are essentially of two types, namely, active sampling and passive sampling. (It should be noted, however, that passive sampling is to some degree always operative concurrently with active sampling.) As the name itself suggests, passive sampling does not require any 'artificial' or external sampling action by the operator; it only requires a suitable material for the pollutant to adhere to under 'natural' or externally undisturbed experimental conditions. Hence, the essential difference between active sampling and passive sampling is that in the first case air samples are collected by means of an air sampling device of some sort. In general, active sampling is realized by drawing or forcing air through a suitable collecting material surface, e.g., filter or material bed, at a constant airflow rate, Q, for a predetermined sampling period, t, by means of a suitable air sampling pump. The amount of pollutant, P, collected by the collecting material can then be written as:

$$P = kQt \tag{1}$$

where, k can be a function of the characteristics of the filtering or adsorbing material (a), the physico-chemical properties of the pollutant (b), time, and other variables. In general, $k = k(a,b,\ldots t)$.

In its simplest case, k is a constant numerical factor independent of

a, b, ... t, and hence, Eq. 1 can be rewritten as $P \propto Qt$, where the sign $\propto$ stands for proportional to.

Because t, the sampling period, can be measured very accurately, it is clear that the accuracy with which P can be determined very much depends on the accuracy with which Q can be ascertained, and above all, with the constancy of the airflow rate (Q) during the sampling period, t.

The accuracy with which Q can be estimated for a given sampling pump depends on a number of factors such as:

1. type of sampling sampling pump;
2. method chosen for determining Q;
3. experimental and environmental conditions;
4. sampling train used; and
5. other factors such as the value or range of values of Q.

This report presents a study on the different factors (items 1 to 5) which affect the accuracy of airflow rate measurements. This investigation was requested by the Atomic Energy Control Board (AECB) under contract (AECB Project) No. 3.124.1, entitled "Assessment of Errors in Airflow Measuring Instruments (Uranium Mines)". The study is of particular interest to AECB uranium mine inspectors and to mine ventilation personnel.

PRELIMINARY REMARKS

In its simplest form, an active air sampling train consists of a filter holder, housing a suitable filter, upstream of an air sampling pump equipped with some sort of airflow monitoring device such as a rotameter. The filter/filter holder arrangement is physically c cted to the inlet of the air sampling pump by means of a length of flex plastic or rubber tubing. In uranium mines and mills, airborne radioact y (mainly radon progeny, thoron progeny, and Long-Lived Radioactive Dust) is collected on a filter and the α-particle activity on it is measured by means of an α-particle counter, i.e.,

'scaler'.

There are a number of methods that can be used to determine the airborne radioactivity concentration in uranium mines and mills. However, because of economical and time constraints, radioactivity measurements are made using the simplest possible technique compatible with proper air quality monitoring as mandated by the pertinent regulatory agencies.

To the knowledge of the author, there are no mandatory specific methodologies in Canada for the assessment of airborne radioactivity in uranium mines and mills. In other words, the mining and milling company is free to determine airborne radioactivity, namely, radon progeny (RnP), thoron progeny (TnP), and Long-Lived Radioactive Dust (LLRD) by whatever method is most convenient provided it is accurate enough for radiation exposure and regulatory purposes. However, regulatory agencies have made, in the past, a number of useful recommendations and drawn guidelines regarding experimental procedures and protocols aimed at introducing some reasonable degree of standardization in the methodology or methodologies used for air quality monitoring purposes.

It can be surmised from the above that the operator, (e.g., mine ventilation personnel) is free to choose the following:

1. The filter material (cellulose, glass fibre, or any other available and/or suitable material), and the size (diameter) of the filter, e.g., 25 mm, 37 mm, 50 mm;
2. The type of sample holder, e.g., nylon, stainless steel, open face, in-line, etc.;
3. The type of sampling pump and its operating airflow rate;
4. The length and diameter of the flexible tubing connecting the filter holder/filter assembly to the inlet of the sampling pump. Also the length and diameter of the tubing connected to the exhaust of the pump should this arrangement be necessary for whatever specific purpose;

5. The kind of tubing material used, e.g., rubber, vinyl. etc.

It is not the purpose of this study to deal with the effects of all of the above items, but only with those which are of direct interest in the context of this work. These include:

1. The pump type.
2. The filter material.
3. The length and diameter of the flexible tubing at the intake and exhaust of the pump.
4. The flow rate of the sampling pump.
5. Environmental conditions.

In addition to the above, the result of using different airflow rate calibration procedures and instrumentation to measure the airflow rate of the several pumps tested, is reported.

EXPERIMENTAL PROCEDURE

It is a well established fact that different types of air sampling pumps are used by mine and mill inspectors from various regulatory agencies such as the AECB, Ministry of Labour (MOL), and other agencies, and ventilation personnel from different uranium mines and mills, in order to measure radon progeny (RnP) and thoron progeny (TnP) concentration levels. The same applies equally well to filter materials, filter sample holders, sampling airflow rates, etc.

In order to assess the potential errors in airflow rate measurements in RnP and TnP measurements four different air sampling pumps were tested, namely:

a) Gilian Model HFS513A

b) SKC Model 224-43XR

c) DuPont Model Alpha-1

d) Ordinary aquarium pump.

Except for the aquarium pump, the airflow rate for the pumps could be

changed within a reasonably wide range, depending on 'filter loading' conditions, from <1 L/min to ~5 L/min with an upstream high resistance filter material, to ~5 L/min with no filter in line. All tests were conducted using the same type of filter holder, namely, a 25 mm Delrin™ nylon open face filter holder, housing either a Gelman Millipore filter (0.8 μm pore, AA type), or a Whatman Glass Fibre™ filter. In addition, the length of the tubing between the filter/filter holder assembly and the intake of the pump, or at the exhaust port of the pump, varied from a few cm to ~4.5 m. Two different internal diameters for the tubing were chosen: 6.5 mm and 4.5 mm. The tubing used is known under the commercial name of Tygon.

Measurements using the Gilian, SKC and Du Pont pumps were carried out covering the airflow rate range 2 to 4 L/min at three specific values, namely, 2 L/min, 3 L/min, and 4 L/min. The airflow rate for the aquarium pump could not be changed, and it operated at a nominal flow rate of ~3 L/min. Airflow rate measurements were conducted using a mass flow rate meter Model 8143A in conjunction with a mass flow transducer Model 8104-1434-FM (0-10 L/min), both manufactured by Matheson (U.S.A.); a conventional, manually operated, bubble test apparatus; a fully automated bubble test meter (BTM) Model Buck Calibrator (0-20 L/min), equipped with a special photocell for quick and automatic flow rate determination; a Wet Gas Test Meter (WGTM) made by GCA/Precision Instruments (U.S.A.), cat. No. 63115; and a Dry Gas Test Meter (DGTM) Model 802 manufactured by Singer (American Meter Division), U.S.A. Most airflow rate measurements were made using the mass flow rate meter apparatus. The latter, in addition to the other airflow rate measuring devices, were used to:

1. calibrate each pump independently;
2. compare the calibration values obtained with the different flow rate measuring devices.

Environmental conditions such as relative humidity (RH), temperature

(T), and barometric pressure (P) during the measurements were carefully recorded. A series of measurements was conducted at temperatures 20°C and -8°C to investigate the effect of T on the airflow rate measurements done with the mass flow rate apparatus and the DGTM.

In summary, each pump (except for the aquarium pump) was tested:

a) at three different airflow rates;

b) with two different filter materials;

c) with two different tubing internal diameters;

d) with over 30 different tubing lengths at the pump intake or pump exhaust; and

e) at two different temperatures.

In addition:

a) Each pump was calibrated using different calibration instrumentation, as pointed out above; and

b) Airflow rate constancy tests were carried out when the pumps were operated on the Q-regulated and Q-unregulated modes. These tests consisted of monitoring the airflow rate (Q) over extended periods of time to determine fluctuations in Q as a function of time. It should be noted that the Gilian, SKC, and Du Pont sampling pumps are provided with an airflow rate, Q, servo control mechanism, i.e., Q adjusts itself to compensate for external filter loading, or other external influences, that tend to alter the pre-set airflow rate. Hence, testing the pumps in the Q-regulated mode is to be understood as testing under normal pump operating conditions. In order to conduct tests in the Q-unregulated mode, the servo control mechanism of the pumps had to be disassembled or bypassed, and the pumps had to be connected to an external source of power operating at a voltage of 6 V.

Finally, the pressure differential built up between the two faces of the upstream filters in the sampling train was measured by means of an

automated manometer with digital readout, and with magnehelics covering different pressure ranges. The majority of the experimental tests were conducted in the flow rate servo-controlled mode, although numerous tests were carried out by-passing the flow control system.

EXPERIMENTAL RESULTS AND DISCUSSION

The results obtained in the present study have been summarized in Figs. 1 to 94, and Tables 1 to 3. For simplicity, the results obtained for the four pumps studied here are presented in sequential fashion, i.e., each pump independently. Comparisons between the performance of the pumps are discussed at the end of the section.

The general experimental arrangement used in these studies is shown in Fig. 1. This arrangement consisted basically of the following items: an airflow rate measuring device (e.g., a mass airflow rate meter, a dry gas test meter, DGTM, or any other conventional device for this purpose) followed by an in-line filter/filter holder system, and the sampling pump to be investigated. In order to measure the pressure differential developed across the filter, a magnehelic of the appropriate pressure differential range, or an automated manometer, was connected between the air upstream and air downstream faces of the filter/filter holder system. In two cases, the pumps were equipped with built-in rotameters in order to set and monitor the airflow rate. In the two other cases, the pumps did not have a rotameter. In these cases, a rotameter in the 0 to 5 L/min range was placed between the filter/filter holder system and the air intake of the sampling pump. The length of the plastic tubing between the filter/filter holder system and the intake of the pump, and the length of the plastic tubing at the exhaust end of the pump could be varied at will in order to investigate the effect of length on the airflow rate of the pump and the pressure differential across the filter.

In order to assist in the understanding of the data presented here, a

brief description of the characteristics of each pump will be given at the beginning of each subsection where the results obtained for each pump are discussed.

A. GILIAN PUMP

The Gilian pump is an airflow sampler which can deliver a variable airflow rate covering the range from 0.75 L/min to somewhat less than 5 L/min. This air sampler is provided with a servo-controlled airflow rate regulating system to maintain the airflow rate within narrow limits of the preset value.

The air sampler is composed of a pneumatic system, a control system, and a rechargeable battery pack, all housed in a sturdy 3.0 mm thick Lexan™ case.

The pneumatic system consists of a pump assembly, two damper assemblies and a flow regulator assembly stacked one above the other and held together by two retaining screws. The pneumatic system also includes a 10 μm nylon filter assembly, a flowmeter and interconnecting tubing assembled in such a way as to allow the entire pneumatic system to be tested as a complete sub-assembly.

The pump is a DC motor driven dual piston that uses a special preloaded valving system. The pump mechanism is sealed to prevent dirt and debris from entering the unit.

The flow compensation control provides for constant airflow from the pump at any preset airflow rate within the performance envelope. The compensation control includes a sensing resistor mounted in the motor leg which provides a voltage signal proportional to the motor load current which is fed to a comparator which in turn adjusts the motor voltage proportionately to the pump load line curves, thereby maintaining a constant airflow rate over the operating range.

The damper assembly consists of a compression spring sandwiched between two silicone diaphragms within a plastic housing which stacks directly above the pump to provide pulsation free flow for close coupling with the flowmeter,

i.e., built-in rotameter. An air intake port connects the damper to the pump intake and a through hole passage is provided in the damper body to allow communicating the pump discharge to the pressure regulator stacked above.

The flow indicator is a built-in rotameter (±20% accuracy) mounted vertically and visible from the outside of the case.

Depending on the particular model, the Gilian air sampler (i.e., pump for short) is equipped with a number of useful and practical features including an automatic timing device and other important features such as digital LED readouts and light indicators to indicate certain functions.

Data for the Gilian pump are shown in Figs. 2 to 38. Figures 2 to 10 show data using the experimental arrangement shown in Fig. 1 with no filter in the filter holder. Figures 2 to 5 show the effect of varying the length of the tubing at the intake of the pump, i.e., L_{int}, on the airflow rate as measured by a mass flow rate meter (MFM) and by the rotameter built-in in the pump. Figures 6 to 10 show similar data when the length of the tubing at the exhaust of the pump, i.e., L_{exh}, is varied. In both cases, the tubing length was varied from less than about 5 cm to approximately 1.1 m. Furthermore, the airflow rate in the pump was set at three different flow rates, namely, 2 L/min, 3 L/min, and 4 L/min. The procedure in each case was to set the airflow rate, Q, at a given value under a fixed set of experimental conditions and then vary either L_{int} or L_{exh}.

Figures 2 to 10 show that in all cases there is a significant effect on the airflow rate (Q) brought about by a variation in L_{int} or L_{exh}, the effect being much more pronounced when L_{exh} is changed. Furthermore, the effect on Q depends on Q itself, and the inner diameter of the tubing. (Note: Figs. 2, 6, 8 and 9 were obtained using tubing of 6.5 mm inner diameter whereas in Figs. 3, 4, 5, 7 and 10 tubing of 4.5 mm inner diameter was used.)

Figures 8 to 10 exhibit a clear resonance effect as a function of L_{exh} for values in the range 0.5 to 0.55 m, particularly at the higher airflow

rates, e.g., 3 L/min and 4 L/min. In these cases, an increase in Q of up to 25 to 28% can be observed. A correspondingly smaller effect (~5%) can be seen at Q = 2 L/min with 4.5 mm inner diameter tubing (see Fig. 7). While in most cases the airflow rate profiles observed for the rotameter and the mass flow meter (MFM) were similar, in some other cases, particularly when L_{int} was the variable, these two profiles did not follow similar variations. The reason for this is as yet unclear. No clear resonance effect could be observed when L_{int} was varied but a steady decrease with increasing L_{int}. Variations of Q of about 17% were observed depending on the value of L_{int} (see Fig. 2).

Figures 11 to 38 show data using the arrangement depicted in Fig. 1 when a filter is in place in the filter holder, i.e., either a glass fibre filter or a Millipore 0.8 μm pore size filter. Figures 11 to 15 show data using a glass fibre filter where the effect of L_{int} on Q has been investigated. Figures 16 to 21 show similar type of data but using a Millipore filter.

Figures 11 to 21 show small variations of the pump airflow rate with increasing L_{int}. In general, these variations are more visible when measured by the MFM than when indicated by the pump's rotameter. No large differences could be observed between the use of a glass fibre filter and a membrane filter, i.e., Millipore filter.

No clear indication could be seen for the airflow rate to either increase or decrease with increasing intake tubing length, L_{int}. No clear evidence of any relationship between the pump's airflow rate (Q) and L_{int} could be observed. However, significant variations in Q_{MFM} could be seen in the range 0.25 to 0.5 L/min (see Figs. 11, 12 and 14) for glass fibre filters, with a maximum fluctuation of ~10% (see Fig. 12). For Millipore filters, variations occurred at different airflow rate ranges.

In all cases a quite significant difference between Q_R (rotameter's reading) and Q_{MFM} reading was observed. Furthermore, the profiles for Q_R and

Q_{MFM} as a function of L_{int} did not follow one another. The latter was equally true for the case where no filter was used (see Figs. 2 to 5).

Figures 22 to 33 show the effect of the exhaust tubing length, L_{exh}, on Q_R and Q_{MFM} when a glass fibre filter is used (Figs. 22 to 26) and when a Millipore filter is used (see Figs. 27 to 33). In all cases a clear correspondence between Q_R and Q_{MFM} can be observed. As with other cases investigated, significant differences between Q_R and Q_{MFM} could be seen. Furthermore, clear evidence of airflow rate resonance effects can be easily observed. The position of the resonance peak varied with the airflow rate to which the pump was initially set up before varying L_{exh}.

When a glass fibre filter was used, the position of the Q resonance peak was as follows:

L_{exh} ~1.05 m for Q_R = 2 L/min (see Fig. 22),

L_{exh} ~0.7 m for Q_R = 3 L/min (see Fig. 23), and

L_{exh} ~0.5 m for Q_R = 4 L/min (see Fig. 24).

In addition, a smaller Q resonance peak at Q_R = 2 L/min occurred for L_{exh} ~0.5 m (see Fig. 22). A maximum fluctuation of up to ~27% in airflow rate could easily be measured. Figures 22 to 24 were obtained for L_{exh} up to about 1.1 m. When L_{exh} was extended up to ~4 m, the results in Figs. 25 and 26 were obtained. (It should be noted that in Fig. 26, the pressure differential across the filter, rather than Q, is the variable measured.) In these cases multiple resonance effects could be observed, the maxima for Q_R = 4 L/min occurring at ~0.5 m (as previously reported), ~1.75 m, and ~3.1 m (see Fig. 25). Similar values were observed at a slightly lower value for (in this case) Q_{MFM} (see Fig. 26).

An interesting feature of Figs. 25 and 26 is not only the case of multiple resonance, but also a decrease in the intensity (height) of the peaks with each subsequent resonance. The peak intensities, taking the last peak as unity, were in the ratio 3:2:1, approximately.

A similar type of behaviour was observed when Millipore filters were used (see Figs. 27 to 33). Examples of this for Q_R = 2 L/min and Q_R = 4 L/min, using plastic tubing of 4.5 mm internal diameter (as opposed to 6.5 mm as in previous cases) are shown in Figs. 27 and 28. Some differences in the location of the resonance peak can be seen for Fig. 28 as opposed to Fig. 24, and it is tempting to ascribe this difference to the internal diameter of the tubing although there is not enough experimental evidence to support this hypothesis.

Figures 29 to 31 show Q_R and Q_{MFM} versus L_{exh} at initial Q_Rs slightly different from those values used before, namely, 2 L/min, 3 L/min and 4 L/min. A similar effect to that reported before is shown, except that the resonance peaks are now slightly shifted in a manner consistent with the different initial Q_Rs used.

Figures 32 and 33 show, respectively, the airflow rate and pressure differential across the filter versus L_{exh} for L_{exh} in the range ~0 to ~5 m. These figures show that for Q_R = 3 L/min, maxima occur at L_{exh} ~0.58 m, 2.28 m and 4.16 m. As before, multiple resonances took place with decreasing peak intensity. The larger values of L_{exh} at Q_R = 3 L/min as compared with those corresponding to Q_R = 4 L/min (namely, 0.5 m, 1.75 m, and 3.1 m) reflect the correspondingly lower values for the pump airflow rate used. Again the peak intensities were in the rough ratio of 3:2:1.

Figure 34 shows the pressure differential measured across a Millipore filter (upper graphs) and a glass fibre filter (lower graphs) versus pump airflow rate. Measurements were conducted with a mass flow meter and by reading the pump's rotameter. Figure 34 shows the following features of interest:

a) there is essentially a strict linear relationship between ΔP (pressure differential) and Q;

b) ΔP increases with increasing Q, as expected; and

c) for a given Q, ΔP is higher for the Millipore filter than for the glass fibre filter, as anticipated.

Figure 35 shows airflow rate constancy tests conducted on the pump for a period of about 9 h of continuous pump operation. Also shown in the graph are the daily mean values corresponding to Q. A maximum variation in Q of about 8% was observed over a one day shift. Figure 36 is similar to Fig. 35 except that ΔP, rather than Q, was measured. A very small maximum ΔP was measured (~2.5%) during a period of ~9 h.

Figures 37 and 38 show the effect of filter loading on the pump airflow rate when the pump was operated on its usual servo-controlling mode (Fig. 37), and when the servo-controlling mechanism was by-passed (Fig. 38), i.e., under unregulated airflow conditions. The measurements were conducted at three different initial airflow rates (as measured without a filter), namely, 3.75 L/min, 2.6 L/min, and 1.7 L/min as measured by the mass flow meter, and which corresponded, respectively, to 4 L/min, 3 L/min, and 2.0 L/min as read on the pump's rotameter.

Pump loading, i.e., filter loading, was attained by adding (glass fibre) filters to the intake side (inlet) of the pump. The pump maintained the airflow rate within very narrow limits, i.e., better than about $\pm$5% for each preset Q_R value. At the highest airflow rate investigated, i.e., Q_R = 4 L/min or Q_{MFM} ~3.75 L/min, constant flow rate could be maintained to better than 3% with a pump loading corresponding to three glass fibre (GF) filters. The pressure differential (ΔP) developed across the filter(s) was as follows:

no filter : 1 cm H_2O

one GF filter : 16 cm H_2O

two GF filters : 32 cm H_2O

three GF filters : 50 cm H_2O

a fourth GF filter increased ΔP to 69 cm H_2O, but the pump failed to maintain a constant flow rate and eventually after a short period the pump shut itself

off. The above table shows that each glass fibre (GF) filter increased ΔP by approximately 16 cm H_2O.

When Q_R was reduced to 3 L/min (Q_{MFM} ~2.6 L/min) and 2 L/min (Q_{MFM} ~1.7 L/min), the pump could comfortably maintain the flow rate to within 6 to 8% with a load of up to five glass fibre filters. The ΔP developed across the filter(s) for Q_R = 3 L/min was as follows:

no filter	: 0.5 cm H_2O
one GF filter	: 11.0 cm H_2O
two GF filters	: 21.5 cm H_2O
three GF filters	: 32.0 cm H_2O
four GF filters	: 43.5 cm H_2O
five GF filters	: 55.0 cm H_2O

The above values indicate that an additional ~11 cm H_2O pressure differential was brought about for each extra GF filter added to the pump intake.

The pressure differential developed across the glass fibre filter(s) for Q_R = 3 L/min was as follows:

no filter	: 0.5 cm H_2O
one GF filter	: 7.0 cm H_2O
two GF filters	: 14.0 cm H_2O
three GF filters	: 20.5 cm H_2O
four GF filters	: 27.5 cm H_2O
five GF filters	: 36.0 cm H_2O

The values given above correspond to a ΔP ~7 cm H_2O for each additional GF filter. The above data indicate a significant decrease in ΔP(per GF filter) with decreasing airflow rate.

Except for Q_R = 4 L/min, the other two cases investigated, i.e., Q_R = 3 L/min and Q_R = 2 L/min, show a slight decrease in airflow rate with increasing filter loading.

Figure 38 shows data under unregulated airflow conditions. In this case the servo-controlled mechanism was disabled and bypassed, and an external voltage power supply was used to operate the pump motor. The data obtained under unregulated conditions are shown in Table 1. The tabulated data show the following:

1. Q_{MFM} decreased with increasing pump loading, i.e., with an increasing number of GF filters placed at the intake of the pump. The decrease in airflow rate depended somewhat on the initial airflow rate, i.e., Q_R measured without a filter. The decrease in pump airflow rate caused by 5 filters as compared with only 1 GF filter was approximately 45% for Q_R = 4.0 L/min, 48% for Q_R = 3 L/min, and 50% for Q_R = 2 L/min;
2. As expected, the pressure differential across the filter(s) increased with increasing number of GF filters. This pressure differential depended on the initial Q_R and was largest for the highest Q_R and decreased with decreasing Q_R;
3. The pressure differential, ΔP, brought about for each additional GF filter increased with increasing number of filters. However, the difference in ΔP measured between n filters and n-1 filters decreased with n (see column labelled $\Delta P/GF$). The value of $\Delta P/GF$ for a given n, n-1 pair increased with increasing initial Q_R, i.e., was largest for Q_R = 4 L/min, and lowest for Q_R = 2 L/min;
4. The external voltage, V, required to attain a given Q_R increased with the desired value for Q_R, but remained independent of the number of filters used; and
5. The current drawn by the pump motor for a given initial Q_R increased with increasing number of GF filters placed at the intake of the pumps, i.e., increased with increasing pump loading.

Other data of interest regarding the Gilian pump will be discussed in conjunction with the behaviour of the other pumps in a subsequent section.

B. THE SKC PUMP

The SKC pump is similar to the Gilian pump. The pneumatic system consists of a pump/valve, pulsation dampener, pressure regulator, flowmeter, and filter assembly.

1. Pump/valve assembly: the pump is of a dual silicone rubber diaphragm type, driven by a high efficiency DC motor. The diaphragm pump is combined with special low pressure, positive acting valves. The pump mechanism is sealed to prevent dirt from entering. The DC motor operates from rechargeable NiCad batteries.
2. The pulsation dampener assembly consists of a pair of silicone rubber diaphragms within a housing. Two such assemblies are used to maintain pulsation-free flow and are located directly above the pump. In the intake stroke, the diaphragms are stretched inward by vacuum. In the exhaust stroke, the diaphragm elasticity forces the diaphragms apart, maintaining a continuous vacuum on the intake to the pump.
3. The pressure regulator is only used for low airflow rate applications, i.e., less than about 0.8 L/min.
4. The flowmeter is a rotameter mounted vertically in the case. It is used to monitor the pump airflow rate.
5. The filter assembly consists of a see-through housing and filter membrane held in place by an 'O' ring. All air passes through the filter assembly. The transparent housing permits the operator to view the pump filter to determine when changing is necessary. The purpose of this filter is to prevent dirt and debris from entering the pump.

Apart from the above, the SKC air sampler is equipped with an electrical control system which consists of a battery pack (as indicated above), a control panel, an advanced motor control circuit and an on-board 'computer'. The motor control system is aimed at providing constant airflow even though the back pressure of the collecting device may have increased

because of dust accumulation on a collecting filter. Thus, as the back pressure increases, the motor voltage is automatically corrected to maintain constant airflow over the operating range.

As with the Gilian air sampler and depending on the model, the SKC air sampler incorporates a number of interesting, useful and practical features including time programmability, battery status indicator, etc. The airflow range covered by the SKC air sampler is from 0.75 L/min to about 5 L/min.

The experimental data obtained for the SKC pump have been summarized in Figs. 39 to 61. Data were obtained for three different 'initial' flow rates, namely, 2 L/min, 3 L/min and 4 L/min as measured by the pump rotameter, i.e., Q_{rot}. It should be noted that except for the data shown in Figs. 54 and 57, the Q_R measured was that corresponding to the filter in place before making any changes in the system, i.e., varying the tubing length at the intake or exhaust. Again, glass fibre (GF) and Millipore filters were used in the experiments. The data presented below follow the same format as that for the Gilian pump. The results and conclusions for the SKC pump are also very similar to those obtained for the Gilian pump.

Figures 39 to 41 show the effect of the intake tubing length, L_{int}, on the pump airflow rate as indicated by the pump rotameter, Q_{rot}, and an external airflow rate measuring device, namely, a mass flow meter, and associated airflow sensor, Q_{MFM}. The data shown in the above figures suggest that the pump rotameter was unaffected by L_{int}. However, Q_{MFM} was affected to some degree for the low airflow rate measurements, i.e., Q_R = 2 L/min (see Fig. 39). A variation of -6% was observed for the latter case. The data corresponding to Figs. 39 to 41 were obtained using a GF filter. The L_{int} covered was from a few cm to ~1.3 m.

Figures 42 to 44 show the same type of data as that corresponding to Figs. 39 to 41 except that a Millipore filter was used. In this case Q_R and Q_{MFM} were unaffected by L_{int}.

Figures 45 to 51 show the effect of the exhaust tubing length, L_{exh}, on Q_R and Q_{MFM} (Figs. 45 to 48 and 50), and on the pressure differential, ΔP, across the GF filter used in these tests. Clear airflow rate resonance effects are observed for all cases. Again, the value for L_{exh} corresponding to the resonance peak decreased with increasing pump airflow rate, i.e., L_{exh} ~1 m for Q_R = 2 L/min, L_{exh} ~0.75 m for Q_R = 3 L/min, and L_{exh} ~0.45 m for Q_R = 4 L/min. The values correspond to a decrease in tubing length of about 0.3 m for each increase of Q_R by 1 L/min. An increase of up to ~16% in airflow rate was observed at L_{exh} ~0.45 m for Q = 4 L/min (see Fig. 48).

Figure 49 shows the effect of L_{exh} on ΔP for Q_R ~4 L/min. The figure shows a strong resonance peak at L_{exh} ~0.46 m with a variation (increase) in ΔP of about 16%.

Figure 50 shows the effect of L_{exh} on the pump airflow rate for an exhaust tubing length in the range from a few cm to about 4.5 m. As for the case of the Gilian pump, multiple resonance phenomena were observed. The resonance peaks were measured at approximately 0.5 m, 2 m and 3.5 m, i.e., with a constant separation of 1.5 m, following a simple 'harmonic' series or multiple of 0.5 m (the first resonance) according to the numerals 1, 4, and 7. Also, as previously reported for the case of the Gilian pump, the intensity of the resonance peaks decreased as the 'harmonic' number, i.e., L_{exh}, increased. The peak intensities, taking the last peak (highest 'harmonic') as reference (unity), were in the ratio 2.5:1.5:1 for Q_R and 5:2:1 for Q_{MFM} which results in a combined, or rough value for the ratios of 3:2:1.

Figure 51 shows the effect of L_{exh} on ΔP. As expected multiple resonance also occurred with peaks appearing at the same positions (L_{exh}) as for the case of Q_R and Q_{MFM}.

Figures 52 to 58 show similar types of data to those corresponding to Figs. 45 to 51, except that a Millipore filter has been used instead of a GF filter. The data were, again, qualitatively similar. Resonance peaks

appeared at L_{exh} ~1.0 to 1.1 m for Q_R = 2 L/min, L_{exh} ~0.58 m for Q_R = 3 L/min, and L_{exh} ~0.53 m for Q_R 3.25 L/min (see Figs. 52 to 54). Some differences in peak positioning were observed for Millipore filters when compared with GF filters. A maximum increase in the resonance peak of ~12% was observed for Q_R = 3.25 L/min, i.e., maximum resonance (maximum peak intensity increase) was observed for higher values of Q_R than for lower values of Q_R.

Figure 55 shows the effect of L_{exh} on ΔP. The figure shows a resonance at L_{exh} ~0.53 m, corresponding to Q_R = 3.25 L/min. The increase in ΔP was ~16%.

Figure 56 shows similar data to those of Figs. 52 to 54 for Q_R = 4 L/min. In this case the resonance occurred at L_{exh} ~0.4 m which is significantly smaller than for the case of Q_R = 3.25 L/min (see Fig. 54), providing further evidence for the decrease of L_{exh} with increasing Q_R.

Figure 57 shows the effect of L_{exh} on the pump airflow rate for a L_{exh} covering the range from a few cm to approximately 4.5 m. As with previous cases, multiple resonance effects are clearly visible which occur at L_{exh} ~0.5 m, L_{exh} ~2.2 m, and L_{exh}~4 m with a constant peak separation of approximately 1.5 m which agrees with data obtained for GF filters. The peak intensity ratio exhibited by Q_{MFM}, taking the smallest peak as reference, was 3:2:1, a value which agrees with previous data.

Figure 58 shows the effect of L_{exh} on the ΔP across the Millipore filter. As expected, multiple resonance also appears at the same locations, i.e., L_{exh}, as in the case of the airflow rate.

Figure 59 shows the relationship between the ΔP that develops across the filter for a given pump airflow rate against a series of flow rates, as measured by the pump rotameter and the mass flow meter, and associated airflow sensor. Data were collected for GF filters and Millipore filters. Figure 59 shows that there is a linear relationship between ΔP and Q. Furthermore, for

a given pump airflow rate, the pressure differential that develops across the filter is larger for Millipore filters than for GF filters, as expected.

Figures 60 and 61 show constancy tests in terms of pump airflow rate (Fig. 60), and in terms of the ΔP across the filter (Fig. 61). In both cases, Millipore filters were used. The figures also show the mean value of Q or ΔP during a period of about 9 h. These two figures show a feature of interest, namely, Q and ΔP decrease for a period of time, i.e., warm-up period, and then they remain fairly constant for the rest of the sampling period. It is shown in Fig. 60 that Q remained constant within $\sim\pm 2.1\%$.

Finally, it is worthwhile noting that a significant difference between Q_R and Q_{MFM} was observed in all the cases investigated. This difference has also been noticed for the Gilian pump and is partly due to the interaction of the two airflow rate measuring devices, the length of tubing separating the mass flow meter's sensor and the pump, and the effect of the filter in the sampling train.

C. THE ALPHA-1 PUMP

The Alpha-1 air sampler is equipped with a number of features which are common to both the Gilian sampler and the SKC air sampler. However, there are also a number of important differences which are worthwhile noticing. The Alpha-1 air sampler is provided with a significantly more advanced degree of programmability than the other two air samplers, although it is difficult to decide whether this results in the end on a practical enhancement of this air sampler's capabilities over the somewhat less microprocessor-control oriented versions characteristic of the Gilian and the SKC air samplers.

The Alpha-1 air sampler is not provided with a rotameter, and hence it is particularly difficult to monitor the airflow rate during the sampling period. Because the control of airflow rates and other components or features of the Alpha-1 air sampler are very similar to the Gilian air sampler and the SKC air sampler, they will not be repeated here. As previously indicated, the

reader should note that although the above devices are strictly speaking air movers or air samplers, the operator usually refers to them as 'pumps', for short.

The experimental data for the Alpha-1 are shown in Figs. 62 to 81. Figures 62 to 69 show the effect of L_{int} on Q_{MFM}. (No data available for Q_R because this pump is not equipped with a built-in rotameter.) Millipore and GF filters were used as for previous tests. A number of initial airflow rates (with the filter in place), as measured by the mass flow meter and associated airflow sensor were investigated.

Figures 62 to 64 present data usng a glass fibre (GF) filter. Three initial Q_{MFM} values were chosen, namely, 1.7 L/min, 2.7 L/min, and 3.91 L/min. The above figures show that L_{int} had very little influence on the pump airflow rate, i.e., at most ~2%.

Figures 65 to 68 show similar kinds of data to that obtained for Figs. 62 to 64, except that a Millipore filter was used instead of a GF filter. The initial Q_{MFM} used were 1.85 L/min, 2.2 L/min, 2.7 L/min and 3.9 L/min. The effect of L_{int} on Q_{MFM} was in this case somewhat larger than for GF filters, namely, ~3.8% (see Figs. 65 and 67).

Figure 69 shows the effect of L_{int} on the ΔP across the filter. A very small decrease in ΔP with increasing L_{int} was noted (-1%).

Figures 70 to 79 show the effect of the tubing exhaust length, Q_{exh}, on Q_{MFM} when a GF filter is used (Figs. 70 to 73), and when a Millipore filter is used (Figs. 75 to 79). The main airflow rates used were 2 L/min, 3 L/min, and 4 L/min. Contrary to the airflow rate resonance effects obtained before with the Gilian and the SKC pumps, no experimental evidence of this phenomenon can be observed for the Alpha-1 pump. Only some Q_{MFM} variations with L_{exh} can be seen, the extent of which could be somewhat influenced by the pump airflow rate.

Figures 74 and 79 show the effect of L_{exh} on ΔP. No significant effect

(≤2% maximum variation) could be seen on ΔP varying L_{exh} from a few cm to ~4 m.

Figures 80 and 81 show airflow rate and ΔP constancy tests for a period of about 9 h. A Millipore filter was used. A maximum variation of about 3% for Q_{MFM} and ΔP was observed for the entire sampling period.

D. THE AQUARIUM PUMP

No information regarding this pump is available. The pump used here was a simple, low-cost diaphragm pump of common use in small tropical fish aquaria. The data collected for this pump are given in Figs. 82 to 88. This pump was not equipped with a built-in rotameter or airflow servo-controlled mechanism as the other three pumps tested were.

Figure 82 shows the effect of L_{int} on the pump airflow rate, Q, with no filter in place. A steady Q-drift was noted with increasing L_{int} which could be due to the pump's drift, and therefore, not particularly related with L_{int}. The initial pump airflow rate, and subsequent airflow rate measurements shown in Figs. 82 to 88 were conducted using the mass flow meter and associated airflow sensor.

Figure 83 shows the effect of L_{int} on Q_{MFM} when a GF filter is used (top graph), and when a Millipore filter is used (lower graph). Based on this test, no significant effect was observed when a GF filter was used, whereas a steady decrease in Q_{MFM} with increasing L_{int} was observed when a Millipore filter was in place.

Figure 84 shows the effect of the tubing length on Q_{MFM} when no filter was used. The upper graph was obtained when L_{exh} was varied and a fixed L_{int} (0.33 m) was used, whereas the lower graph was obtained when L_{int} was varied and the L_{exh} was fixed at a given length, namely, 1.08 m. It is interesting to note that in this case resonance effects were observed when varying both L_{int} and L_{exh}. The maximum increase in Q_{MFM} in both cases was of about 25%.

Figure 85 shows the effect of L_{exh} on Q_{MFM} when a GF filter was used (top graph), and when a Millipore filter was in place (lower graph). As

before, clear resonance effects were observed which occurred at L_{exh} ~0.5 m for the GF filter with an initial Q_{MFM} = 2.8 L/min, and at L_{exh} ~0.6 m for the Millipore filter with an initial Q_{MFM} = 2.5 L/min. The increase in Q_{MFM} was about 22% for the GF filter, and ~17% for the Millipore filter.

Figure 86 shows a constancy test for the pump airflow rate when no filter was in place. Figure 87 shows a constancy test for Q_{MFM} when a Millipore filter was used. Figure 88 shows a constancy test for ΔP using a Millipore filter. In the first case (Fig. 86), a steady decrease in Q_{MFM} occured (~12%) as a function of sampling time. In the other two cases, Q_{MFM} or ΔP fell rather rapidly in the beginning (Figs. 87 and 88, respectively), and then fluctuated above and below a given airflow rate, or ΔP level.

FURTHER TESTS

Apart from the tests already discussed several other tests and measurements were conducted, namely,

1. Relationship between pump airflow rate and the pressure differential developed across the filter;
2. Effect of ambient temperature on the pump airflow rate;
3. Comparison of pump airflow rate measured by several methods;
4. Effect of measuring pump airflow rate at the intake and exhaust ports of the sampling pump.

The above items will be discussed in turn below.

A. RELATIONSHIP BETWEEN PRESSURE DIFFERENTIAL AND AIRFLOW RATE

The relationship between the pump airflow rate and the pressure differential developed across the filter was investigated. The data shown below are the combined data for (all) four pumps tested. Pump airflow rate measurements at the intake and exhaust ports of the pumps were conducted. The results of the tests are presented in Figs. 89 to 92. Figures 89 and 90 were obtained using GF filters, whereas Figs. 91 and 92 were obtained using

Millipore filters. Figures 89 and 91 include airflow rate measurements conducted at the intake port of the pumps only. Figures 90 and 92 include airflow rate measurements conducted at both the intake and exhaust ports of the pumps. In all the cases investigated a linear relationship between the pump airflow rate, Q, and the pressure differential, ΔP, developed across the filter was obtained. The slopes for Figs. 89 to 92 are different because the ΔP developed across the filters for a given Q depends on the filter material.

B. EFFECT OF AMBIENT TEMPERATURE ON THE RELATIONSHIP BETWEEN ΔP AND Q

Measurements of ΔP and Q for all pumps were conducted at two different temperatures, namely, 21°C and -8°C. The effect of temperature, T, on the relationship between ΔP and Q is shown in Figs. 93 and 94. In these tests, Millipore filters were used. Two pump airflow rate measuring devices were used independently, namely, a mass flow meter/airflow sensor system (0-10 L/min range) and a Dry Gas Test Meter (DGTM). Figures 93 and 94 show the results obtained with the former and the latter devices, respectively. Both figures show that for any given Q, ΔP is lower at the lower temperature, i.e., -8°C, than at the higher temperature, i.e., 21°C.

Table 2 shows the data used to plot Figs. 93 and 94 in a form suitable for direct comparison of the effect of T on Q and ΔP, independently.

C. MEASUREMENT OF AIRFLOW RATE BY SEVERAL METHODS

The pump airflow rate was measured by means of several airflow rate measuring devices, namely:

a) a Wet Gas Test Meter (WGTM),

b) a Dry Gas Test Meter (DGTM),

c) a Mass Flow Meter and its associate airflow sensor,

d) a Bubble 'tube', and

e) an automated bubble 'tube' equipped with a specially designed airflow cell and an automatic photo-timing device.

Table 3 shows data corresponding to the measurement of airflow rates for the four sampling pumps tested, measured with the airflow rate measuring devices indicated in items a) to e). Also shown in the table are the pressure differentials developed across the filters used (GF and Millipore filters) in the tests. Airflow rate measurements were conducted at both the inlet and the exhaust ports of the several pumps tested. Measurements were conducted on two different days, one day using a GF filter, the next day using a Millipore filter. The average environmental conditions during the tests were as follows:

Temperature (T) : 22.6 to 23.3°C

Relative Humidity (RH) : 15 to 19%

Barometric Pressure : 96.0 to 98.1 kPa

Table 3 shows the following interesting features:

a) Data with the Millipore filters seemed to be slightly more consistent than the data obtained with GF filters.

b) In general, Q_{MFM} was the lowest reading.

c) Measurements carried out with the other airflow rate measuring devices agreed fairly well with each other, i.e., ≷5%.

d) There was not much difference in the airflow rates measured at the intake and the exhaust ports of the sampling pumps.

e) The (average) ratio of the maximum value to the minimum value for the pumps airflow rates measured by the different airflow rate measuring devices was about 13%.

The differences between Q_{MFM} and other airflow rate measurements can tentatively be ascribed to the air density dependence on temperature.

MAIN CONCLUSIONS

The main conclusions that can be derived from this study are the following:

1. Sampling airflow rate (Q) and pressure differential (across the filter), ΔP, resonance effects were observed for all the sampling pumps, except the Alpha-1, when the tubing length at the exhaust port of the pump, or the intake port of the pump, or both, was varied. A maximum increase of over 25% could be observed in some cases. The tubing length at which this phenomenon occurred depended on the pumps sampling airflow rate, and to some extent on the filter type and internal diameter of the tubing. The length of the tubing, L, at which resonance occurred decreased with increasing sampling airflow rate.
2. Multiple resonance effects were observed when L was varied from a few cm length to about 4.5 m. In this L range, three resonance peaks appeared equally spaced with decreasing intensity (in the ratio 3:2:1) as L increased in value.
3. There was no marked difference between the airflow rates measured for any given pump using different airflow rate measuring devices, either at the intake or the exhaust ports of the pumps. It is estimated that Q can be estimated within an error of about $\pm$6%. It should be noted that by error, is meant here to be the maximum deviation from the average value of all the airflow rates measured by all the airflow rate measuring devices combined.
4. Measurements conducted with the mass flow meter/airflow sensor system gave, in general, the lowest values for the sampling airflow rate.
5. The qualitative behaviour of the pumps were not significantly affected by the type of filter material or filter used, i.e., GF filters or Millipore filters.
6. All the pumps tested equipped with airflow rate servo-control mechanisms operated quite satisfactorily, i.e., Gilian pump, SKC pump, and Alpha-1 pump. From these pumps, only the latter (Alpha-1) did not exhibit resonance phenomena.

Items 1 and 2 are very important because they can substantially affect the accuracy of experimental results. Situations where the effect of tubing length is not considered to have any effect on airflow rate abound, and the operator should be aware that this may constitute a significant and unexpected source of error.

ACKNOWLEGEMENTS

The author would like to acknowledge the contribution of Drs. Samir and Hussein for their contribution to this project during an IAEA fellowship. The author is also grateful to E. Edwardson of our laboratory for his assistance in some experimental aspects of this work. Finally, the author would like to thank the AECB for the financial support to carry out this project, and to Dr. P. Duport (AECB) for his advice and helpful technical discussions.

Table 1 - Operation of the Gilian pump under unregulated airflow conditions.

No. of GF Filters	Q_{MFM} (L/min)	ΔP (cm H_2O)	V (volt)	I (mA)	ΔP/GF	$\frac{Q_{MFM(1)}}{Q_{MFM}(5)}$
0	1.7	0.5	1.37	35		
					6.0	
1	1.5	6.5	1.37	50		
					4.5	
2	1.3	11.0	1.37	--		
					4.0	1.5
3	1.2	15.0	1.37	70		
					3.5	
4	1.1	18.5	1.37	--		
					3.5	
5	1.0	22.0	1.37	86		
0	2.7	0.5	2.09	50		
					9.5	
1	2.3	10.0	2.09	72		
					7.5	
2	2.0	17.5	2.09	--		
					6.0	1.48
3	1.9	23.5	2.09	103		
					5.5	
4	1.7	29.0	2.09	--		
					5.5	
5	1.55	34.5	2.09	125		
0	3.7	1.0	2.97	71		
					13.0	
1	3.2	14.0	2.97	98		
					10.0	
2	2.8	24.0	2.97	--		
					9.0	1.45
3	2.6	33.0	2.97	139		
					8.0	
4	2.4	41.0	2.97	--		
					8.0	
5	2.2	49.0	2.97	167		

Notes: 1) Q_{MFM} and ΔP stand for airflow rate measured by the mass flow meter and pressure differential across the filter(s), respectively.
2) V and I stand, respectively, for voltage and current supplied to the pump motor.
3) ΔP/GF indicates the pressure differential, per GF filter, for each successive pair of filters.
4) $Q_{MFM}(1)/Q_{MFM}(5)$ represents the decrease in pump airflow rate brought about by the use, i.e., loading, of 5 GF filters as compared with using only 1 GF filter.
5) GF is used to denote glass fibre.

Table 2 - Effect of temperature on pump flow rate and filter pressure differential.

Meas. at	Pump Type	Rotameter Setting (L/min)	Temperature: 21°C				Temperature: -8°C			
			Mass Flowmeter		Dry Test Meter		Mass Flowmeter		Dry Test Meter	
			Flowrate (L/min)	Pressure Drop (cm H_2O)	Flowrate (L/min)	Pressure Drop (cm H_2O)	Flowrate (L/min)	Pressure Drop (cm H_2O)	Flowrate (L/min)	Pressure Drop (cm H_2O)
Intake	Aquarium	None	2.9	44	2.86	42.5	3.0	38	3.17	39.5
	Gilian	2	1.82	26.5	1.91	26.5	1.9	23.5	1.98	23.5
		4	3.8	57	3.79	57	3.8	48	3.53	49
	SKC	2	1.7	25	1.79	25	1.7	22.5	1.82	22.5
		4	3.26	50	3.41	50	3.6	45.5	3.29	46
	Alpha-1	2	2.0	28	2.08	28	2	25	1.95	24.5
		4	3.98	62	4.37	62	4.32	57	4.13	57
Exhaust	Aquarium	None	3.06	45.5	3.53	49.5	3.3	41	3.15	42.5
	Gilian	2	1.91	26.5	1.92	27	2	23.5	1.9	23.5
		4	3.82	57	pump failure	65	3.8	48.5	pump failure	pump failure
	SKC	2	1.76	25.5	1.83	25	1.8	23	1.76	22.5
		4	3.3	50	3.75	52	3.66	46	3.61	48.5
	Alpha-1	2	1.94	28	1.95	28	2	25	1.84	25
		4	4.0	62	3.95	62	4.26	57	4.04	56

Table 3 - Comparison of pump airflow rates measured by different airflow rate measuring devices.

Filter: Glass Fibre Date: February 27, 1990

Meas. at	Pump Type	Rotameter Setting (L/min)	Mass Flowmeter (L/min)	Dry Test Meter (L/min)	Wet Test Meter (L/min)	Buck Calibrator (L/min)	Bubble Tube (L/min)	ΔP (cm H_2O)	$\frac{Q_{max}}{Q_{min}}$
Intake	Aquarium	None	3.08	3.24	3.18	3.173	3.02	23	1.07
	Gilian	2	1.8	1.97	1.98	1.982	1.97	14	1.10
		3	2.6	2.97	2.95	2.948	2.92	20	1.13
		4	3.62	3.96	3.89	3.91	3.88	29	1.09
	SKC	2	1.6	1.7	1.78	1.81	1.77	13	1.13
		3	2.4	2.7	2.71	2.683	2.83	19	1.18
		4	3.24	3.74	3.56	3.551	3.53	26	1.15
	Alpha-1	2	1.86	2.06	2.05	2.044	2.01	15	1.11
		3	2.76	3.07	3.06	3.086	3.06	21.5	1.12
		4	3.8	4.33	4.22	4.205	4.16	31	1.14
Exhaust	Aquarium	None	3.34	3.7	3.59	*	3.59	23	1.11
	Gilian	2	1.88	2.06	2.1	2.115	2.14	14	1.14
		3	2.64	2.89	3.54	3.14	3.13	21	1.34
		4	3.7	4.77	4.54	*	3.95	29	1.22
	SKC	2	1.62	1.79	1.85	1.781	1.83	13	1.14
		3	2.46	2.91	2.95	2.573	3	19.5	1.22
		4	3.32	4.14	3.73	*	3.56	26	1.25
	Alpha-1	2	1.82	2.07	2.09	2.064	2.05	14	1.15
		3	2.76	2.93	3.1	3.144	3.02	22	1.14
		4	3.8	4.03	4.29	4.263	4.25	31	1.13

Cont.

Table 3 - continued

Filter: Millipore DATE: March 2, 1990

Meas. at	Pump Type	Rotameter Setting (L/min)	Mass Flowmeter (L/min)	Dry Test Meter (L/min)	Wet Test Meter (L/min)	Buck Calibrator (L/min)	Bubble Tube (L/min)	ΔP (cm H_2O)	$\frac{Q_{max}}{Q_{min}}$
Intake	Aquarium	None	2.5	2.79	2.58	2.481	2.63	42	1.12
	Gilian	2	1.78	1.99	1.95	1.959	1.92	27.5	1.12
		3	2.6	2.93	2.9	2.87	2.87	42	1.13
		4	3.48	3.7	3.86	3.858	3.91	56	1.12
	SKC	2	1.6	1.72	1.8	1.806	1.78	24.5	1.13
		3	2.42	2.55	2.7	2.702	2.63	38	1.12
		4	3.28	3.51	3.54	3.516	3.59	51	1.09
	Alpha-1	2	2	2.08	2.03	2.036	2	28	1.04
		3	2.8	3.04	2.98	2.986	2.97	42	1.09
		4	3.98	4.37	4.09	4.25	4.09	62	1.10
Exhaust	Aquarium	None	2.74	2.98	3.12	3.108	2.88	39.5	1.14
	Gilian	2	1.8	1.96	1.98	2.026	1.986	27.5	1.12
		3	2.6	2.97	3.15	3.016	3.1	42.5	1.21
		4	3.52	PF	PF	*	3.78	56	1.07
	SKC	2	1.6	1.81	1.85	1.865	1.84	24.5	1.16
		3	2.46	2.64	2.85	2.714	2.77	38	1.16
		4	3.3	3.47	3.5	*	3.36	52	1.06
	Alpha-1	2	1.94	1.95	2.05	2.039	1.99	28	1.06
		3	2.74	2.94	2.93	2.977	2.92	43	1.09
		4	4	3.95	4.16	4.153	4.08	62	1.05

Notes: * No bubble produced.
PF indicates pump failure.
ΔP stands for pressure differential (drop)
Q_{max}, Q_{min} stand, respectively, for maximum and minimum airflow rate measured by airflow measuring device.

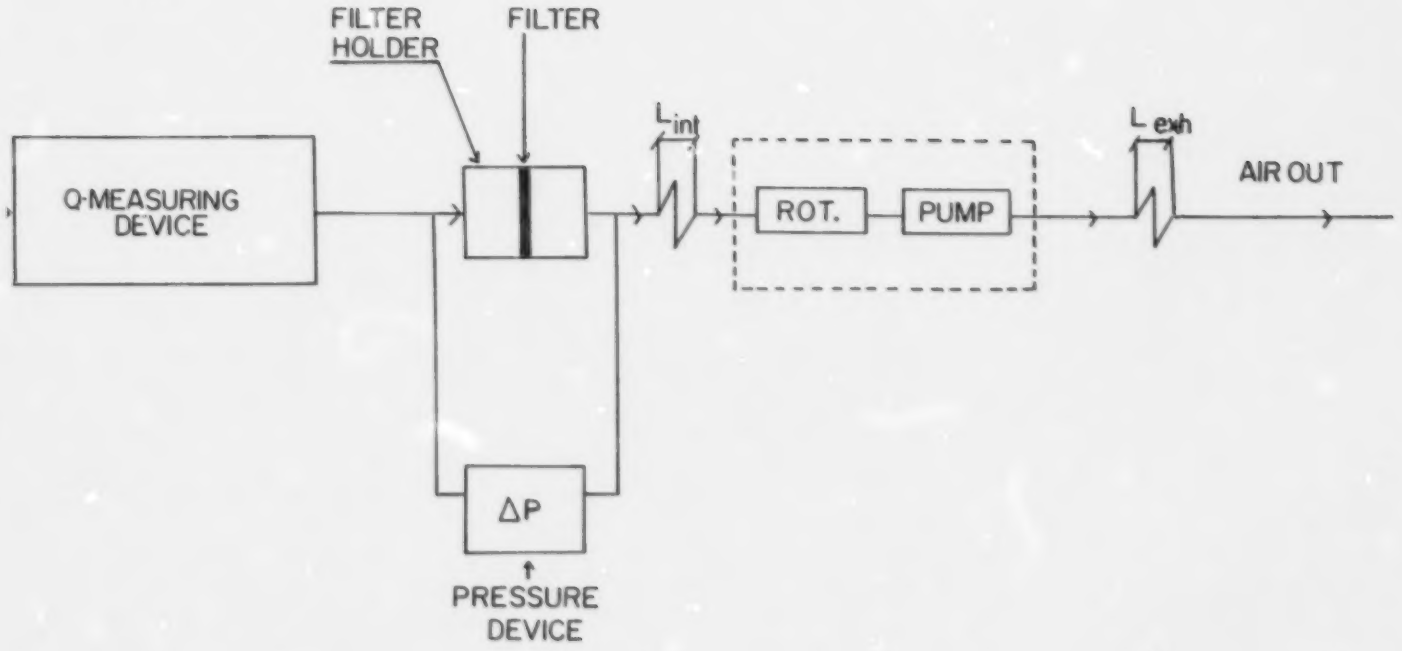

Fig. 1 - Experimental arrangement used.

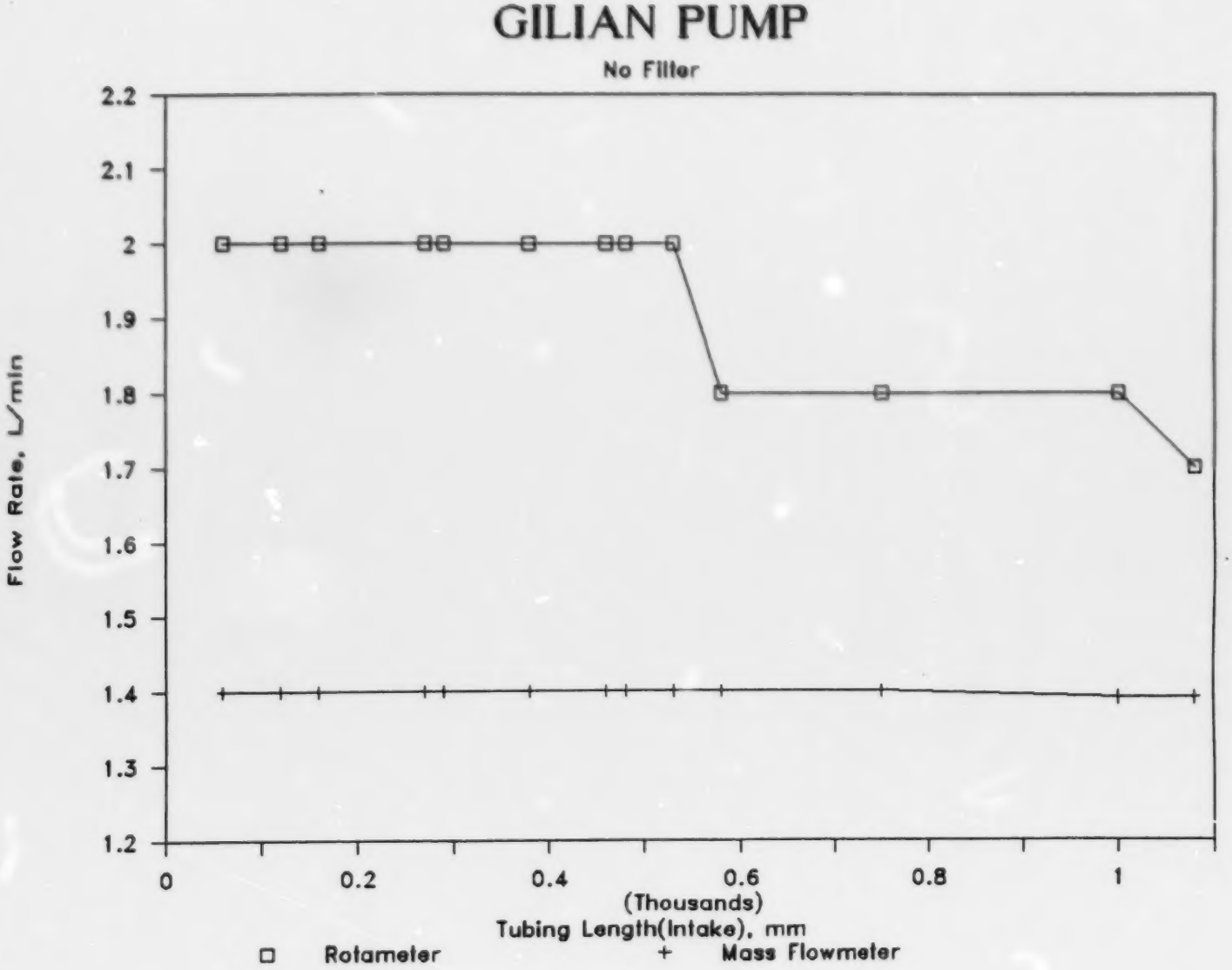

Fig. 2 - Airflow rate versus intake tubing length for the Gilian pump. (no filter)

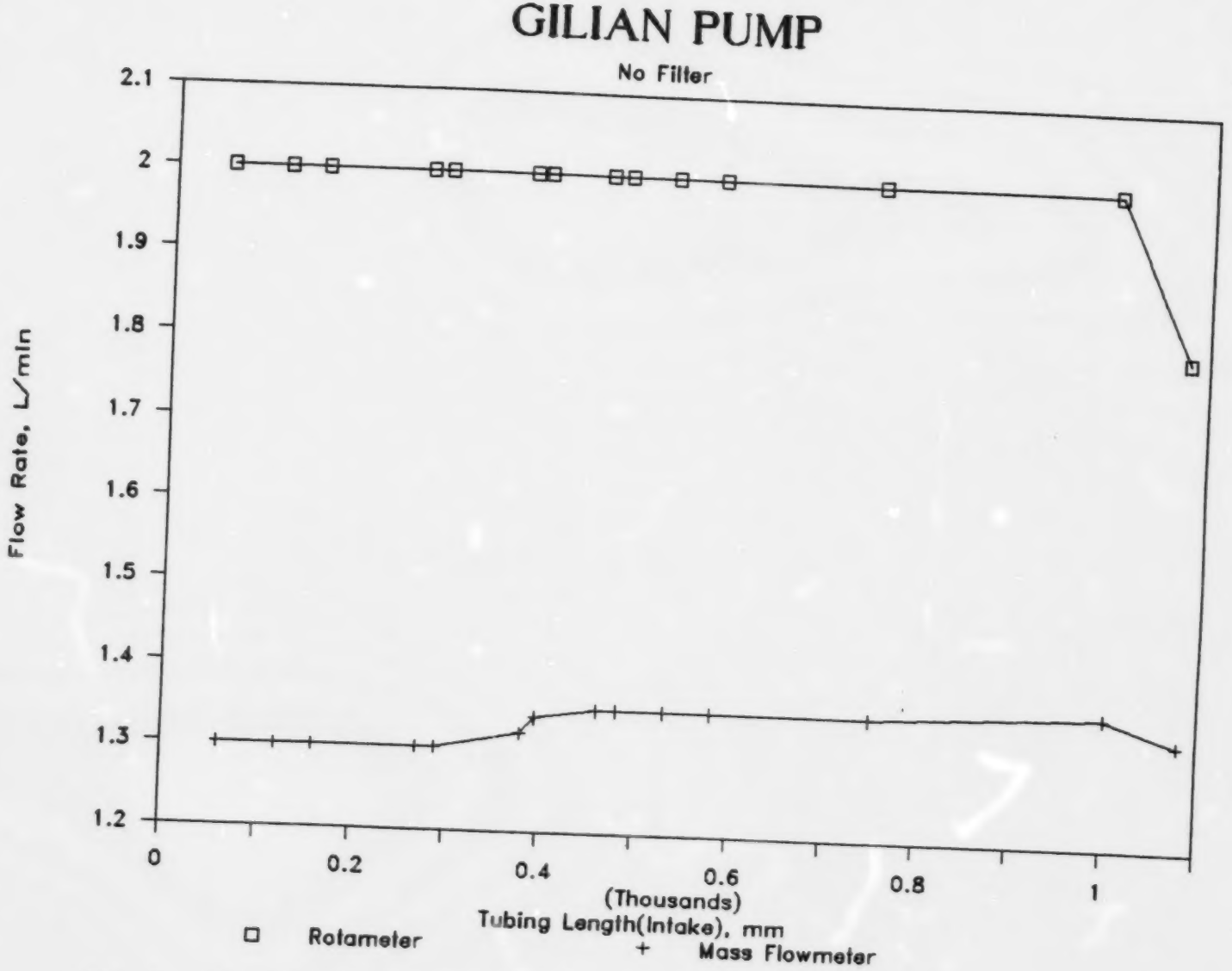

Fig. 3 - Airflow rate versus intake tubing length for the Gilian pump. (no filter)

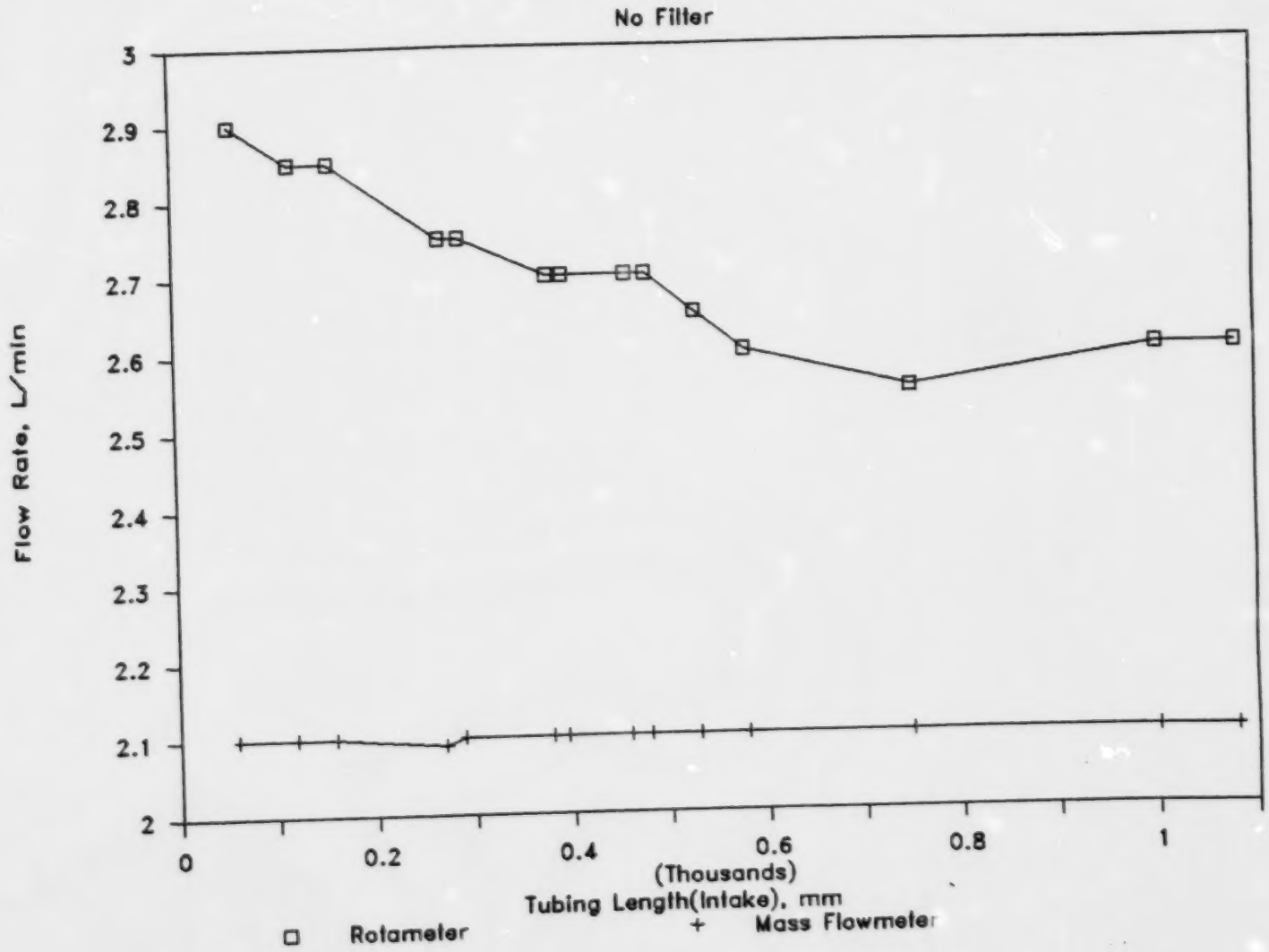

Fig. 4 - Airflow rate versus intake tubing length for the Gilian pump. (no filter).

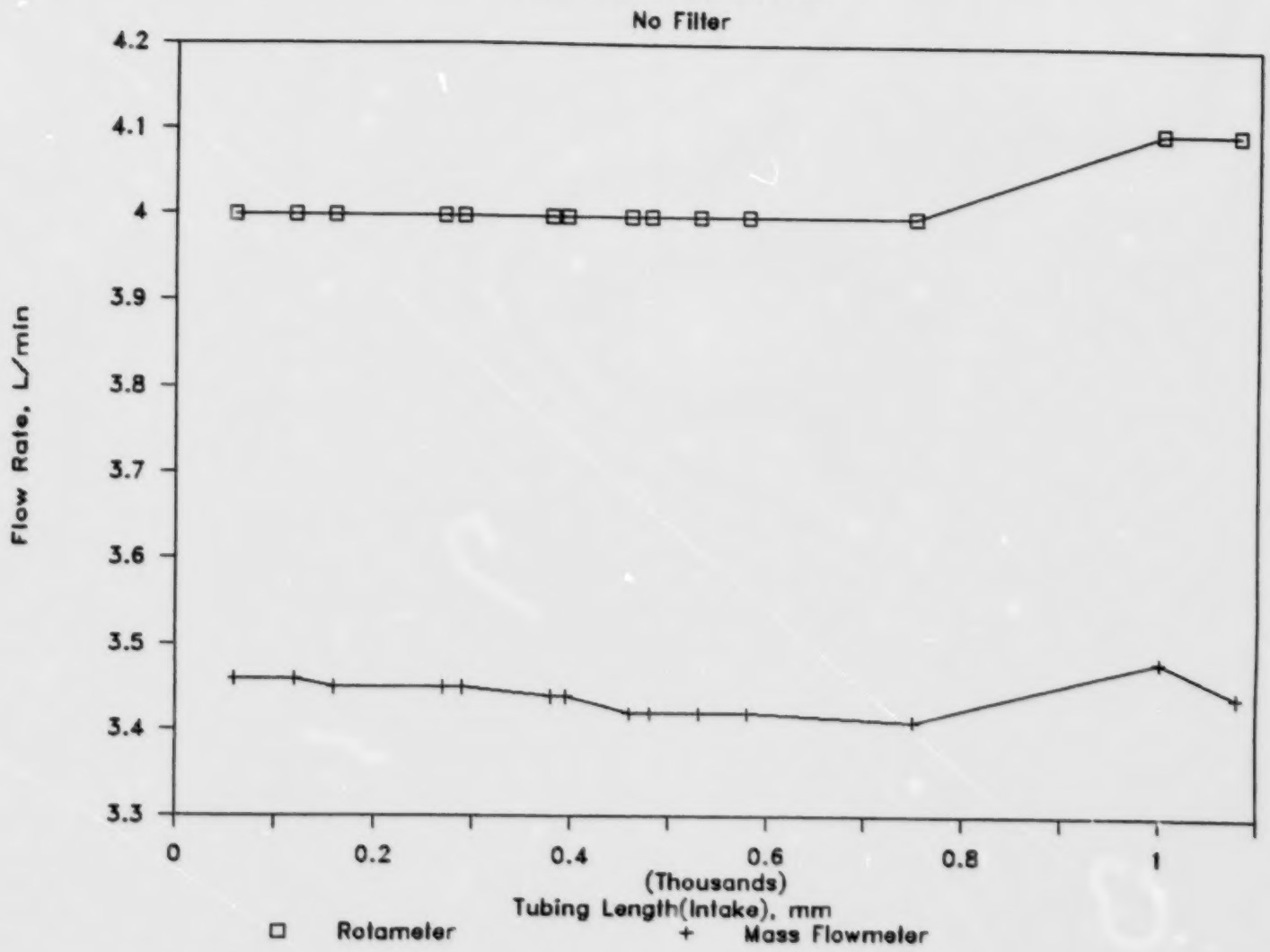

Fig. 5 - Airflow rate versus intake tubing length for the Gilian pump. (no filter)

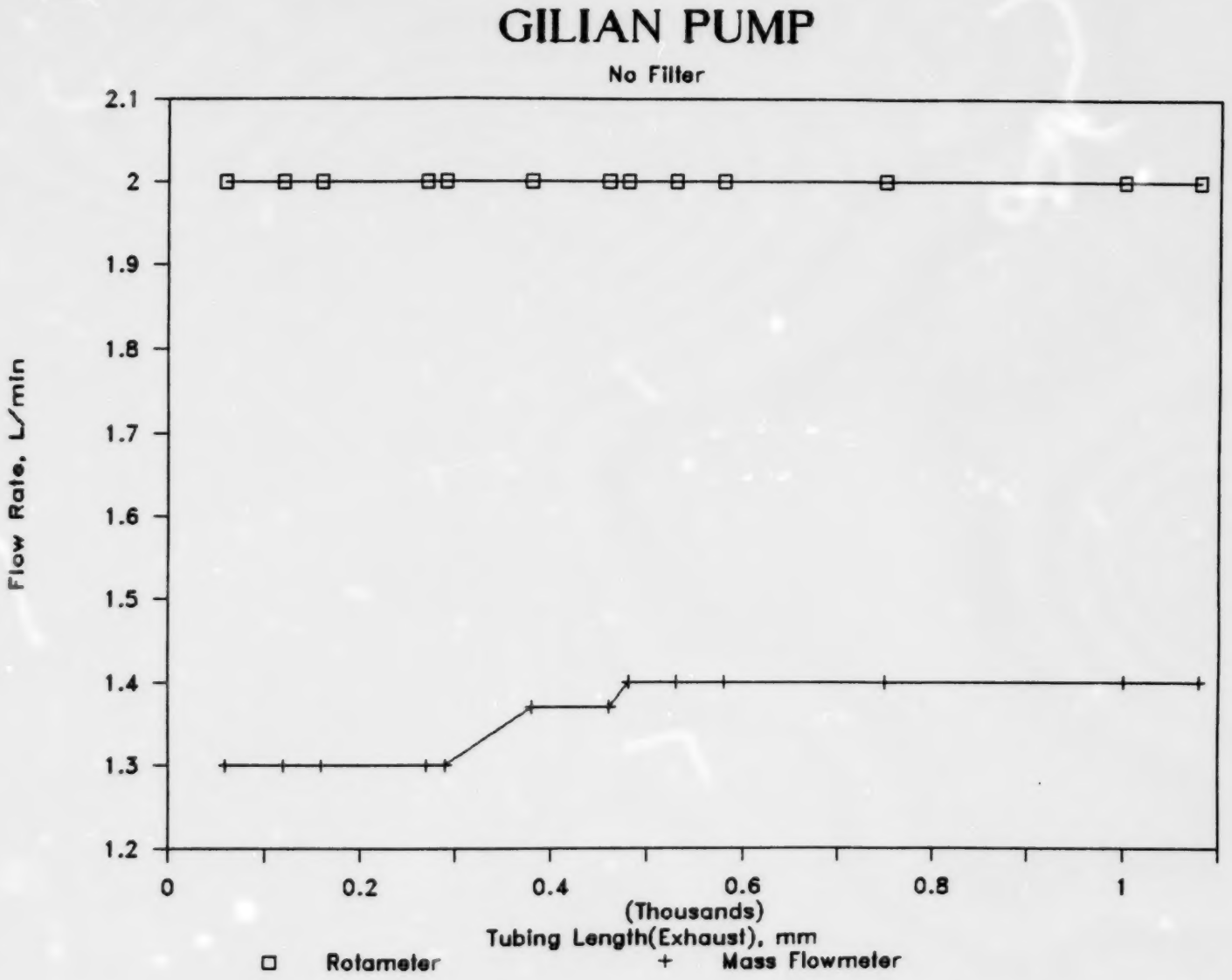

Fig. 6 - Airflow rate versus exhaust tubing length for the Gilian pump. (no filter)

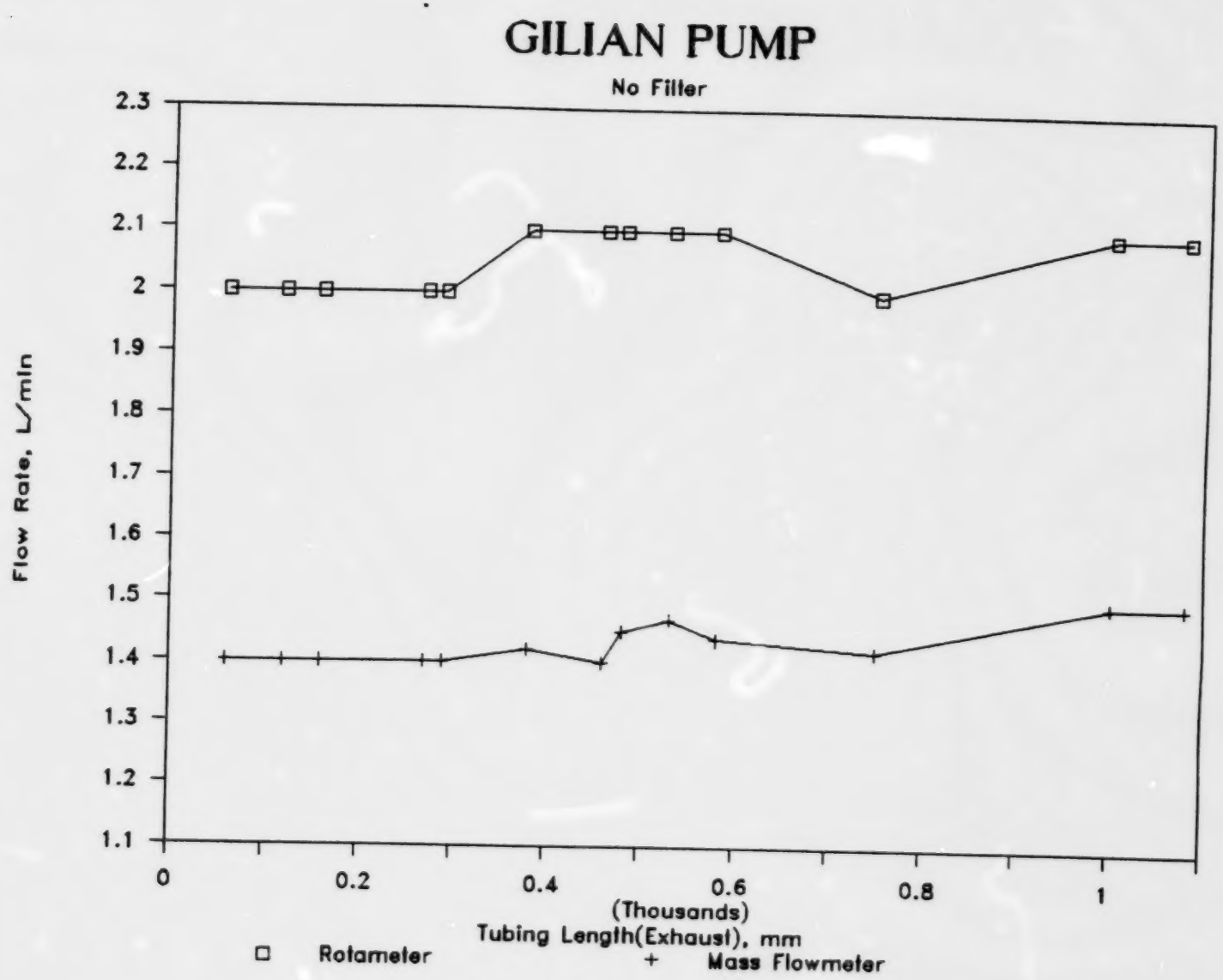

Fig. 7 - Airflow rate versus exhaust tubing length for the Gilian pump. (no filter)

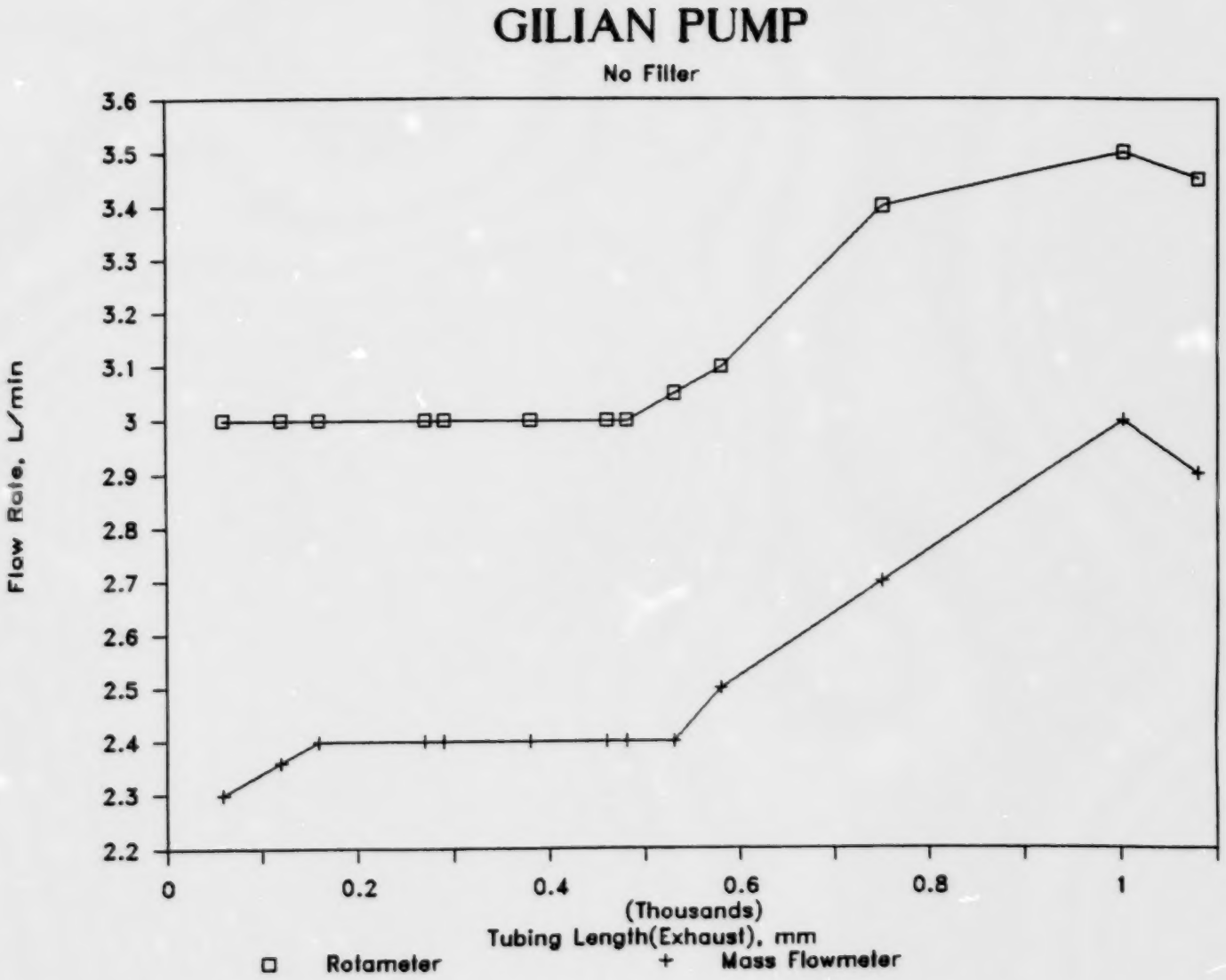

Fig. 8 - Airflow rate versus exhaust tubing length for the Gilian pump. (no filter)

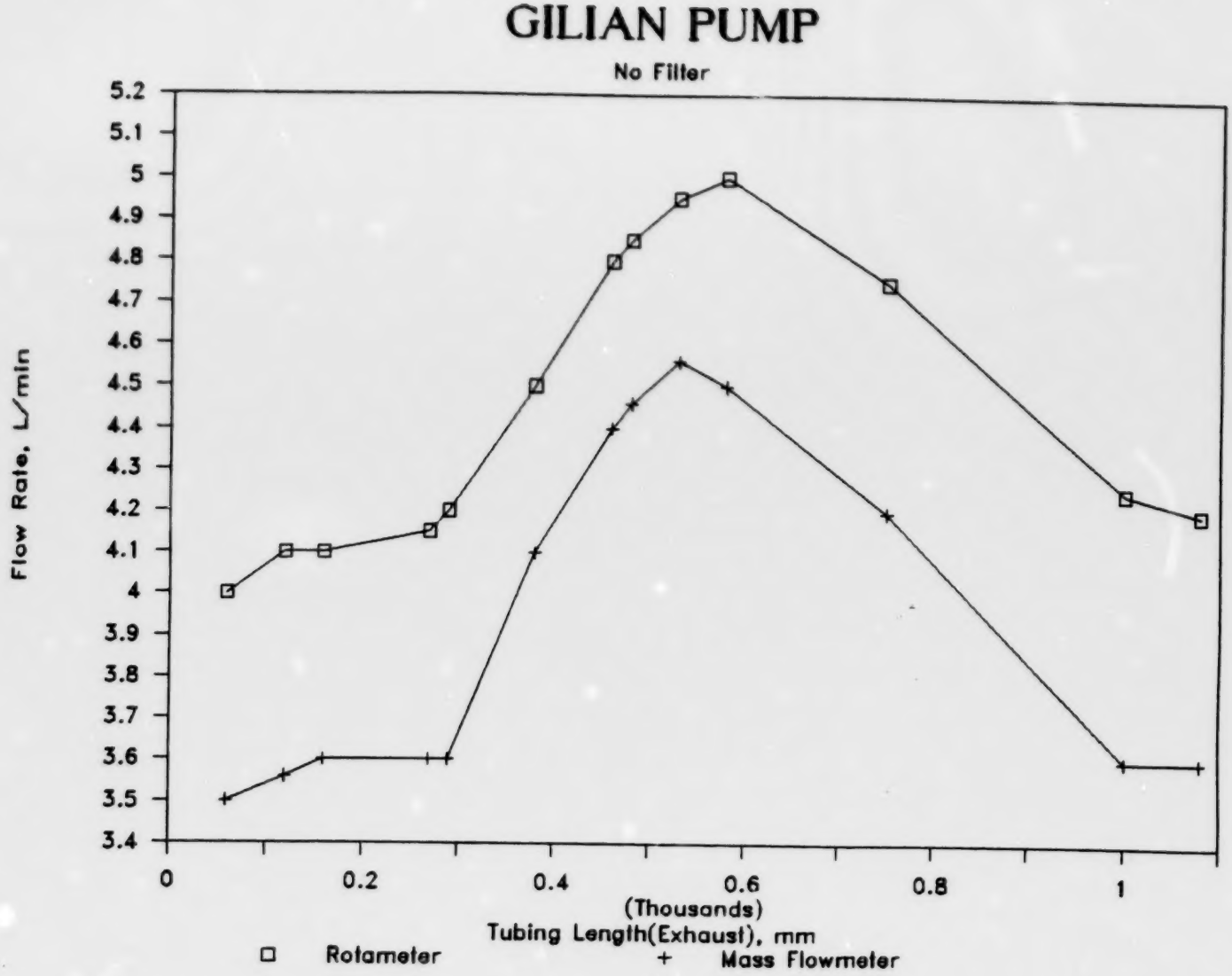

Fig. 9 - Airflow rate versus exhaust tubing length for the Gilian pump. (no filter)

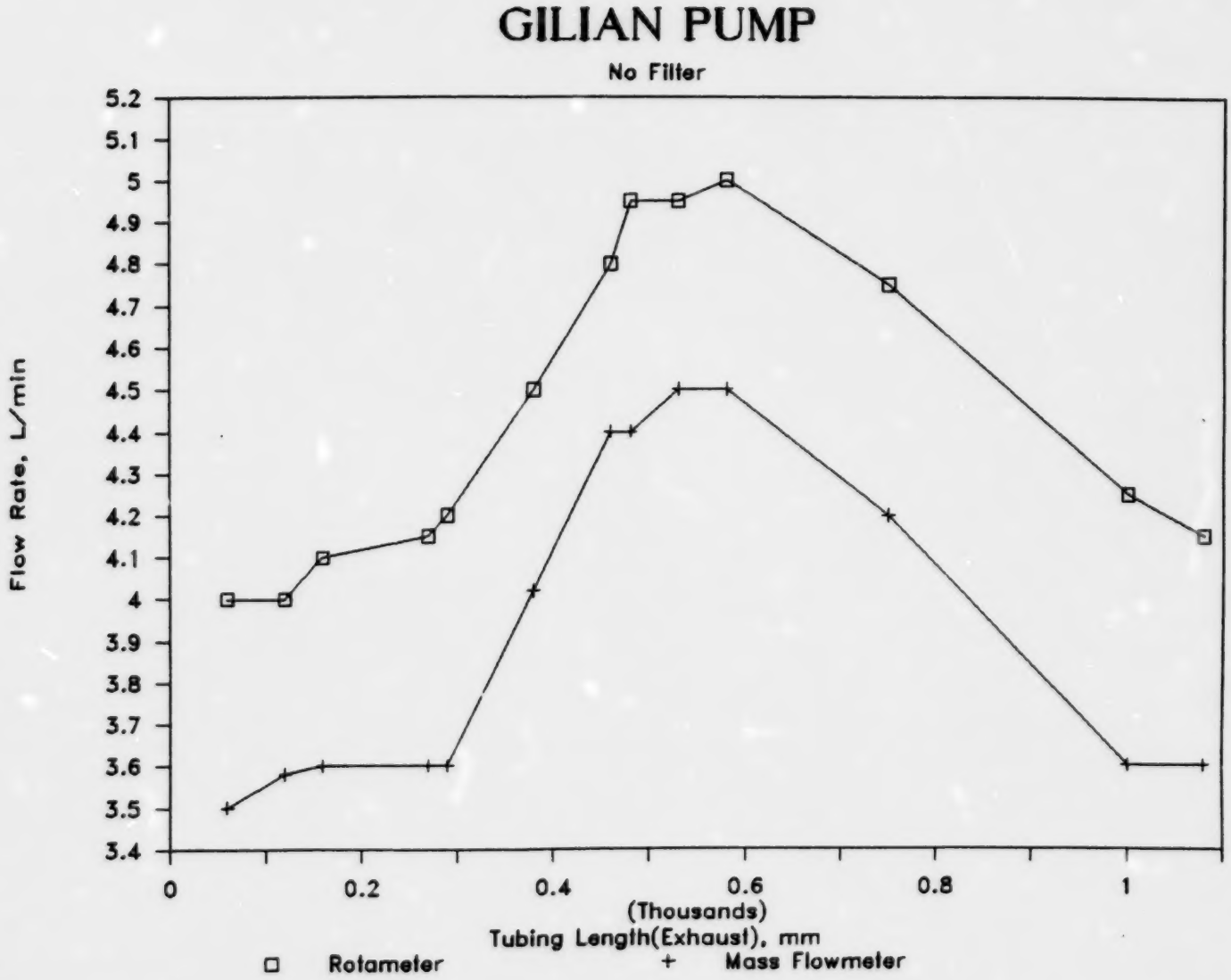

Fig. 10 - Airflow rate versus exhaust tubing length for the Gilian pump. (no filter)

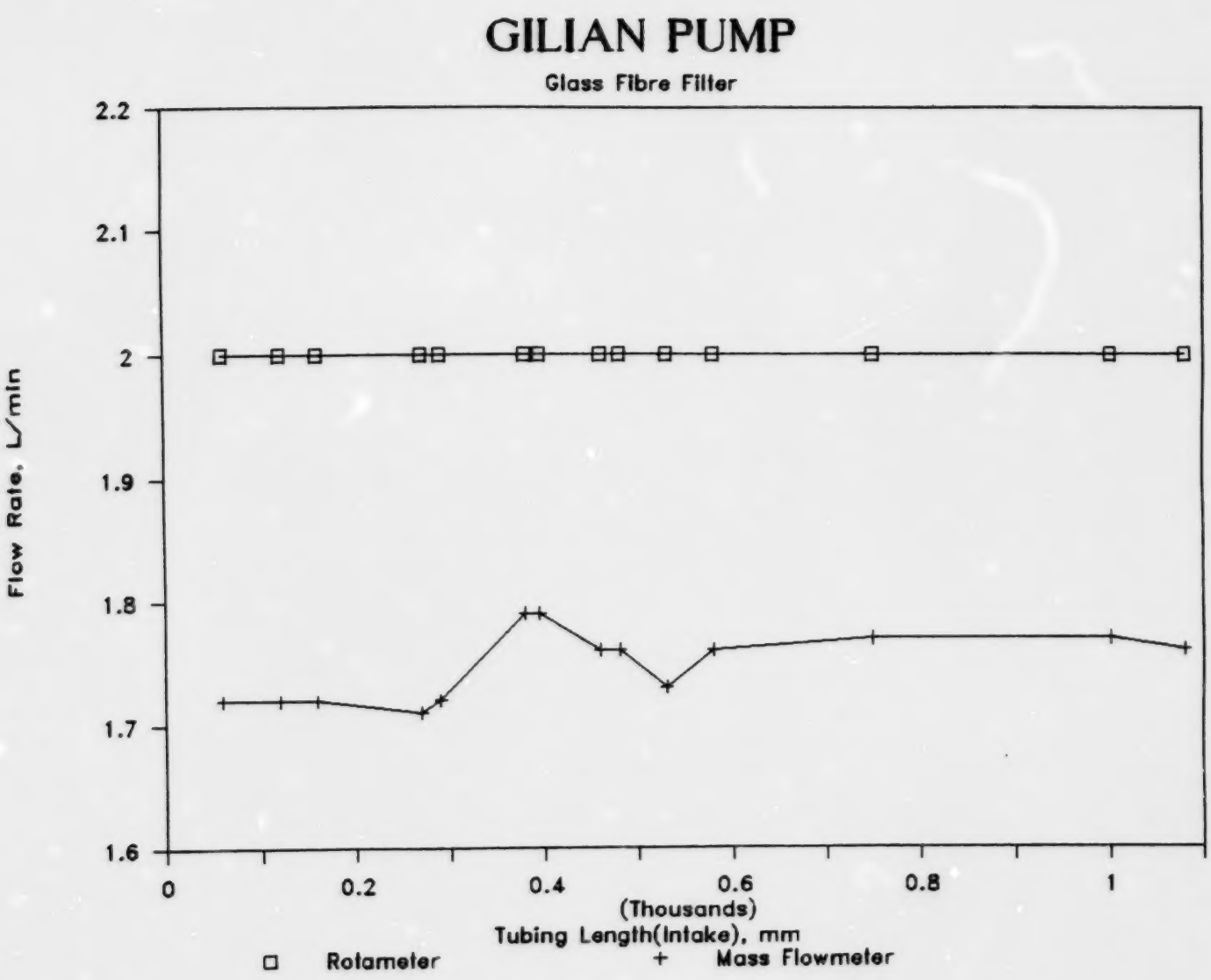

Fig. 11 - Airflow rate versus intake tubing length for the Gilian pump. (Glass fibre filter)

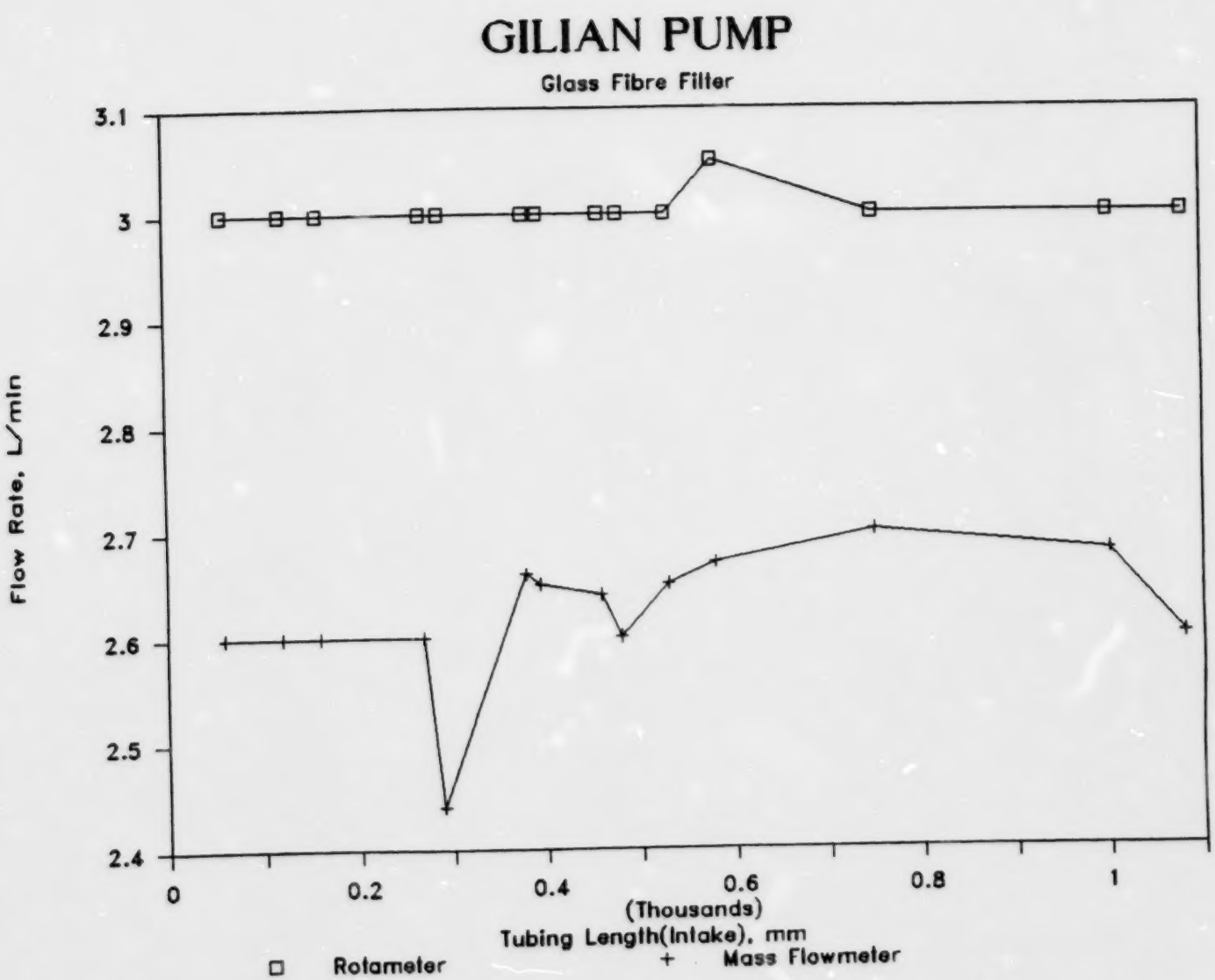

Fig. 12 - Airflow rate versus intake tubing length for the Gilian pump. (Glass fibre filter)

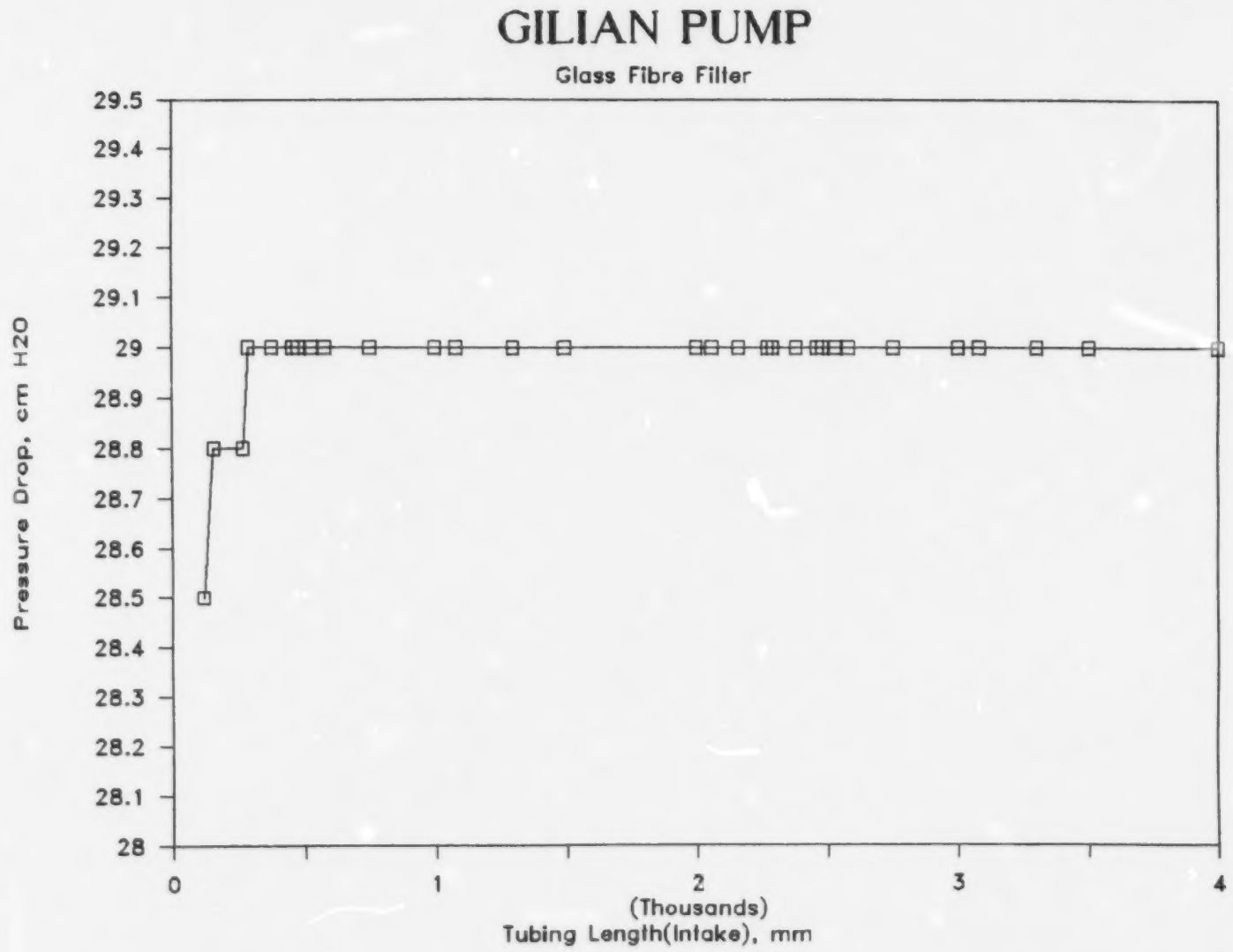

Fig. 13 - Pressure drop across the filter versus intake tubing length. (Glass fibre filter)

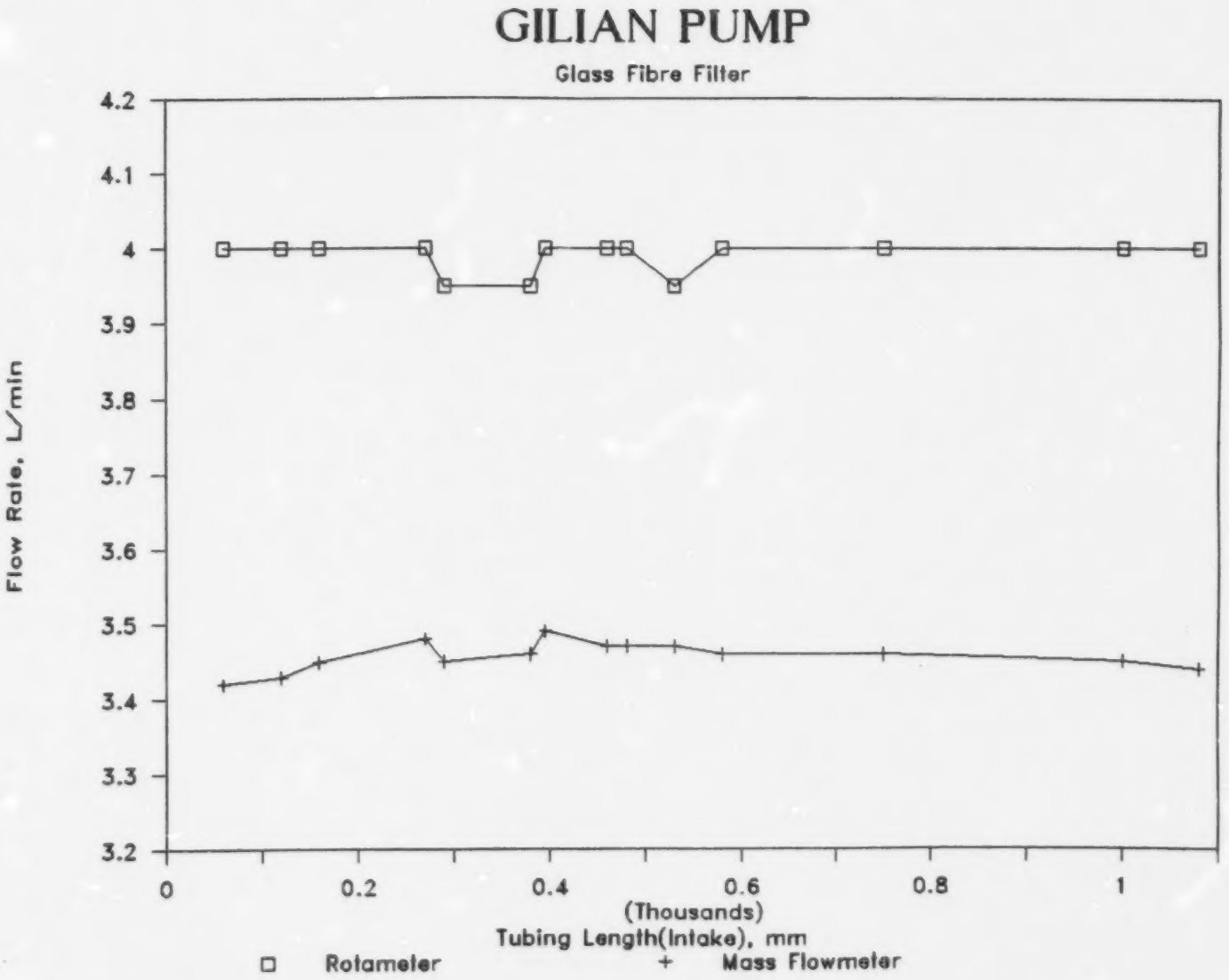

Fig. 14 - Airflow rate versus intake tubing length for the Gilian pump. (Glass fibre filter)

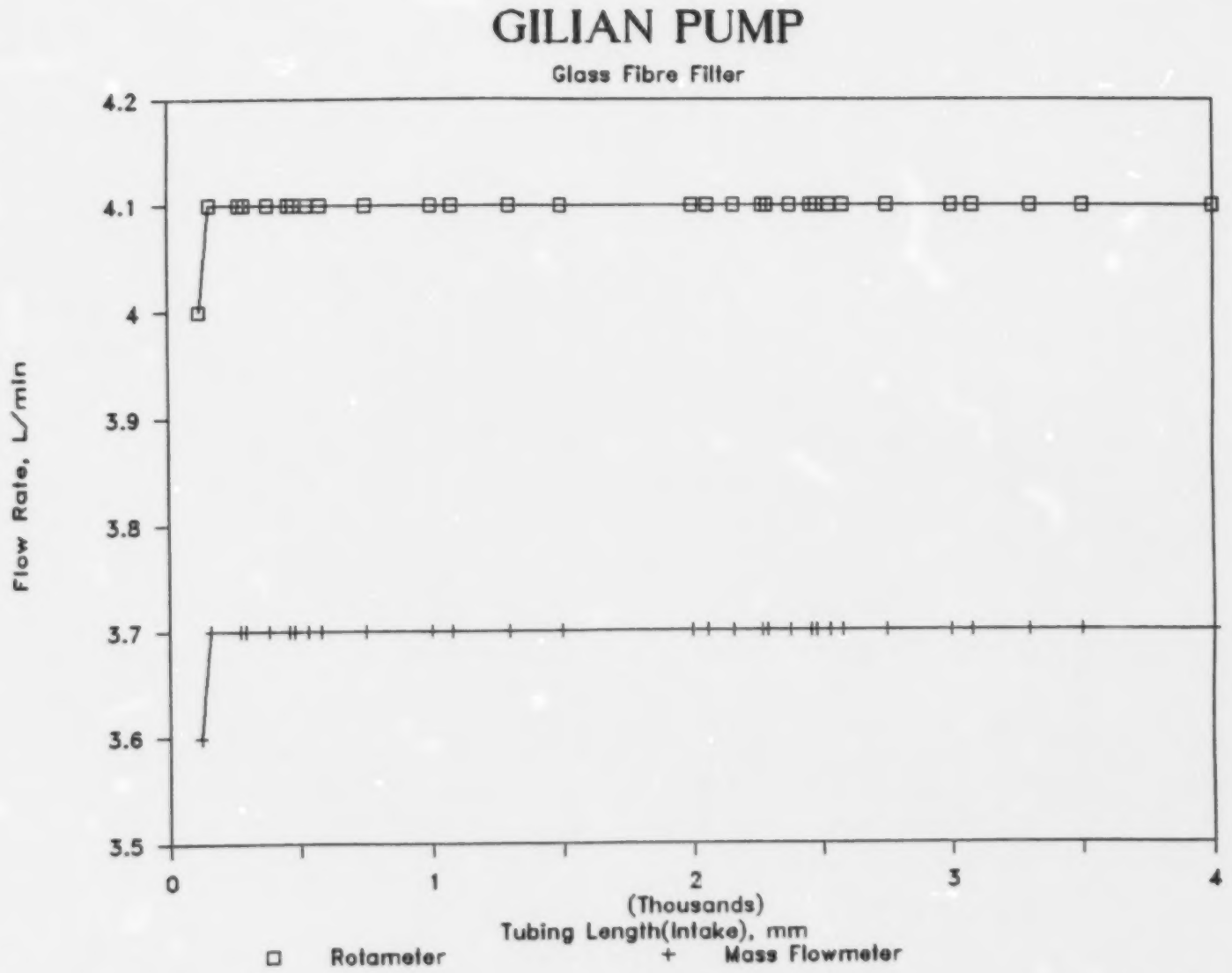

Fig. 15 - Airflow rate versus intake tubing length for the Gilian pump. (Glass fibre filter)

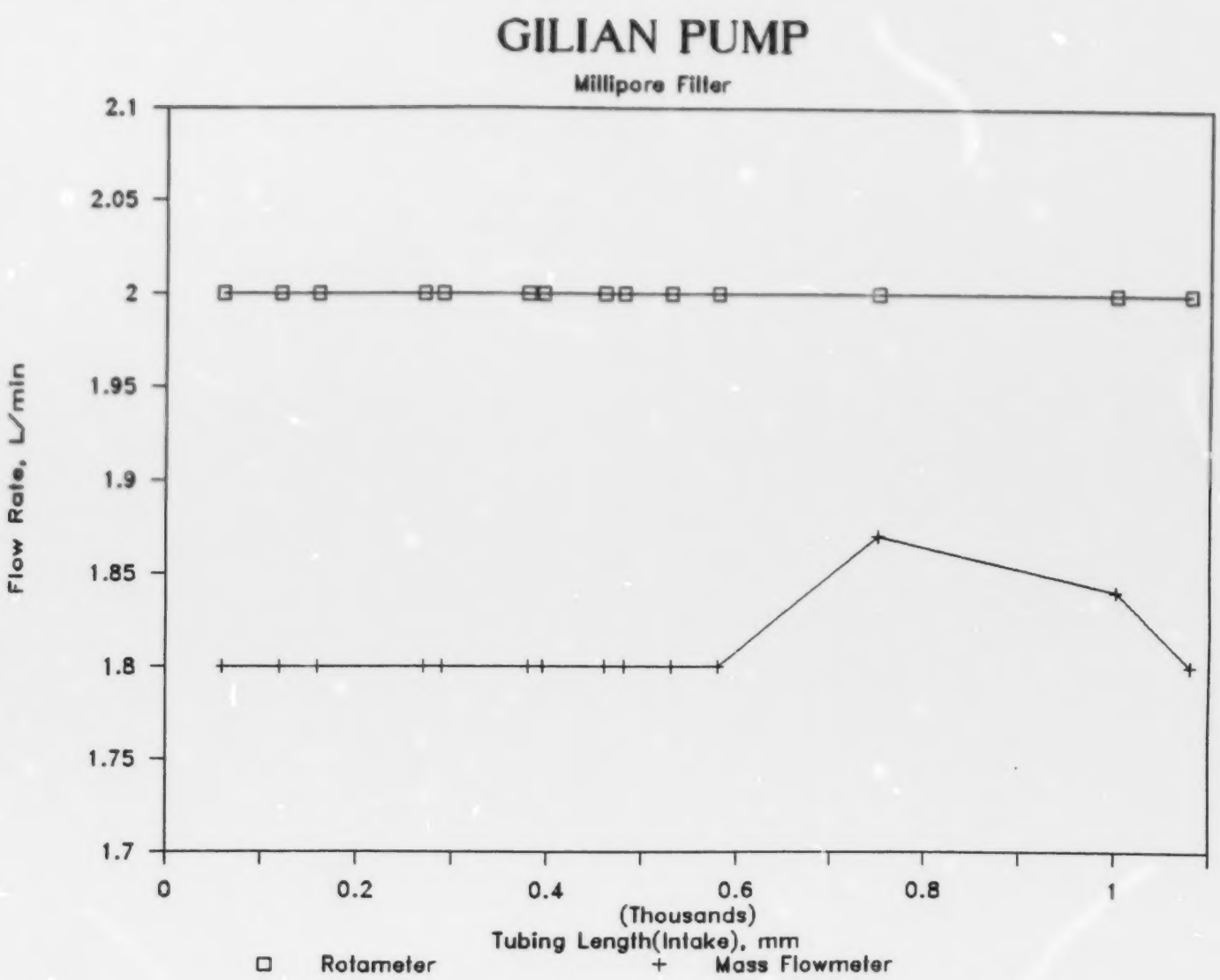

Fig. 16 - Airflow rate versus intake tubing length for the Gilian pump. (Millipore filter)

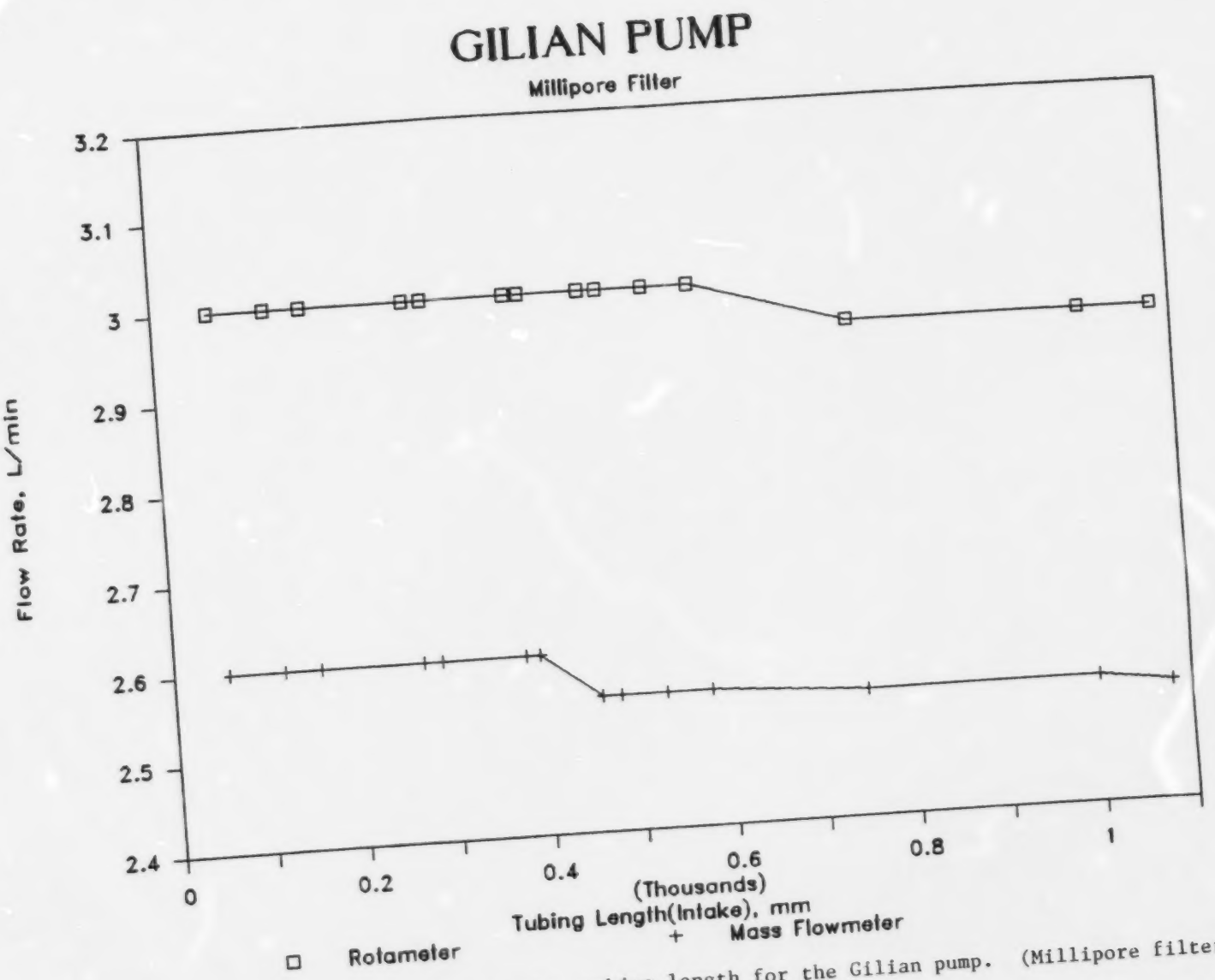

Fig. 17 - Airflow rate versus intake tubing length for the Gilian pump. (Millipore filter)

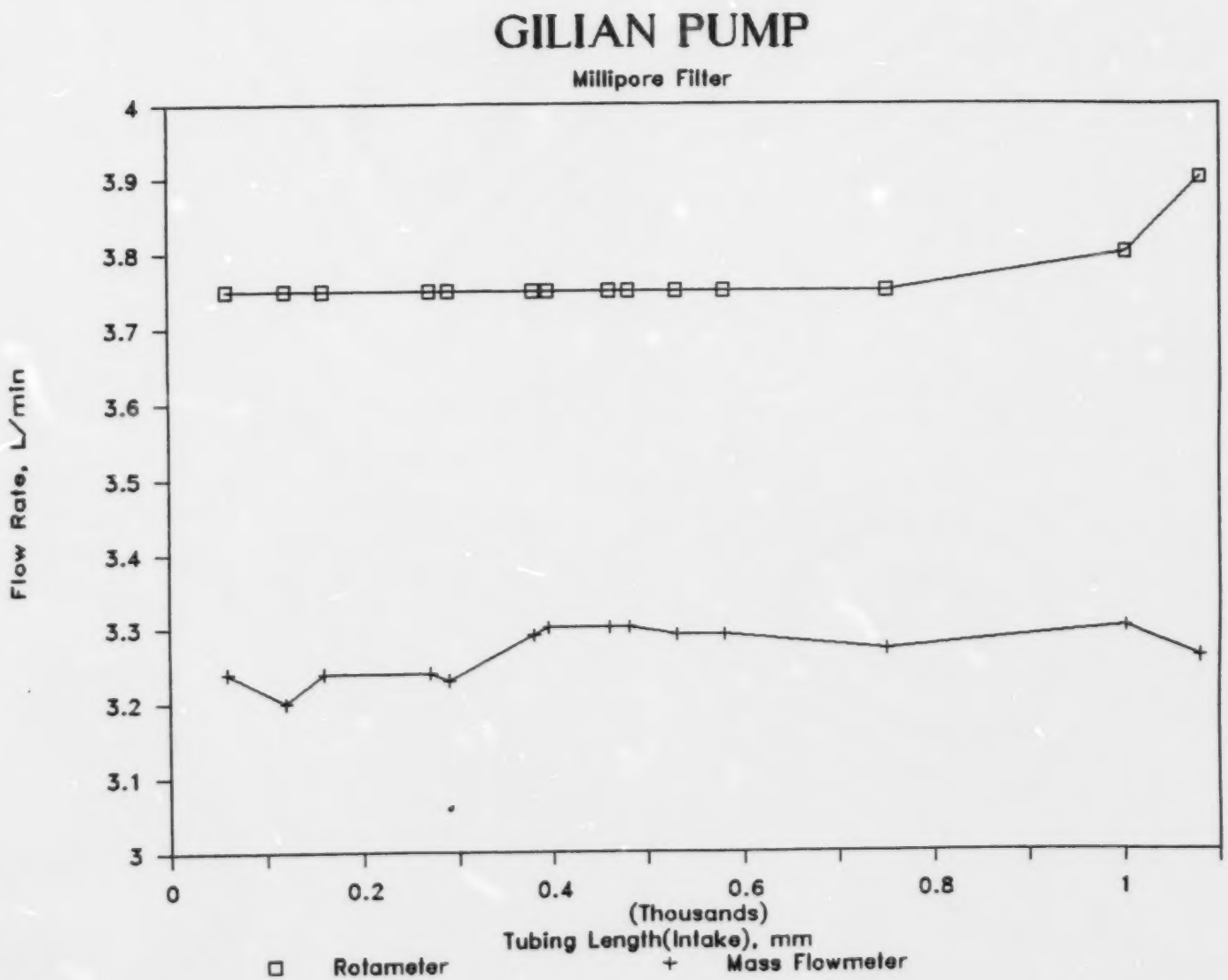

Fig. 18 - Airflow rate versus intake tubing length for the Gilian pump. (Millipore filter)

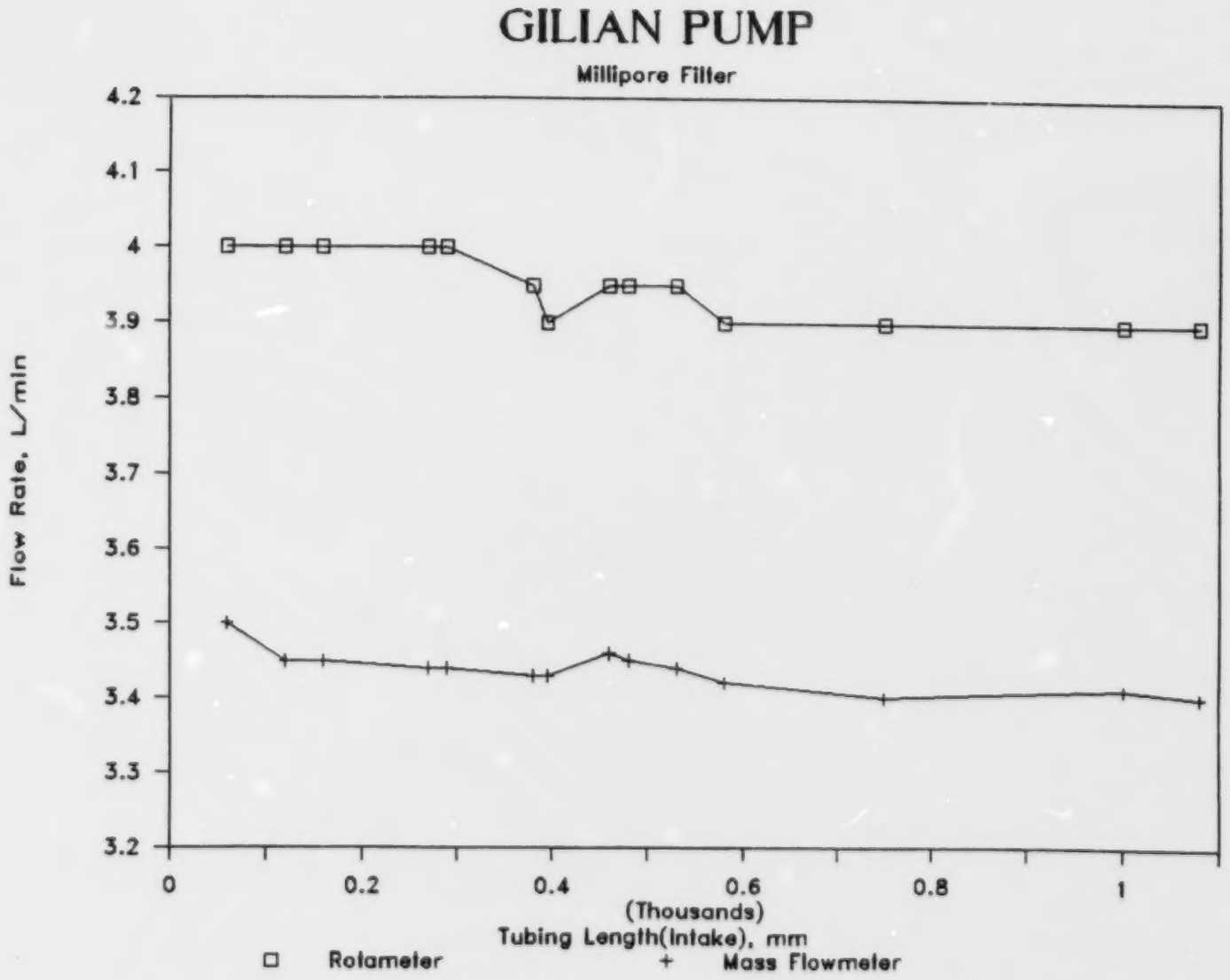

Fig. 19 - Airflow rate versus intake tubing length for the Gilian pump. (Millipore filter)

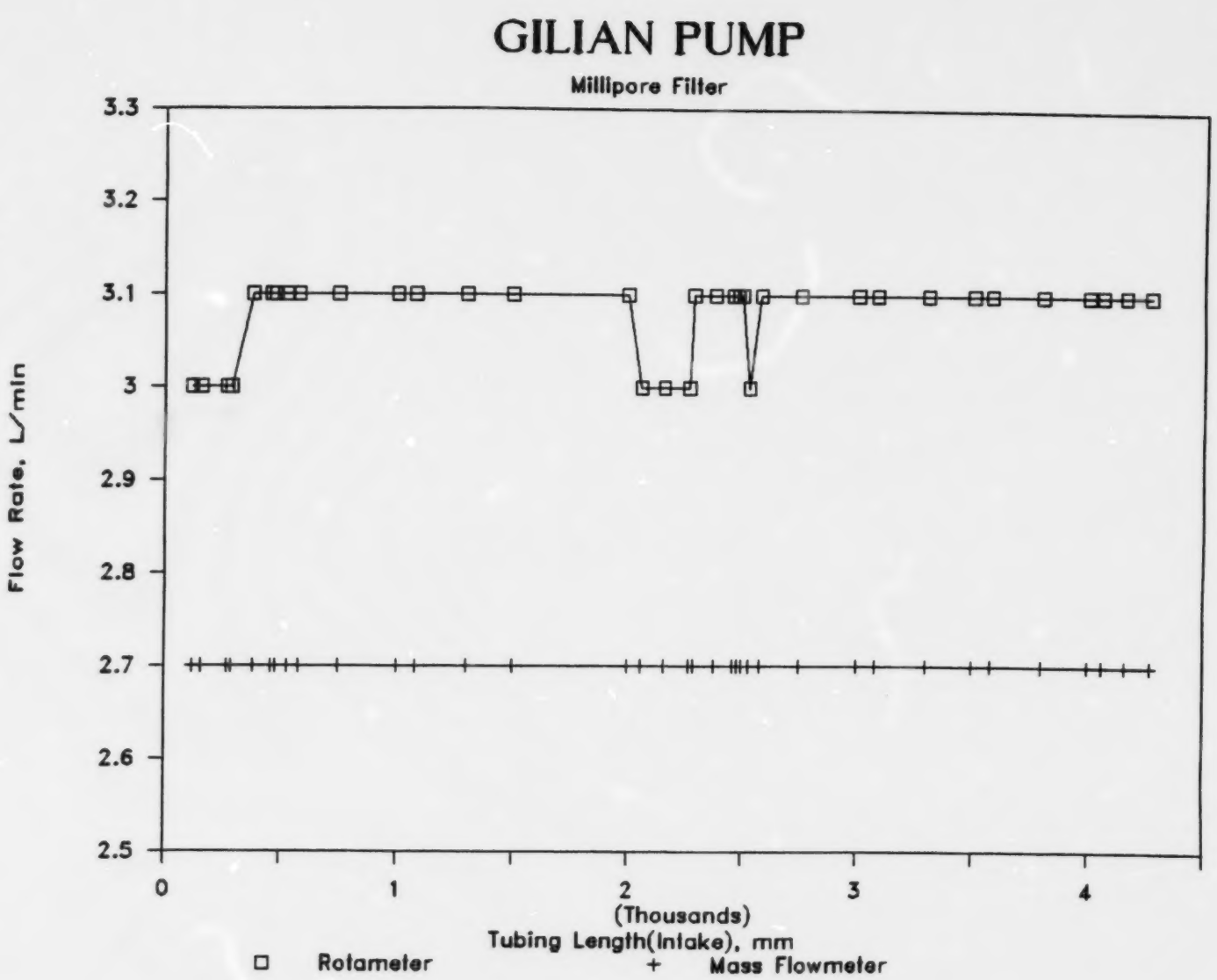

Fig. 20 - Airflow rate versus intake tubing length for the Gilian pump. (Millipore filter)

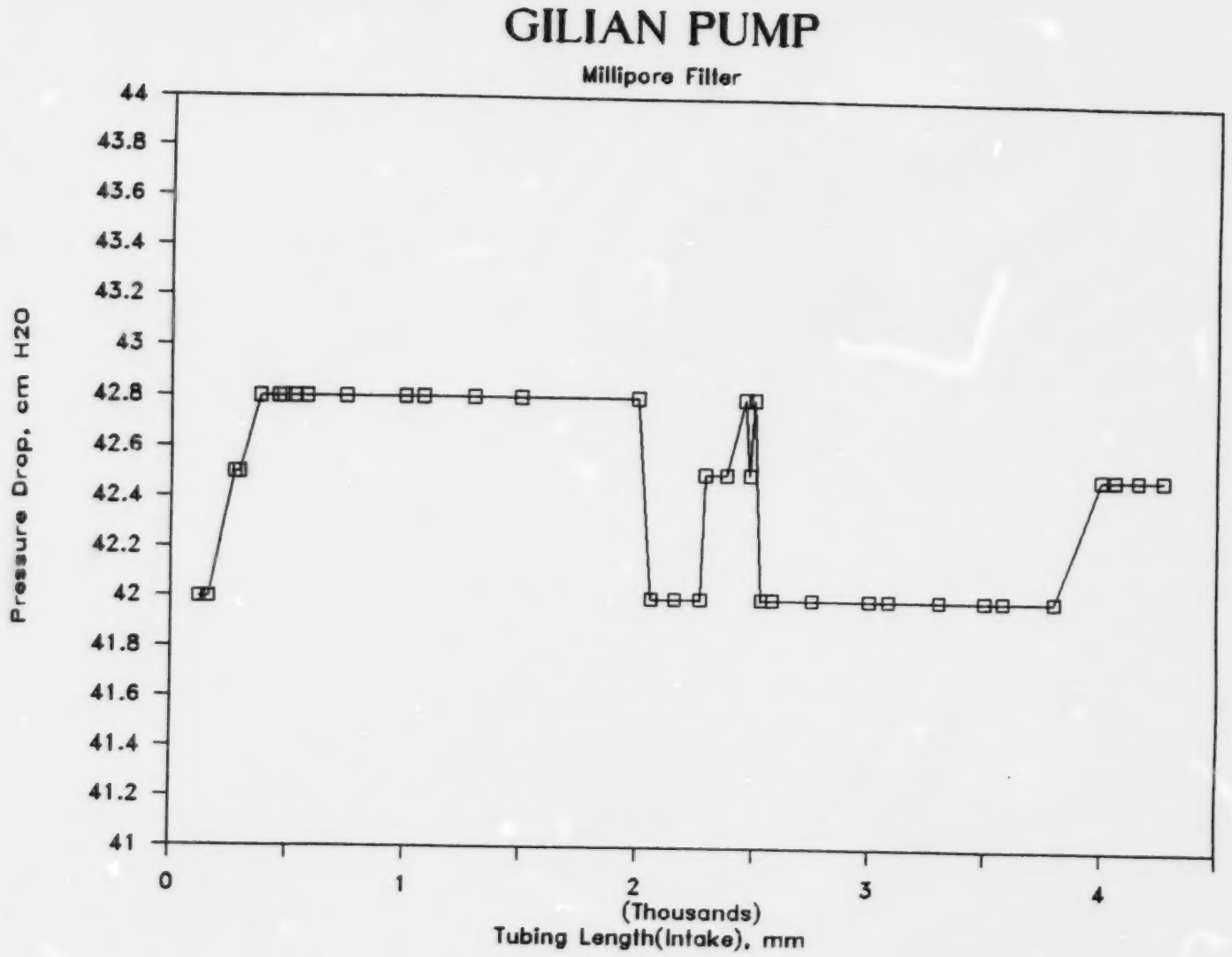

Fig. 21 - Pressure drop across the filter versus intake tubing length for the Gilian pump. (Millipore filter)

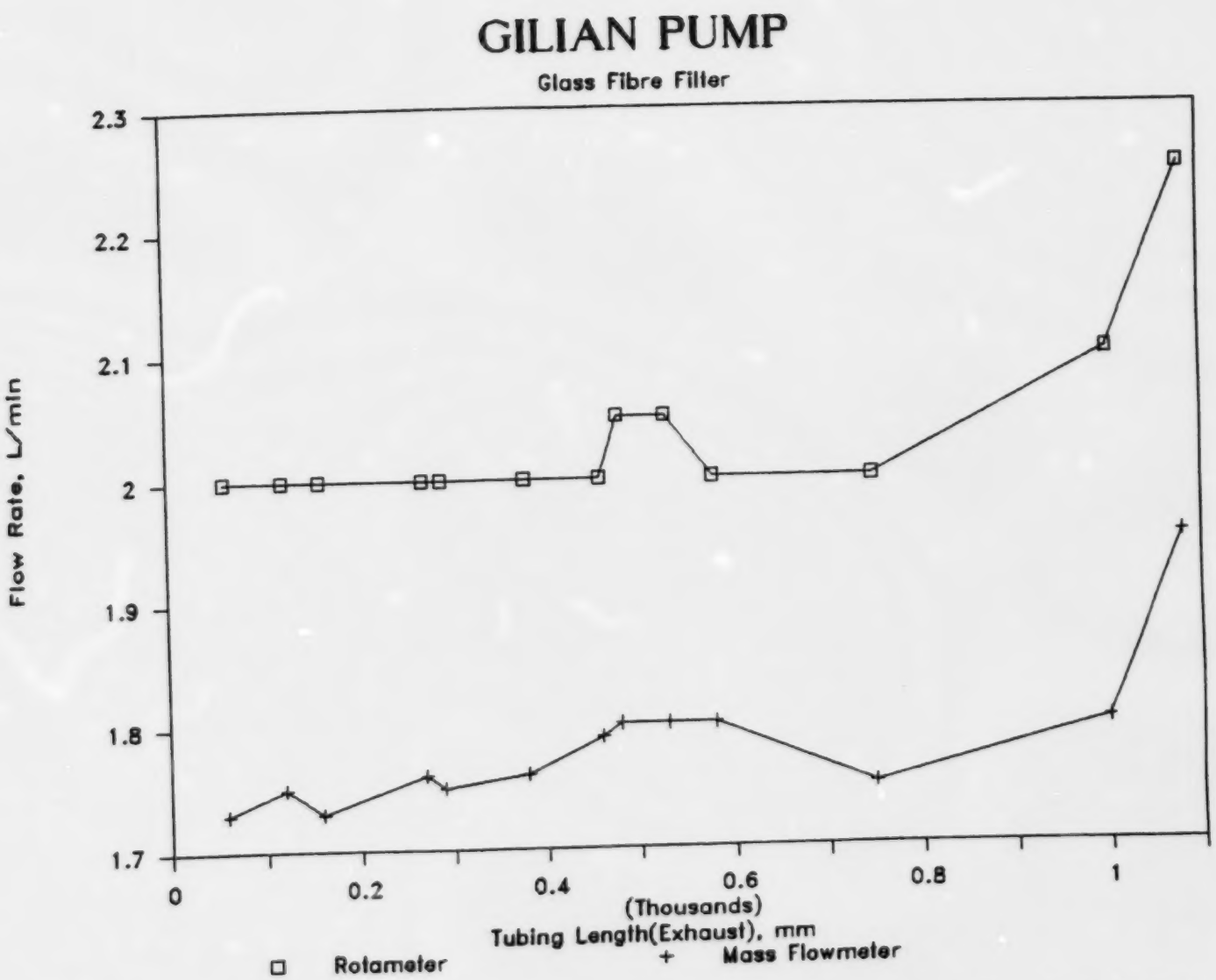

Fig. 22 - Airflow rate versus exhaust tubing length for the Gilian pump. (Glass fibre filter)

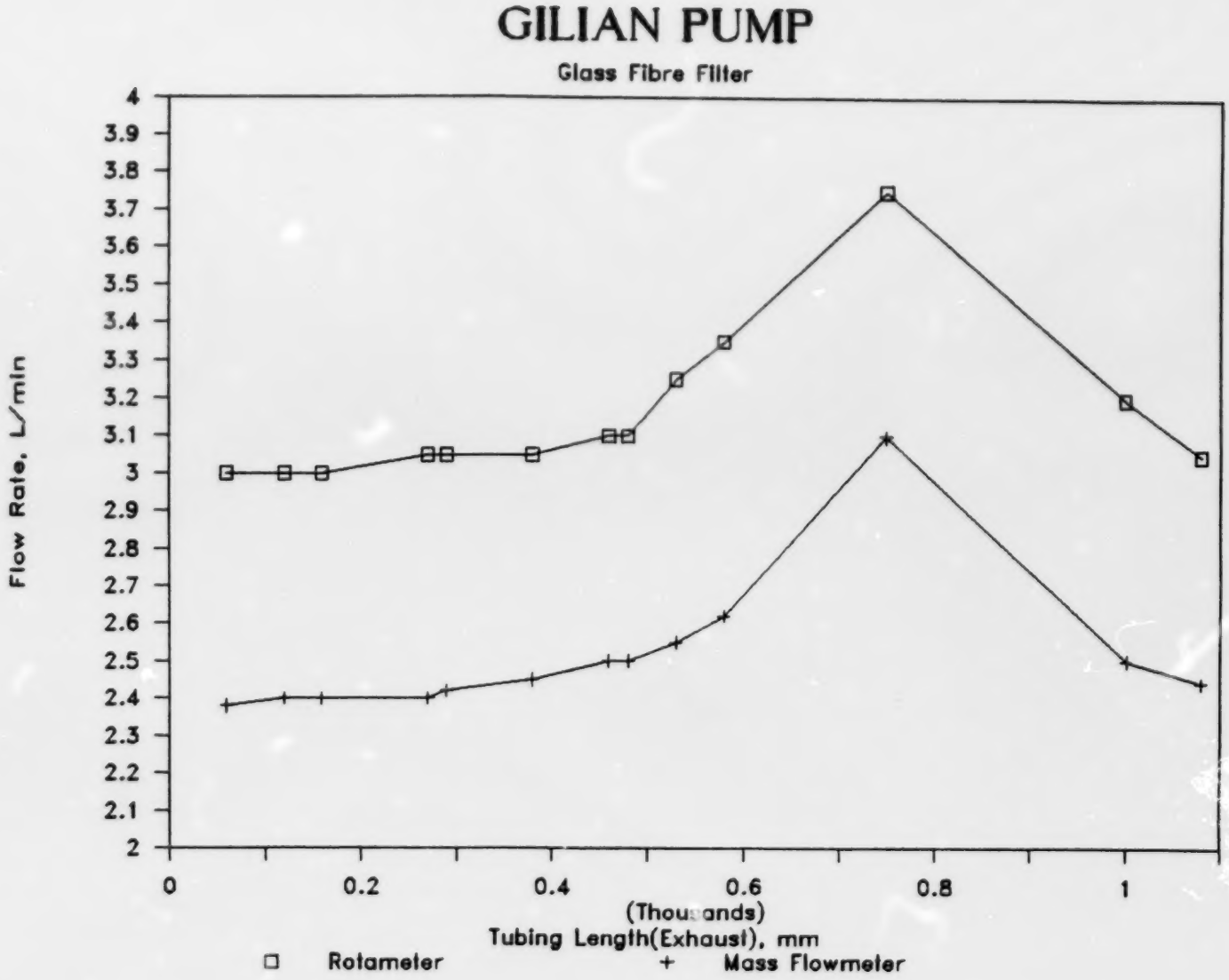

Fig. 23 - Airflow rate versus exhaust tubing length for the Gilian pump. (Glass fibre filter)

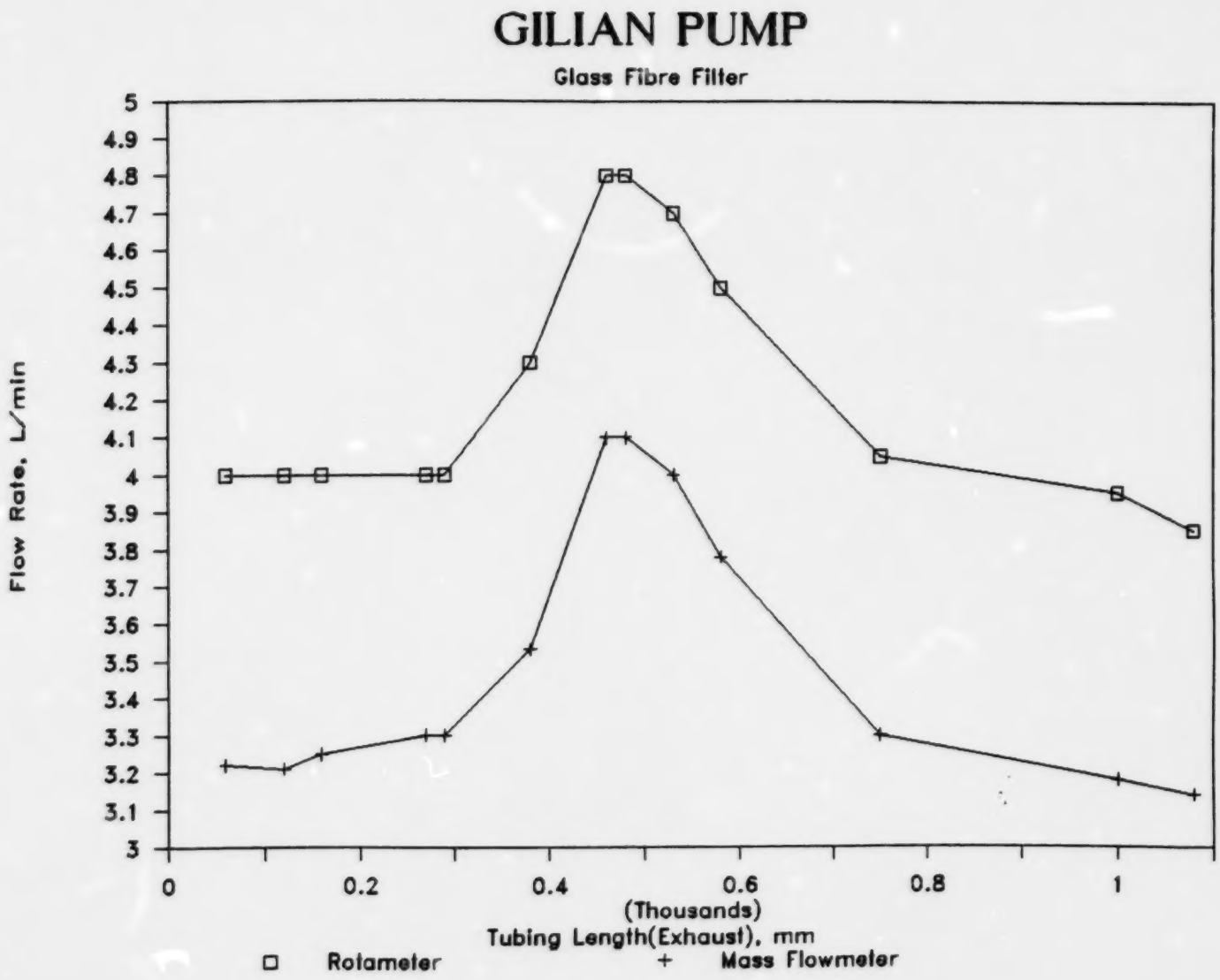

Fig. 24 - Airflow rate versus exhaust tubing length for the Gilian pump. (Glass fibre filter)

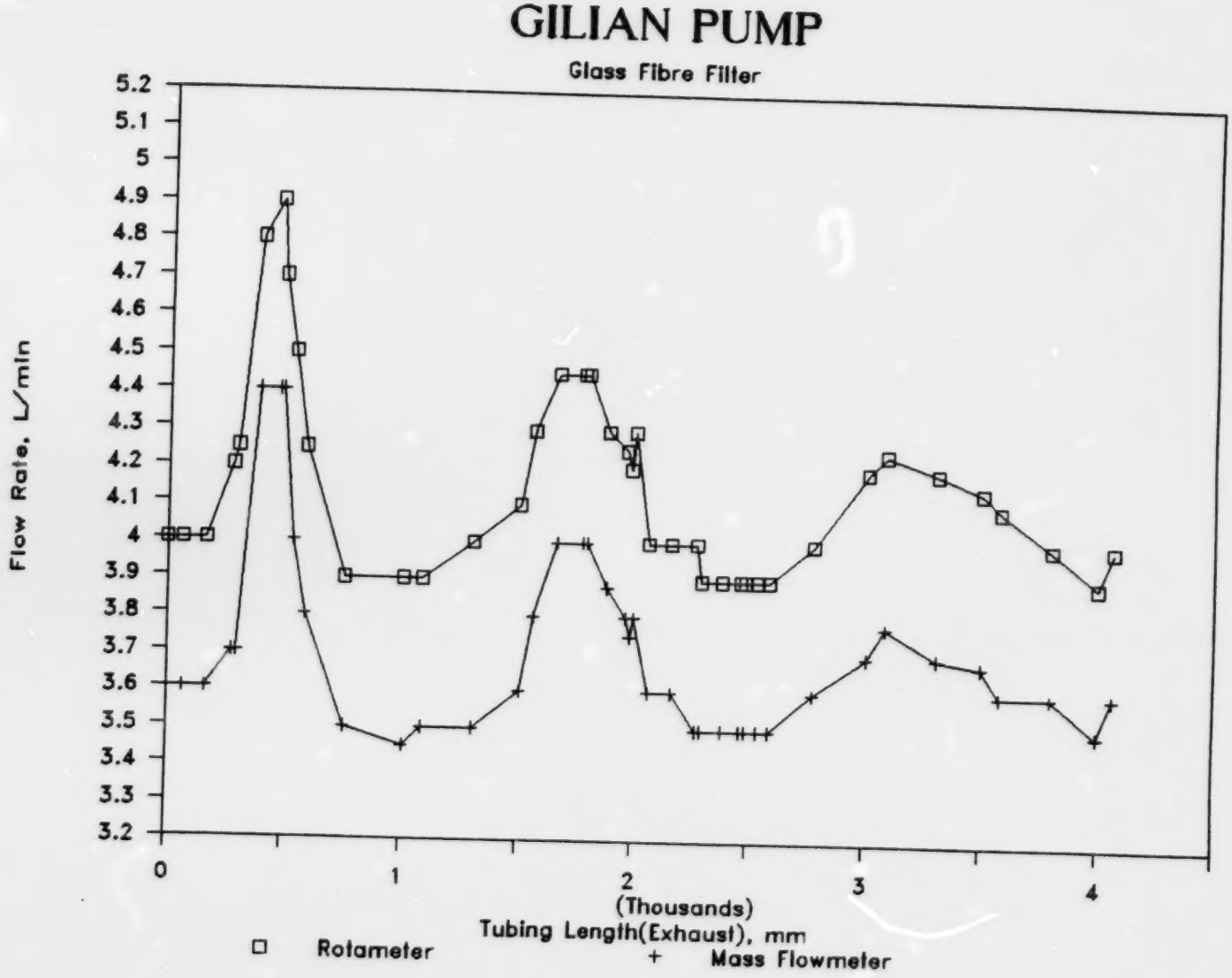

Fig. 25 - Airflow rate versus exhaust tubing length for the Gilian pump. (Glass fibre filter)

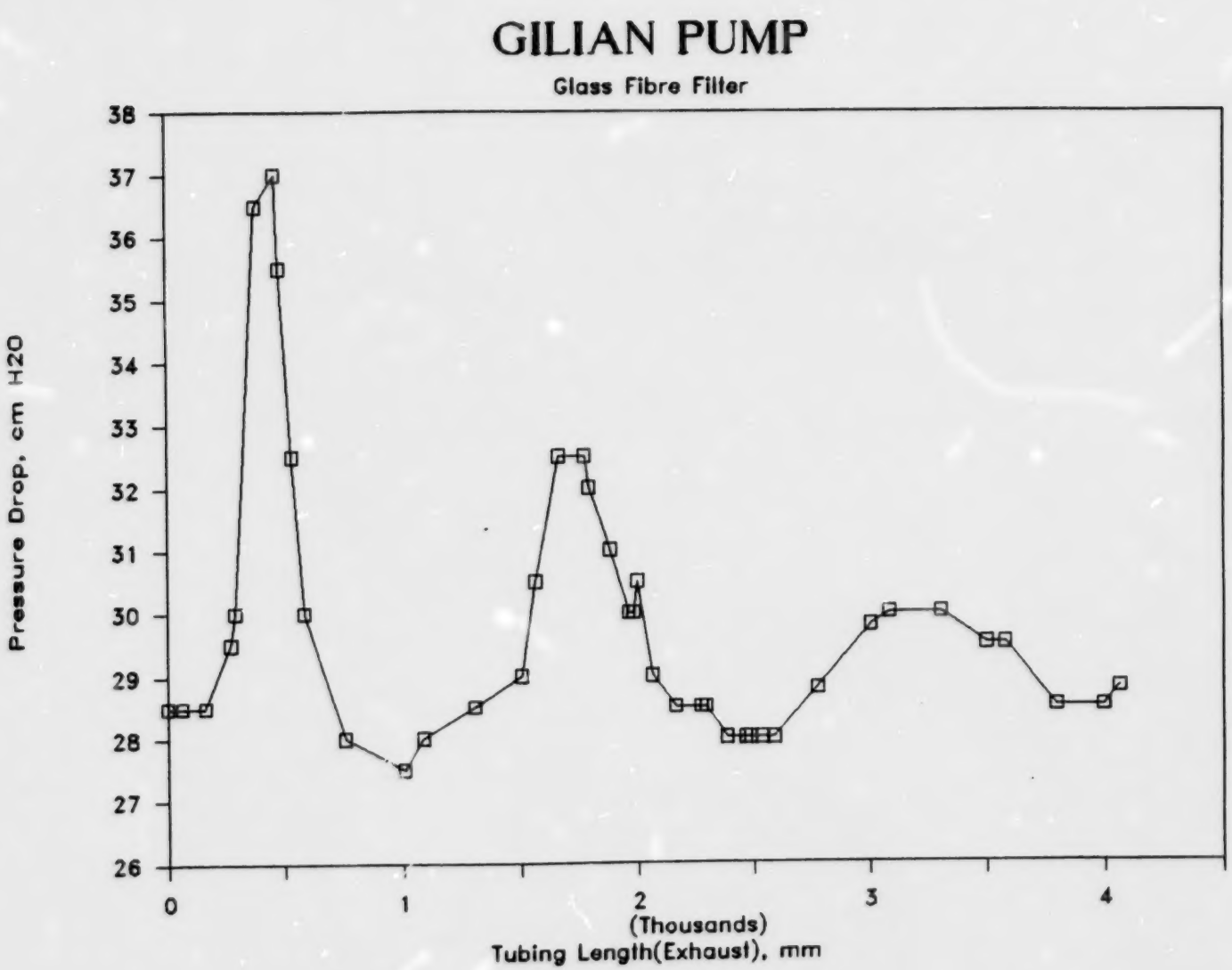

Fig. 26 - Pressure drop across the filter versus exhaust tubing length for the Gilian pump. (Glass fibre filter)

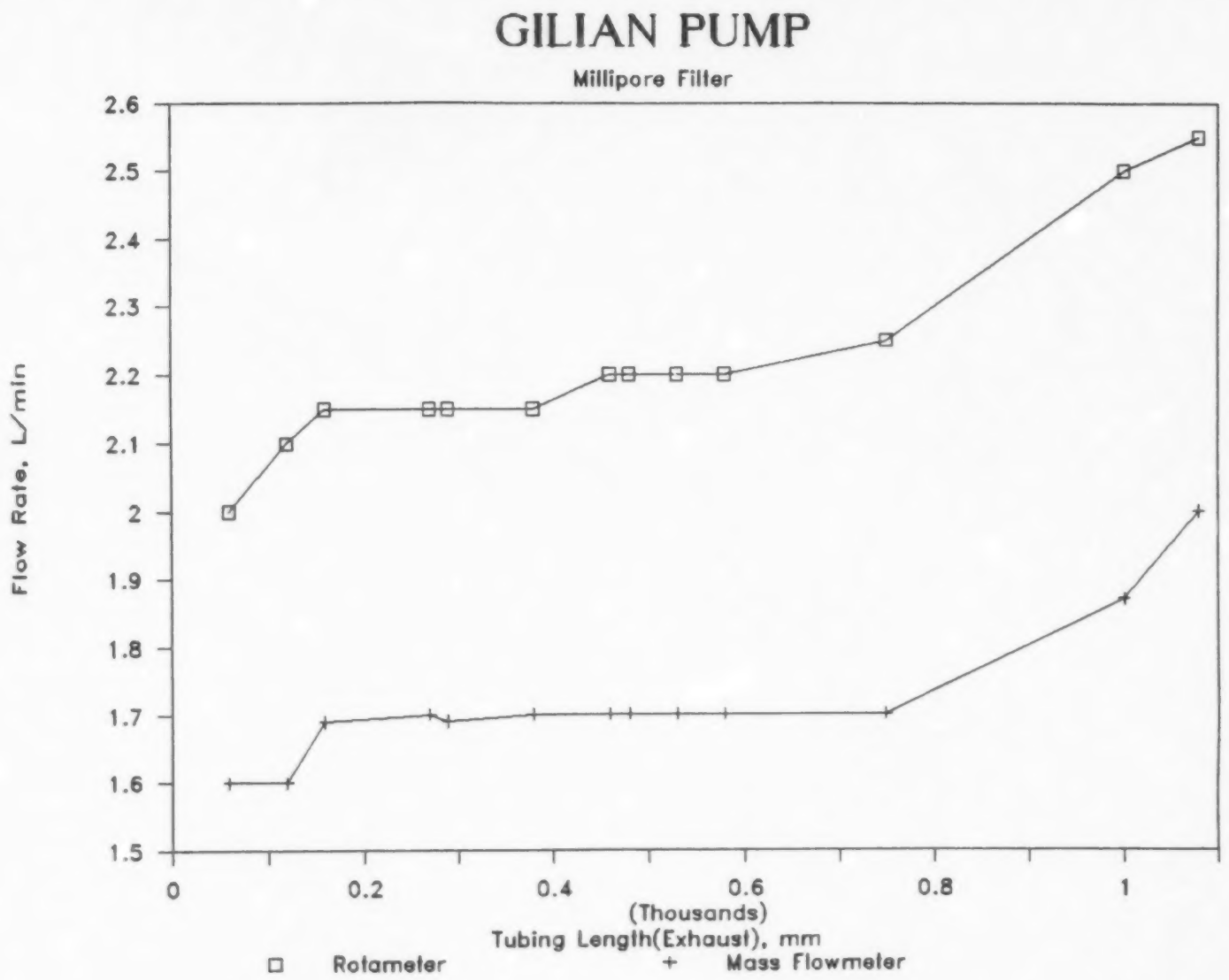

Fig. 27 - Airflow rate versus exhaust tubing length for the Gilian pump. (Millipore filter)

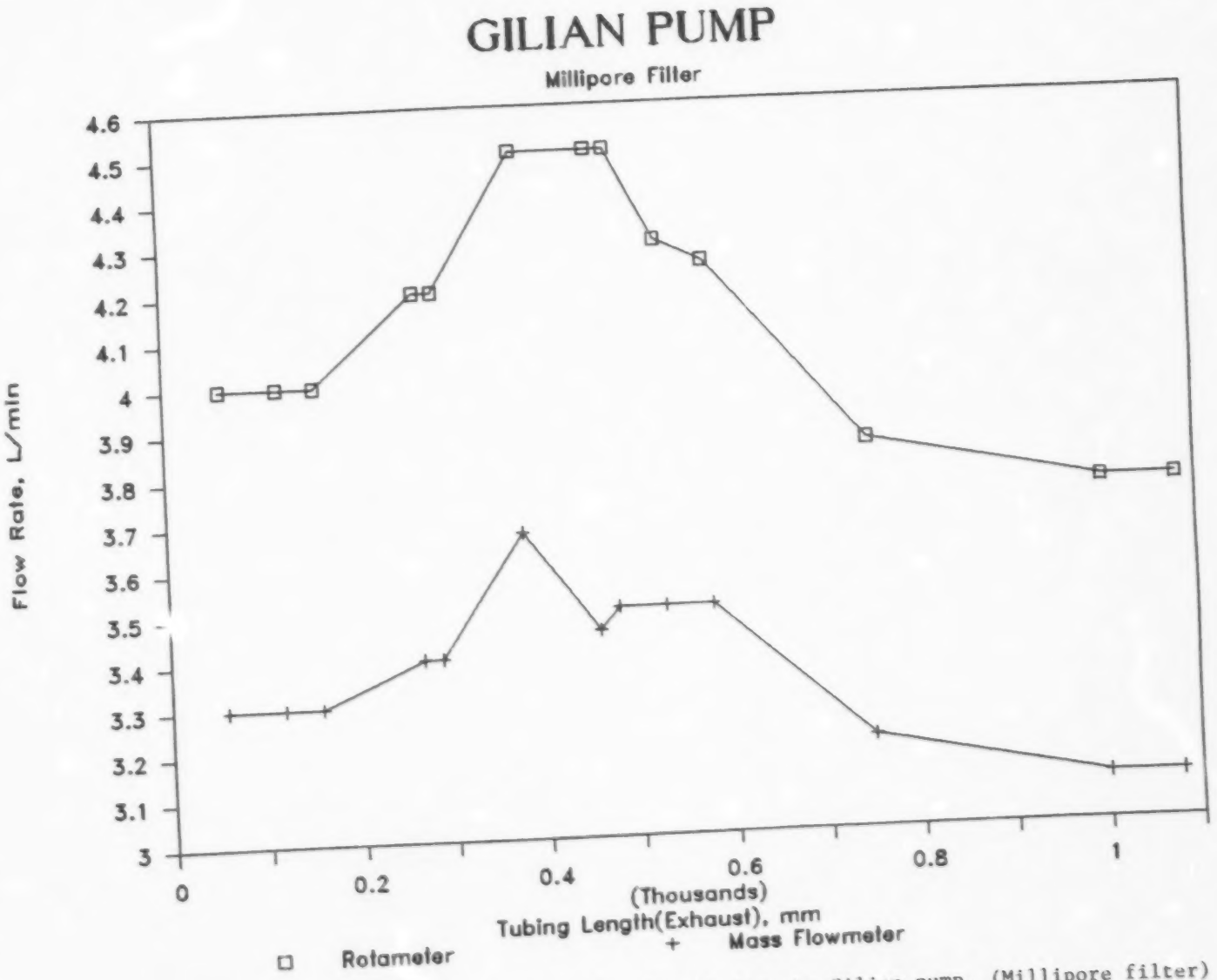

Fig. 28 - Airflow rate versus exhaust tubing length for the Gilian pump. (Millipore filter)

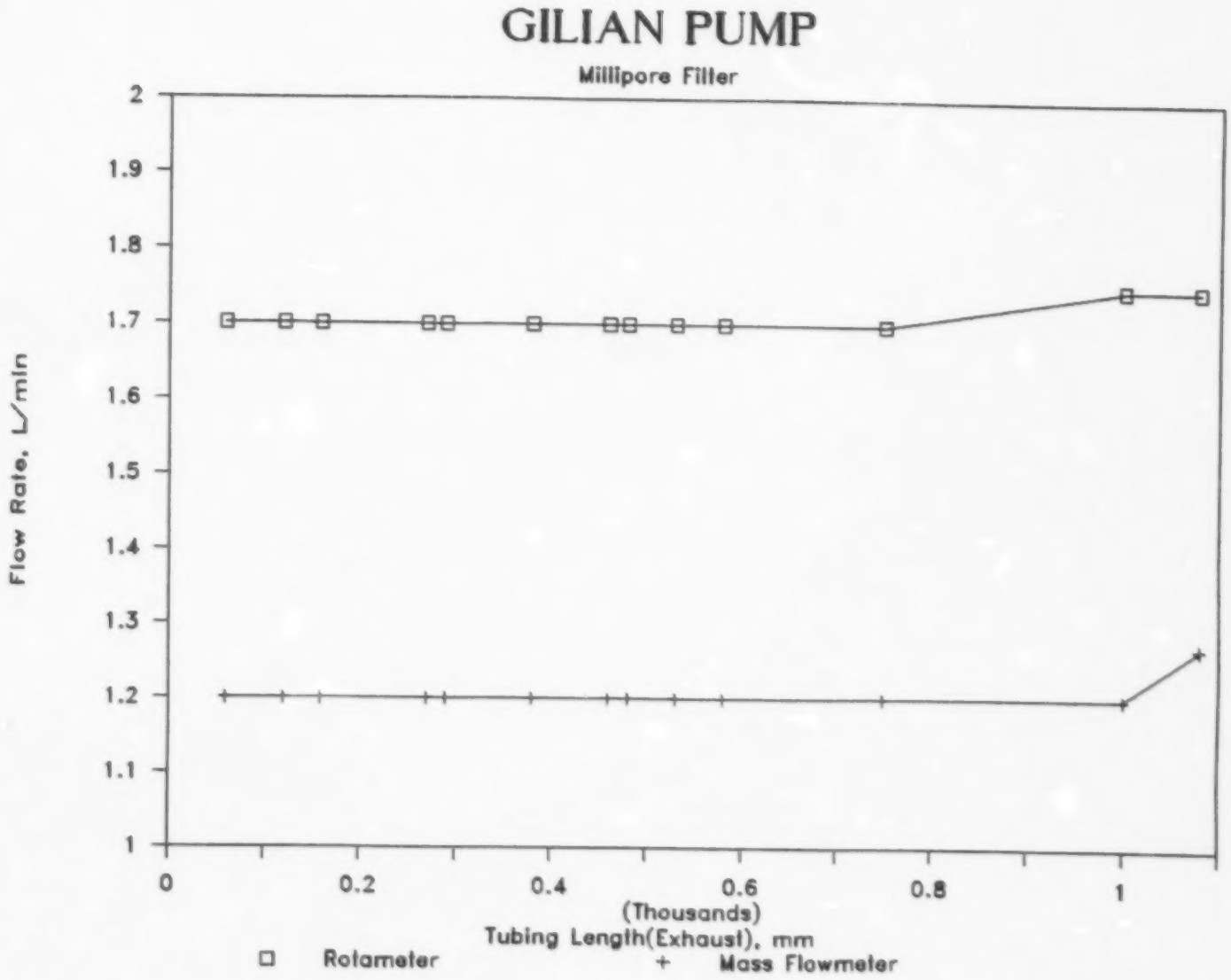

Fig. 29 - Airflow rate versus exhaust tubing length for the Gilian pump. (Millipore filter)

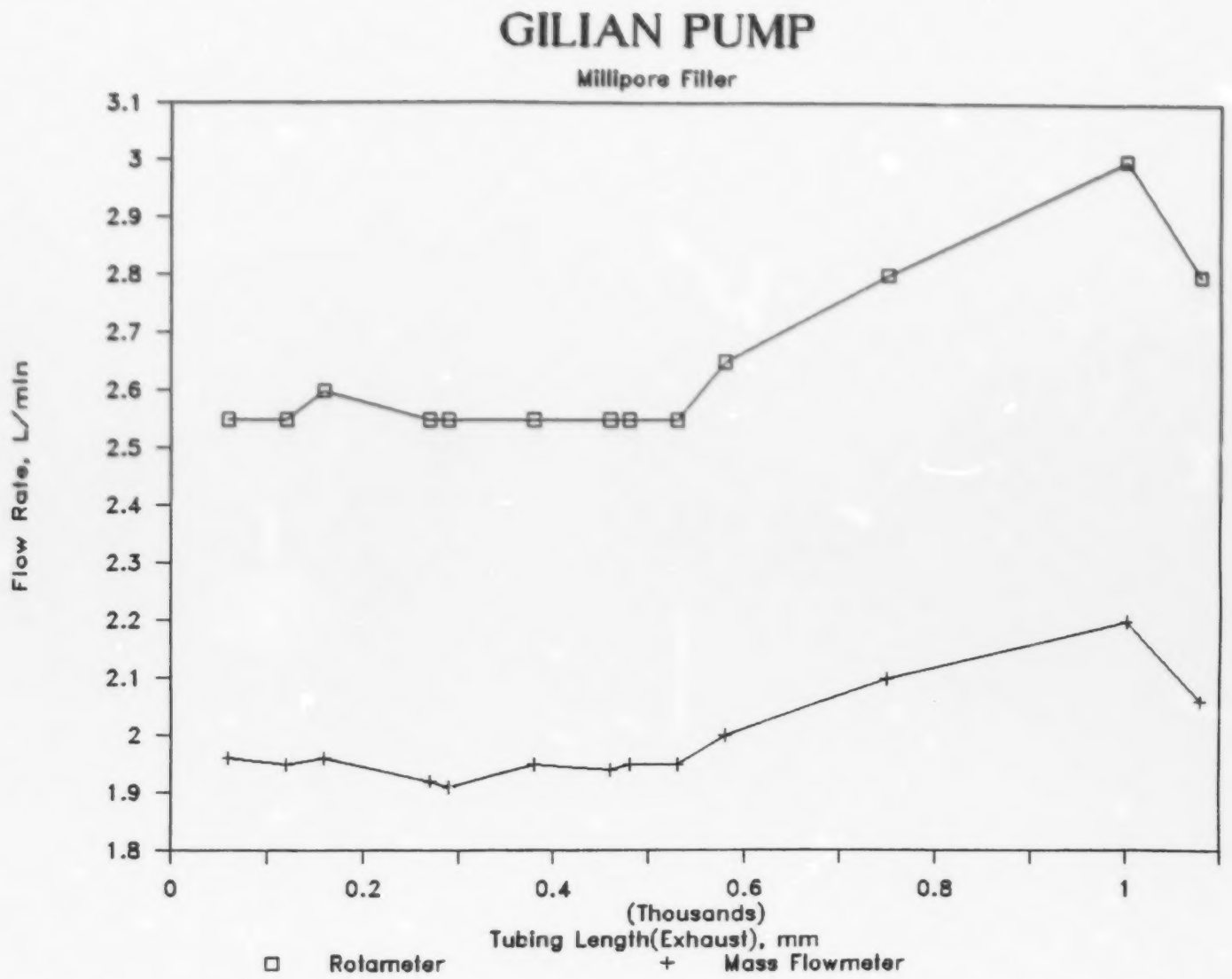

Fig. 30 - Airflow rate versus exhaust tubing length for the Gilian pump. (Millipore filter)

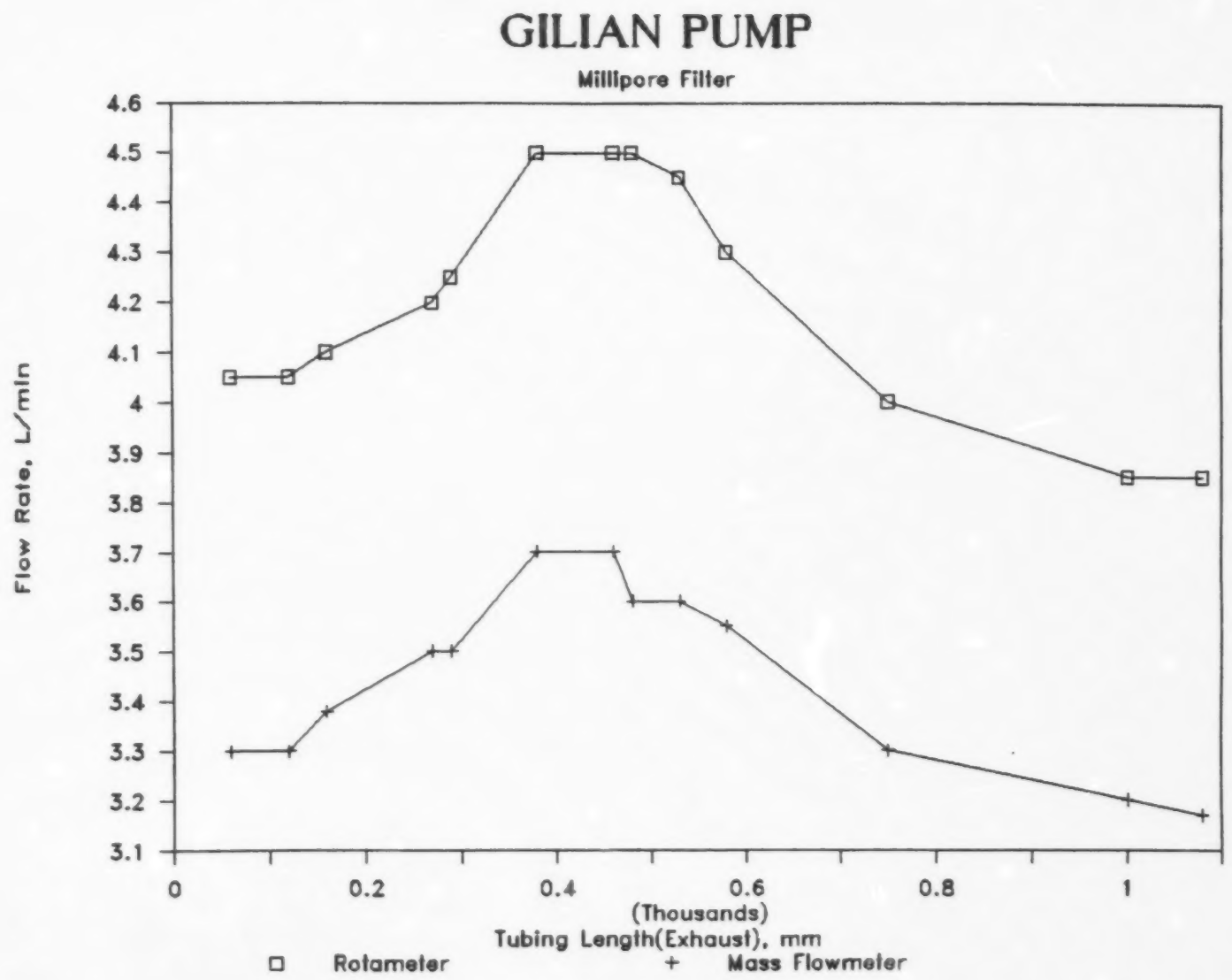

Fig. 31 - Airflow rate versus exhaust tubing length for the Gilian pump. (Millipore filter)

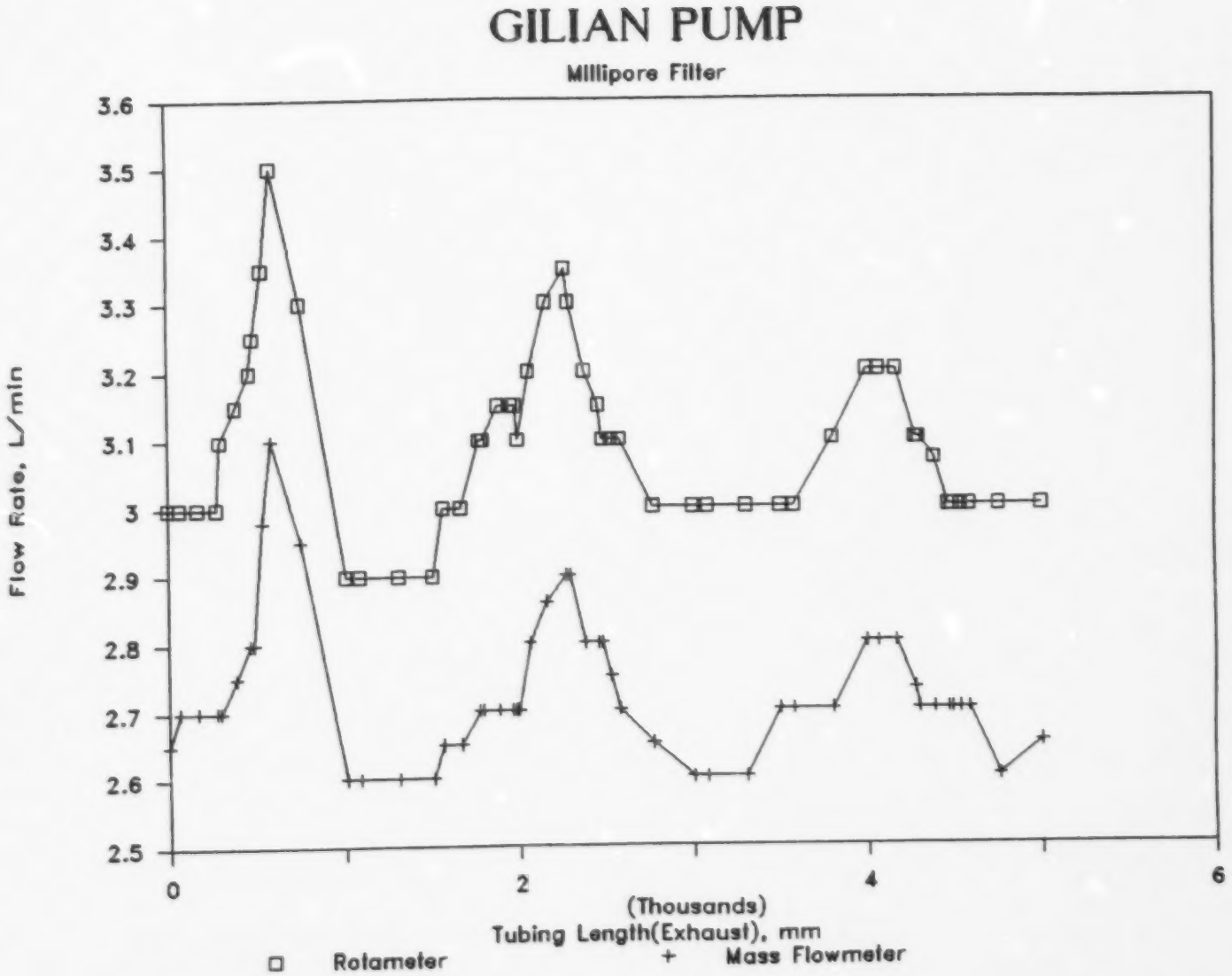

Fig. 32 - Airflow rate versus exhaust tubing length for the Gilian pump. (Millipore filter)

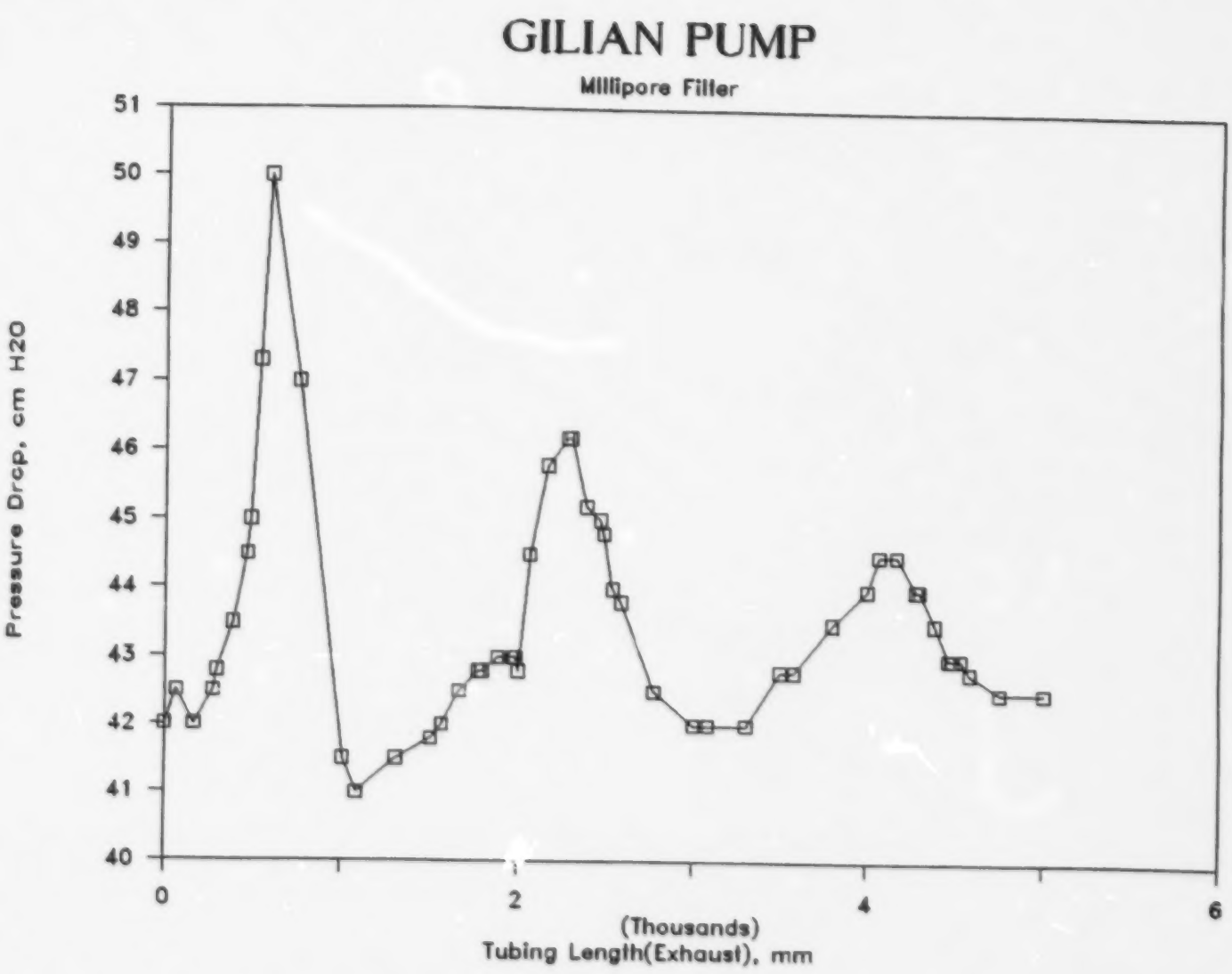

Fig. 33 - Pressure drop across the filter versus exhaust tubing length for the Gilian pump. (Millipore filter)

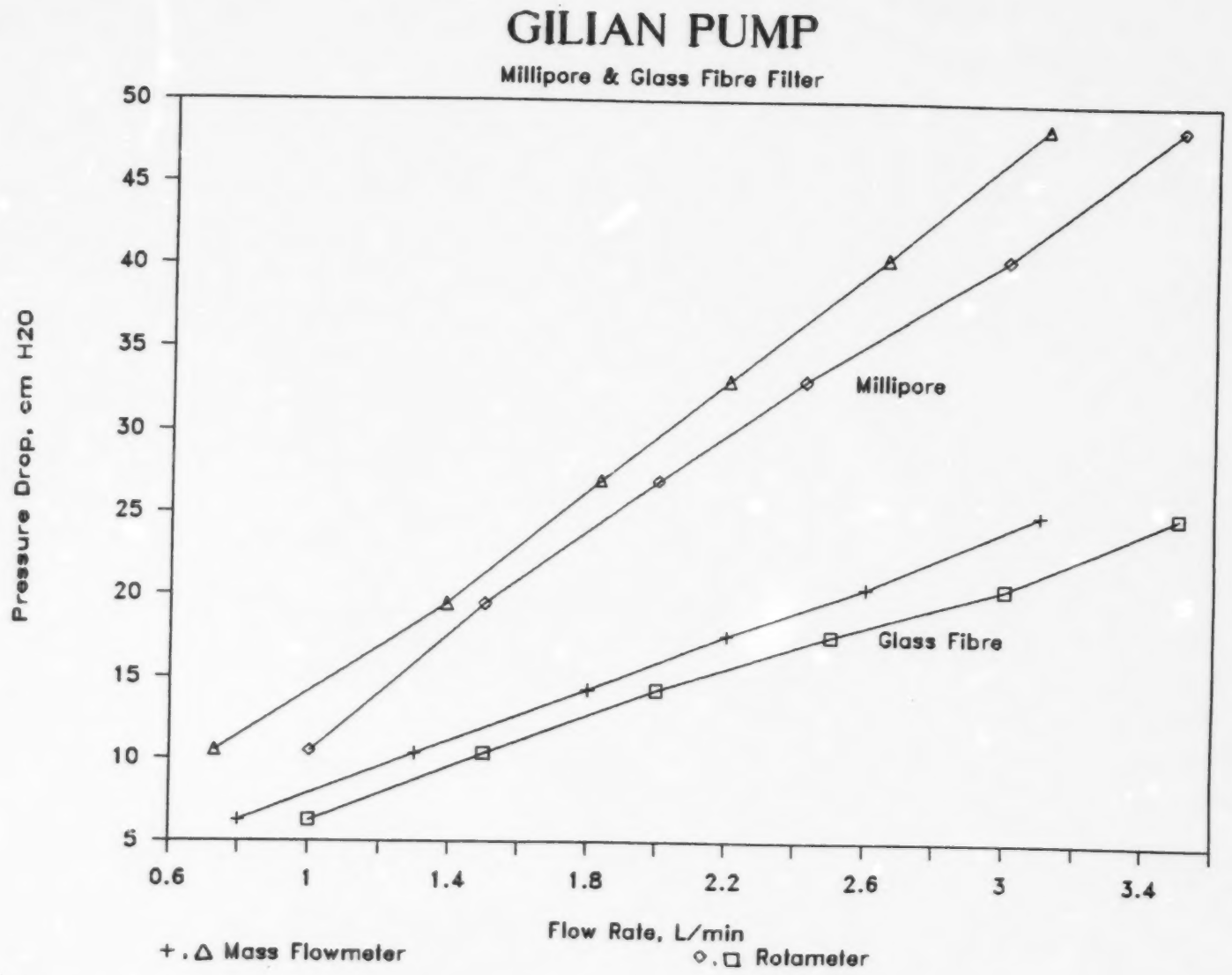

Fig. 34 - Pressure drop across the filter versus airflow rate for Millipore filters (upper graphs), and Glass fibre filters (lower graphs). Gilian pump.

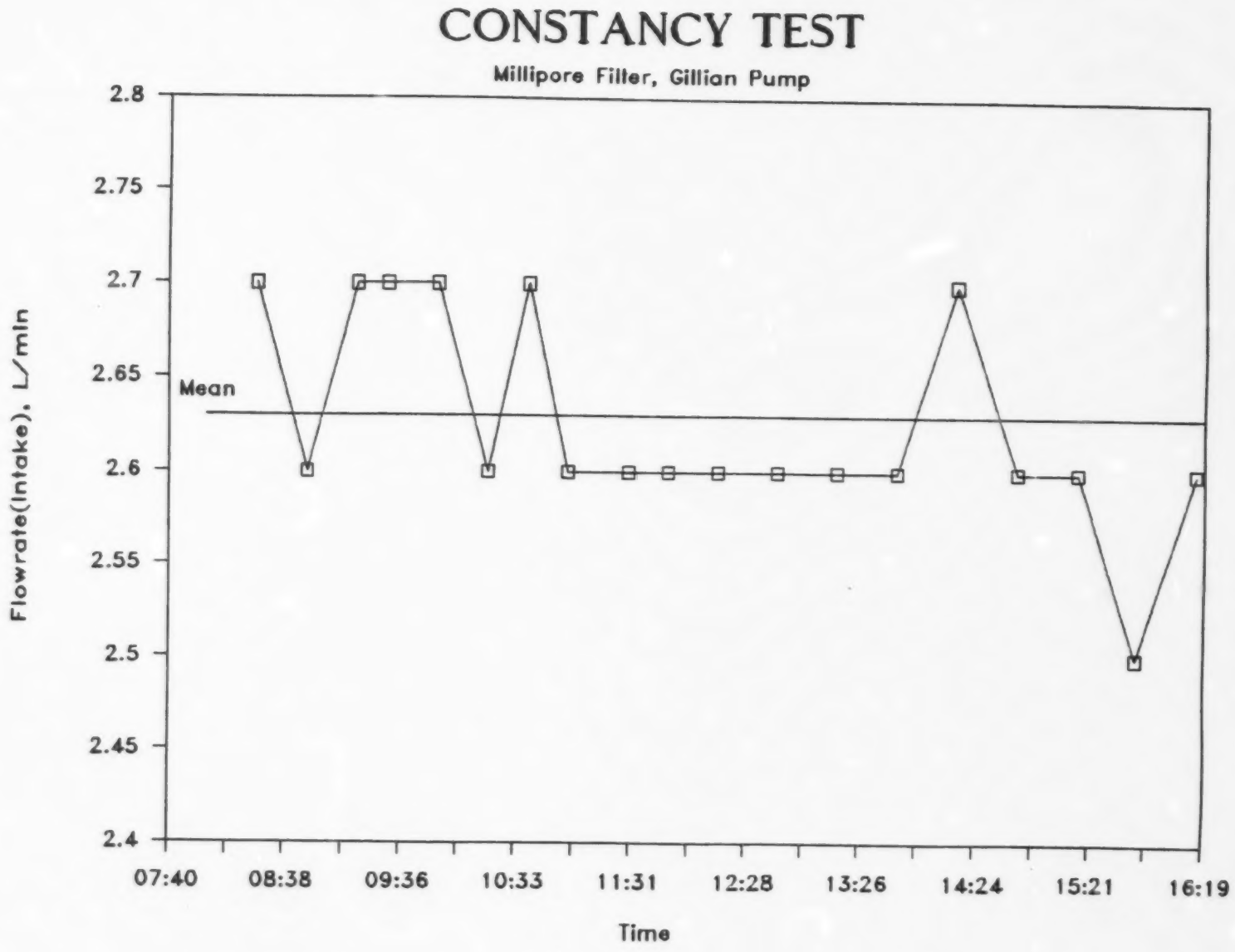

Fig. 35 - Airflow rate versus time for the Gilian pump.

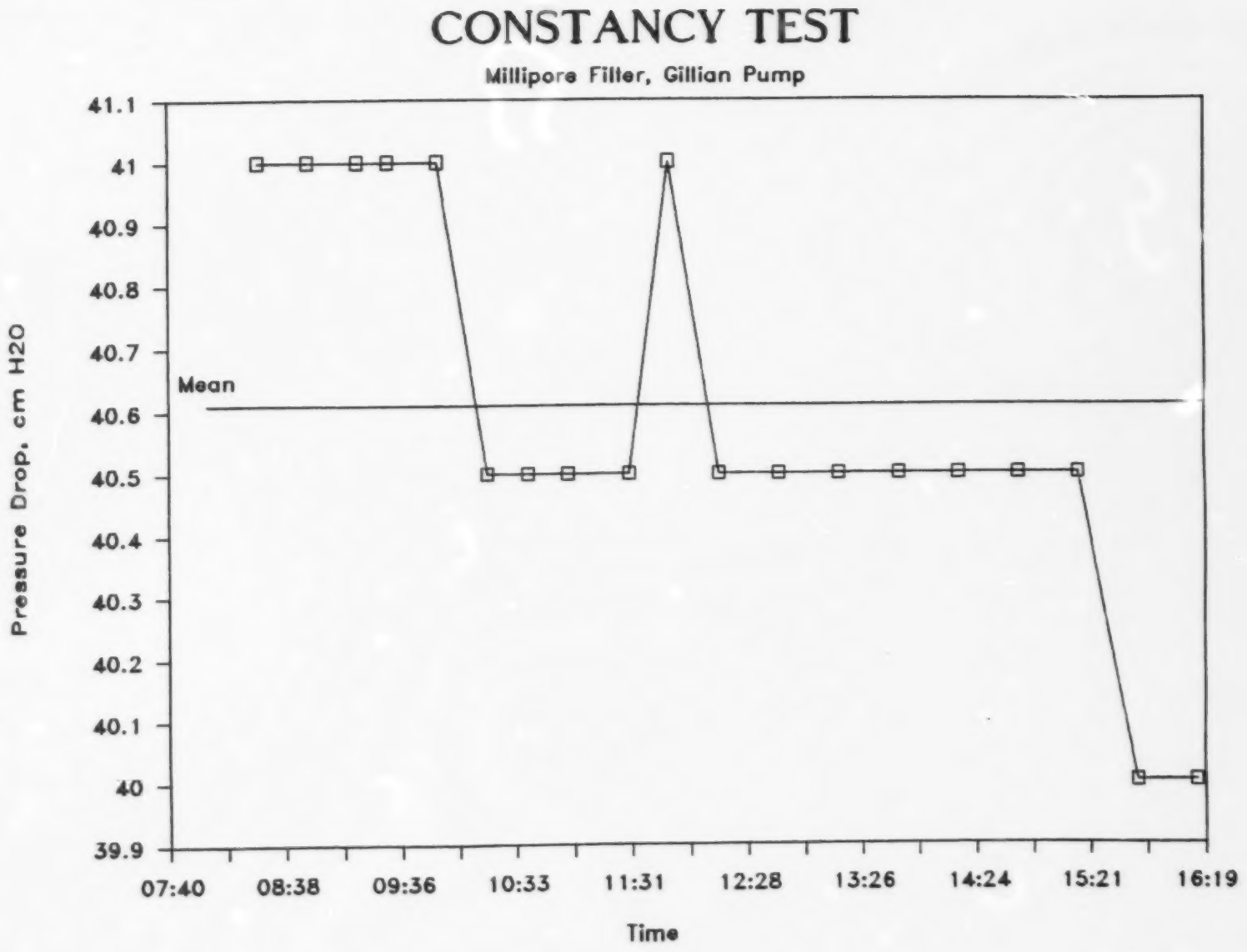

Fig. 36 - Pressure drop across the filter versus time for the Gilian pump.

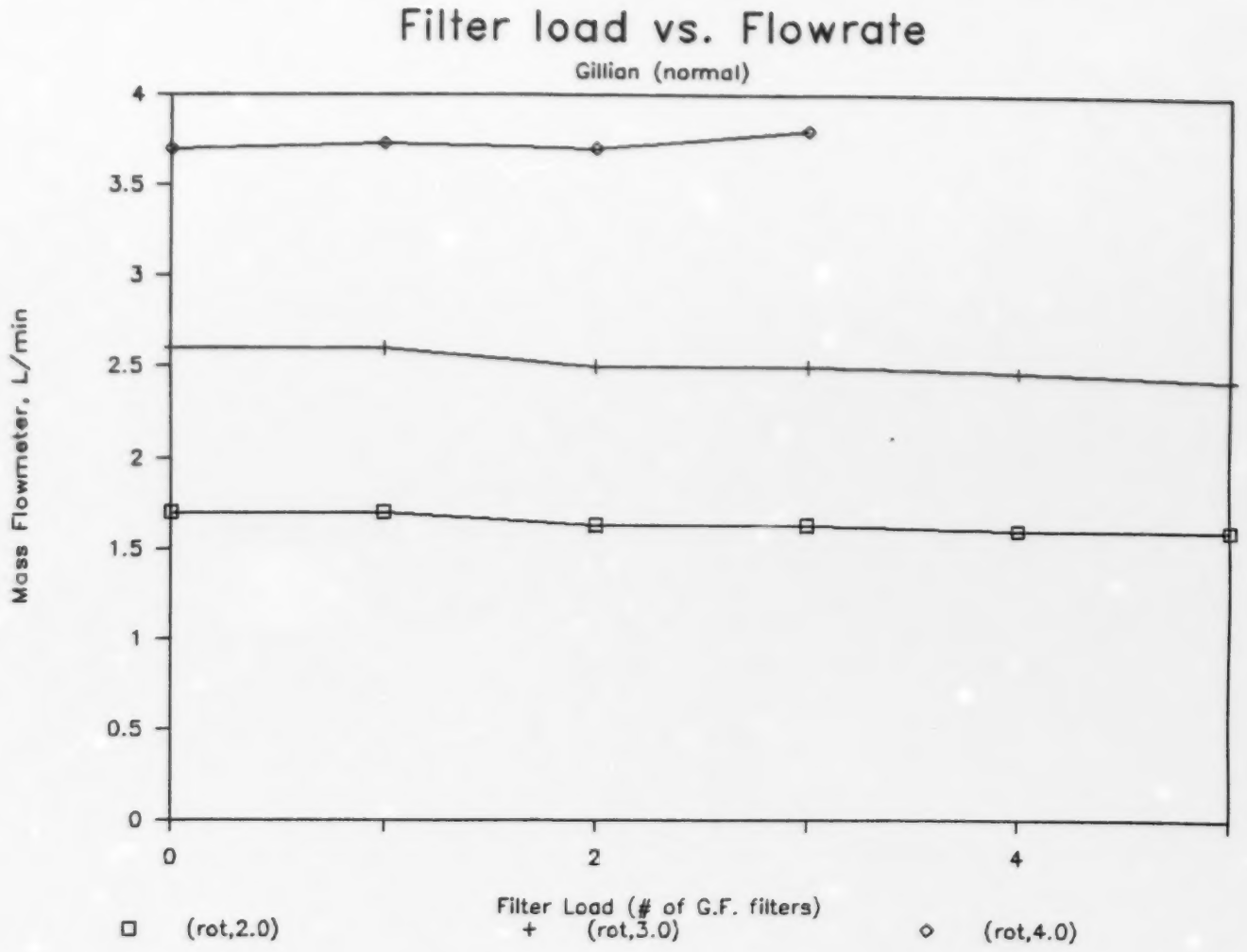

Fig. 37 - Airflow rate versus number of glass fibre filters for the Gilian pump operating on the flow regulated mode.

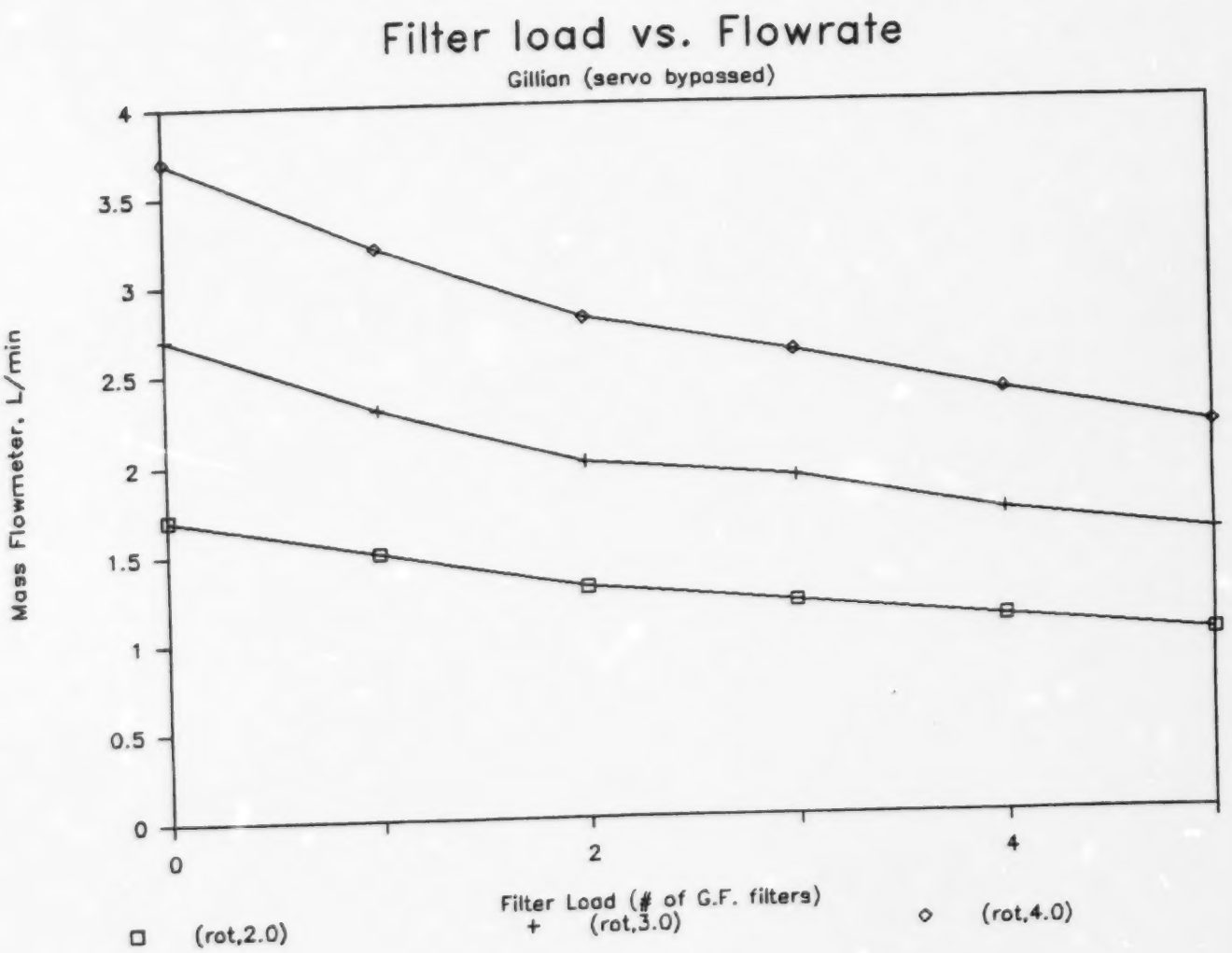

Fig. 38 - Airflow rate versus number of glass fibre filters for the Gilian pump, non-flow regulating mode.

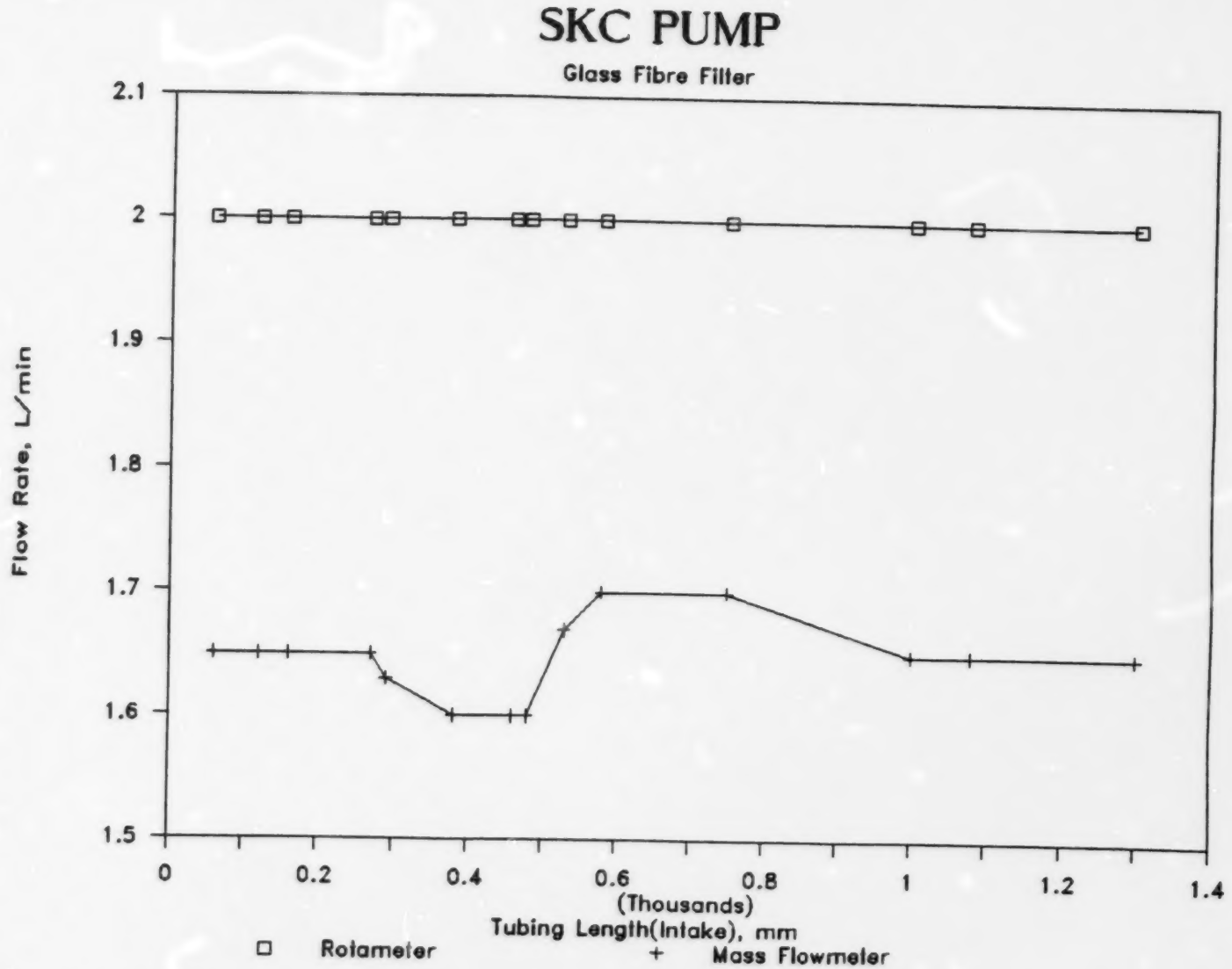

Fig. 39 - Airflow rate versus intake tubing length for the SKC pump. Glass fibre filter.

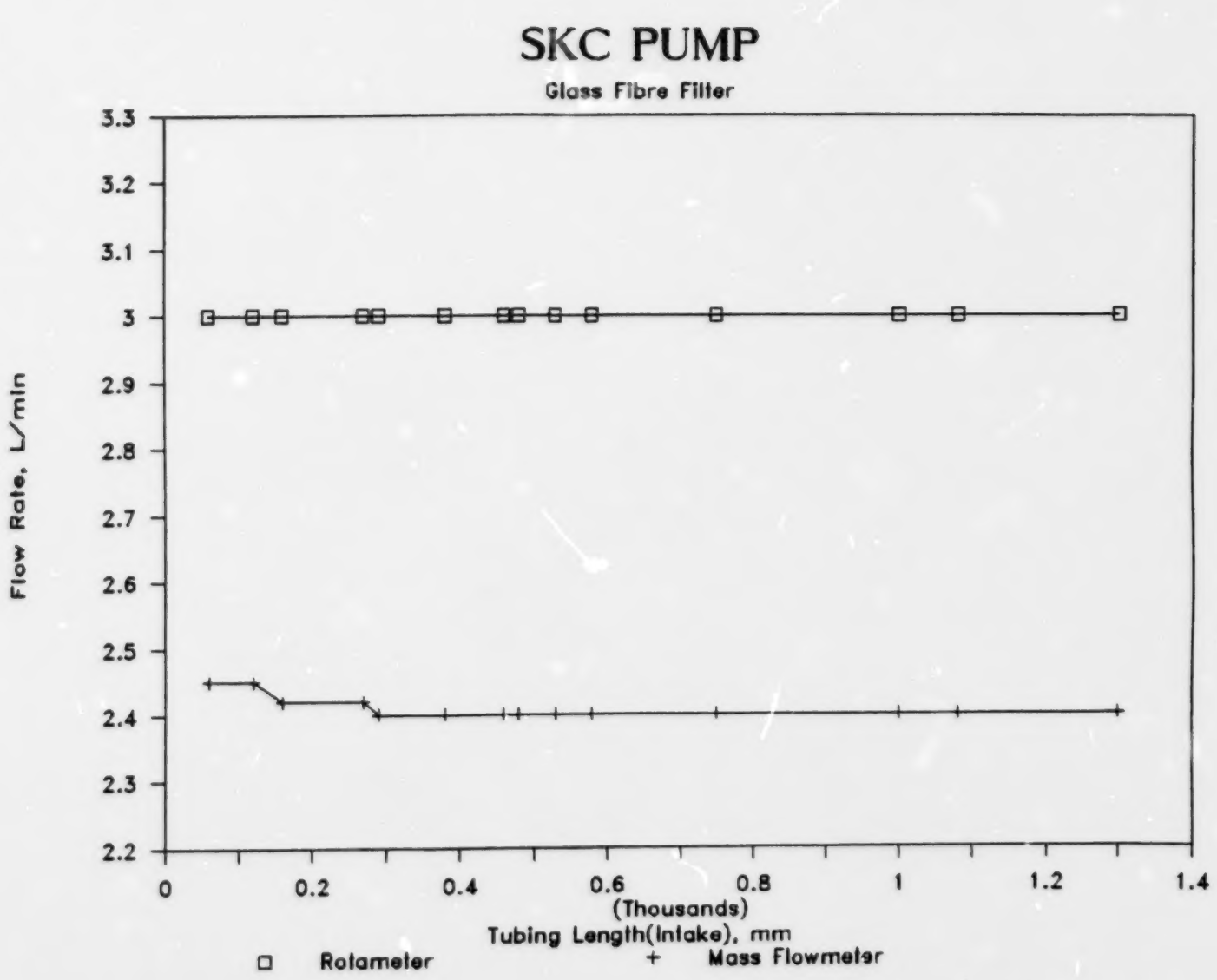

Fig. 40 - Airflow rate versus intake tubing length for the SKC pump. Glass fibre filter.

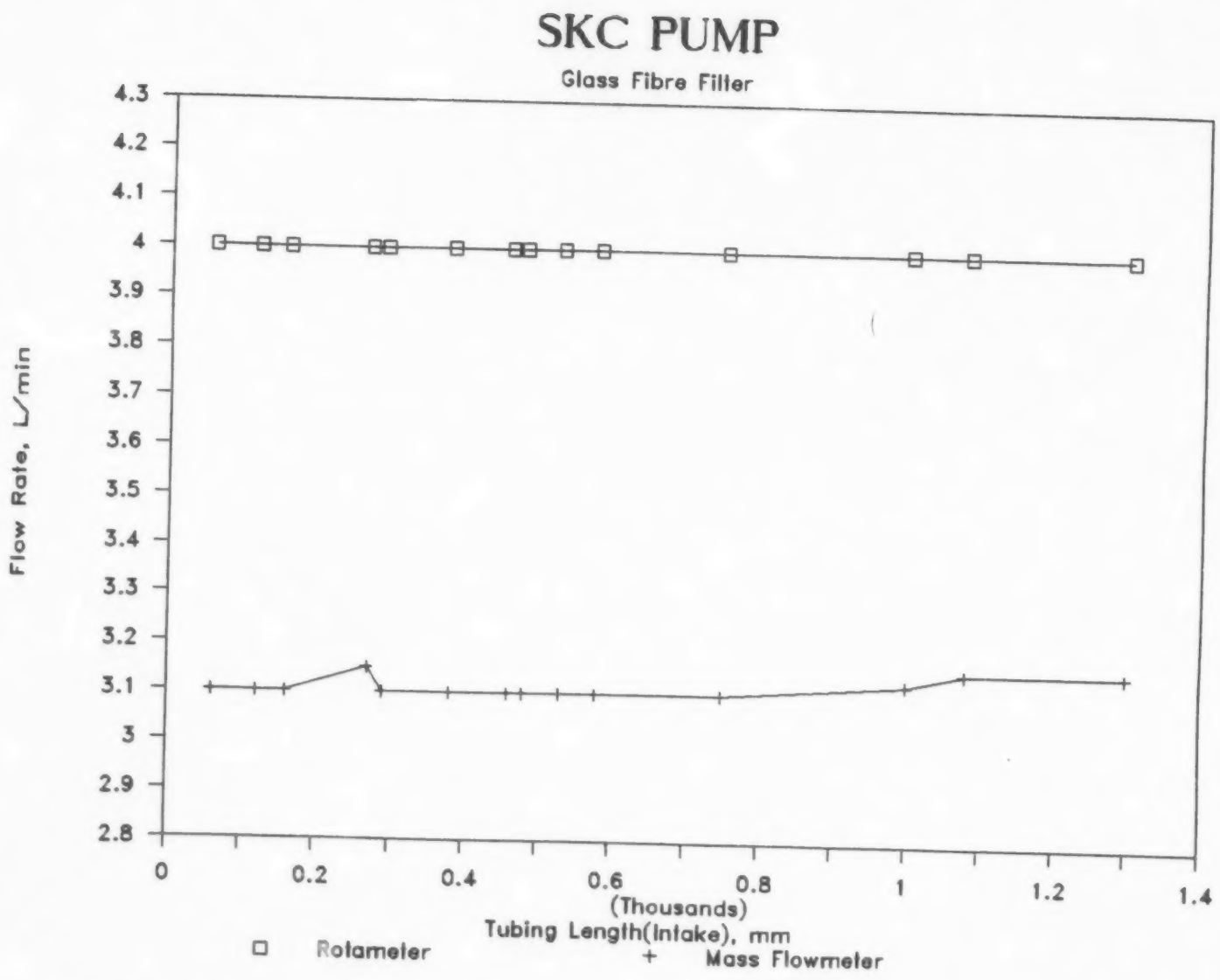

Fig. 41 - Airflow rate versus intake tubing length for the SKC pump. Glass fibre filter.

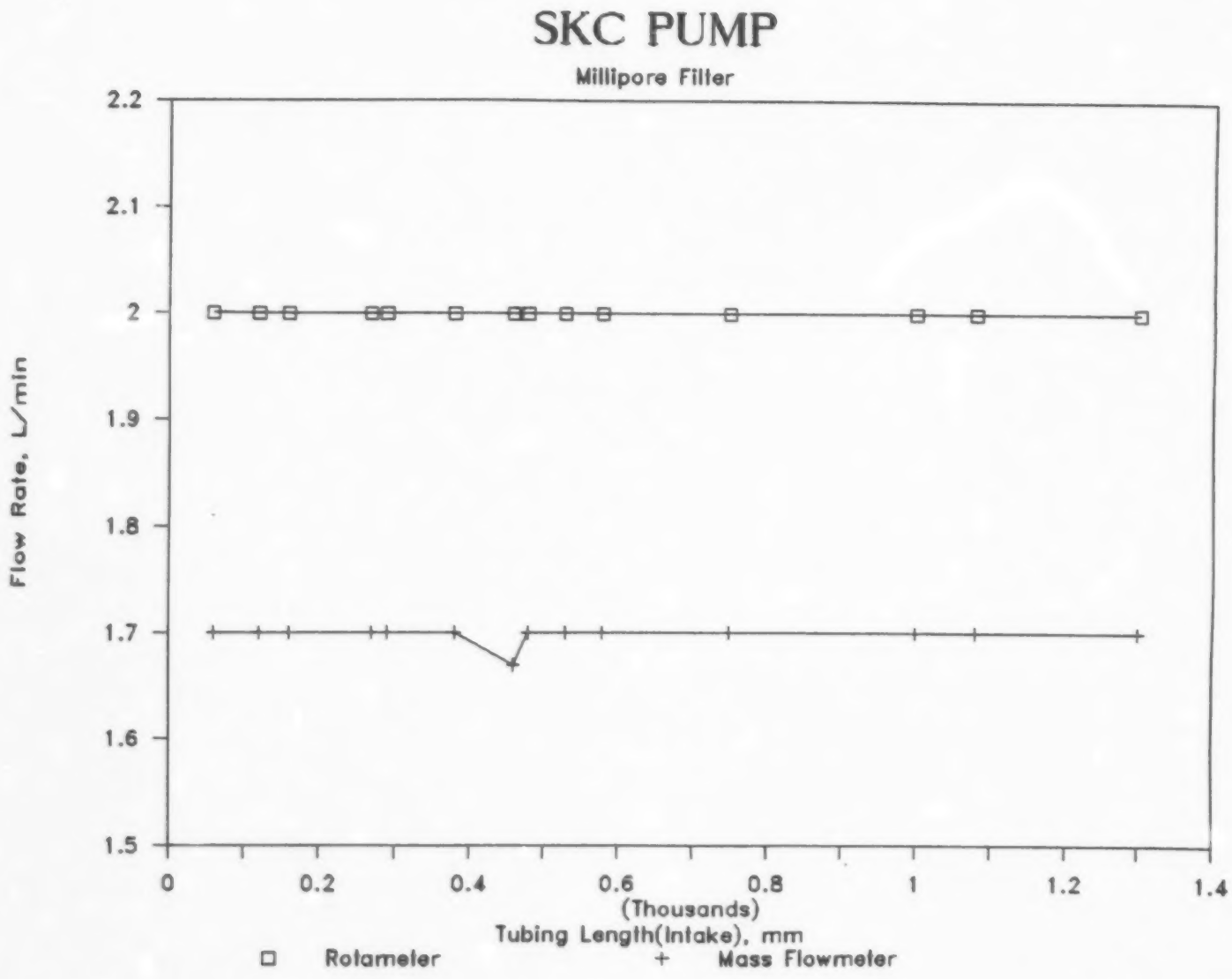

Fig. 42 - Airflow rate versus intake tubing length for the SKC pump. Millipore filter.

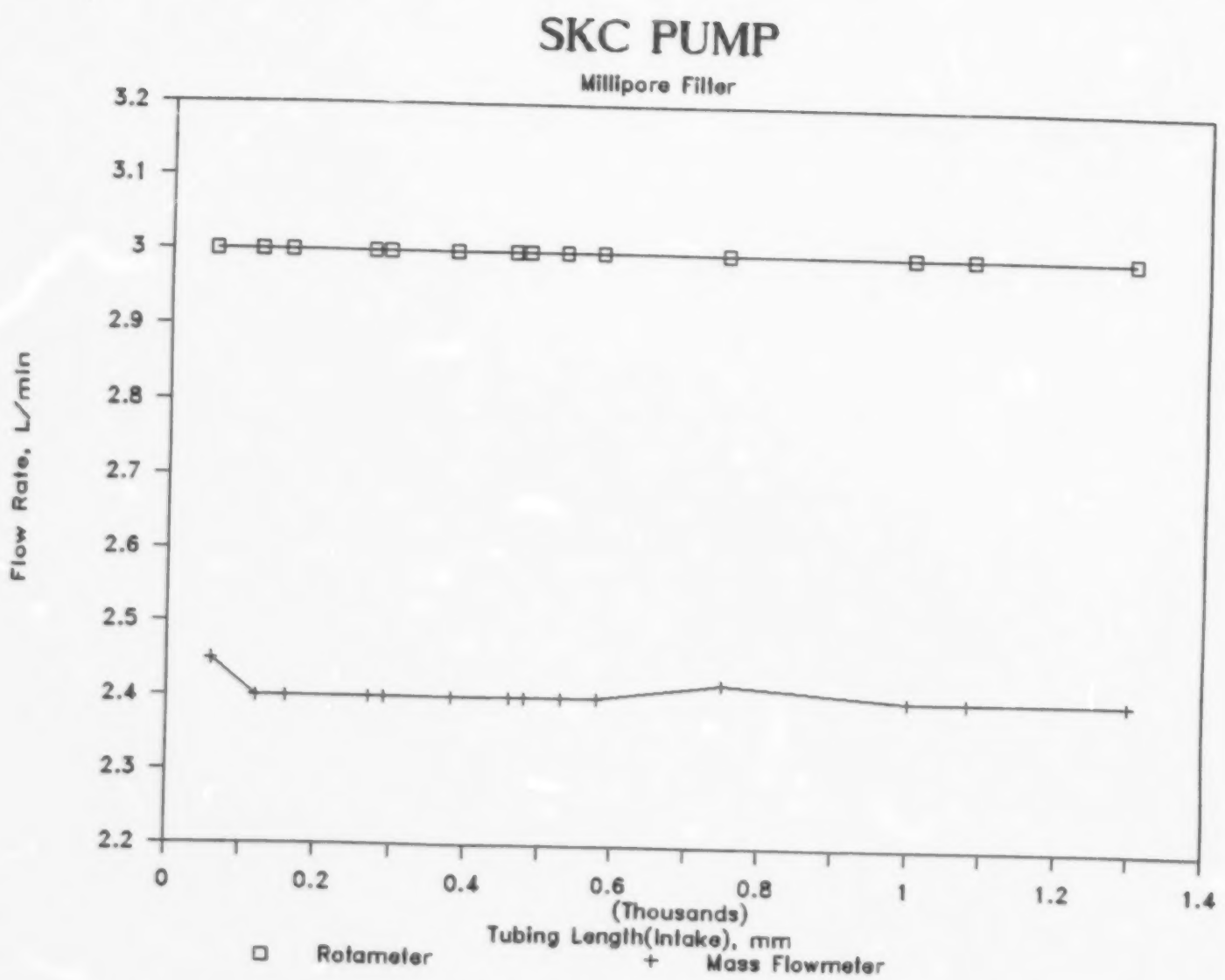

Fig. 43 - Airflow rate versus intake tubing length for the SKC pump. Millipore filter.

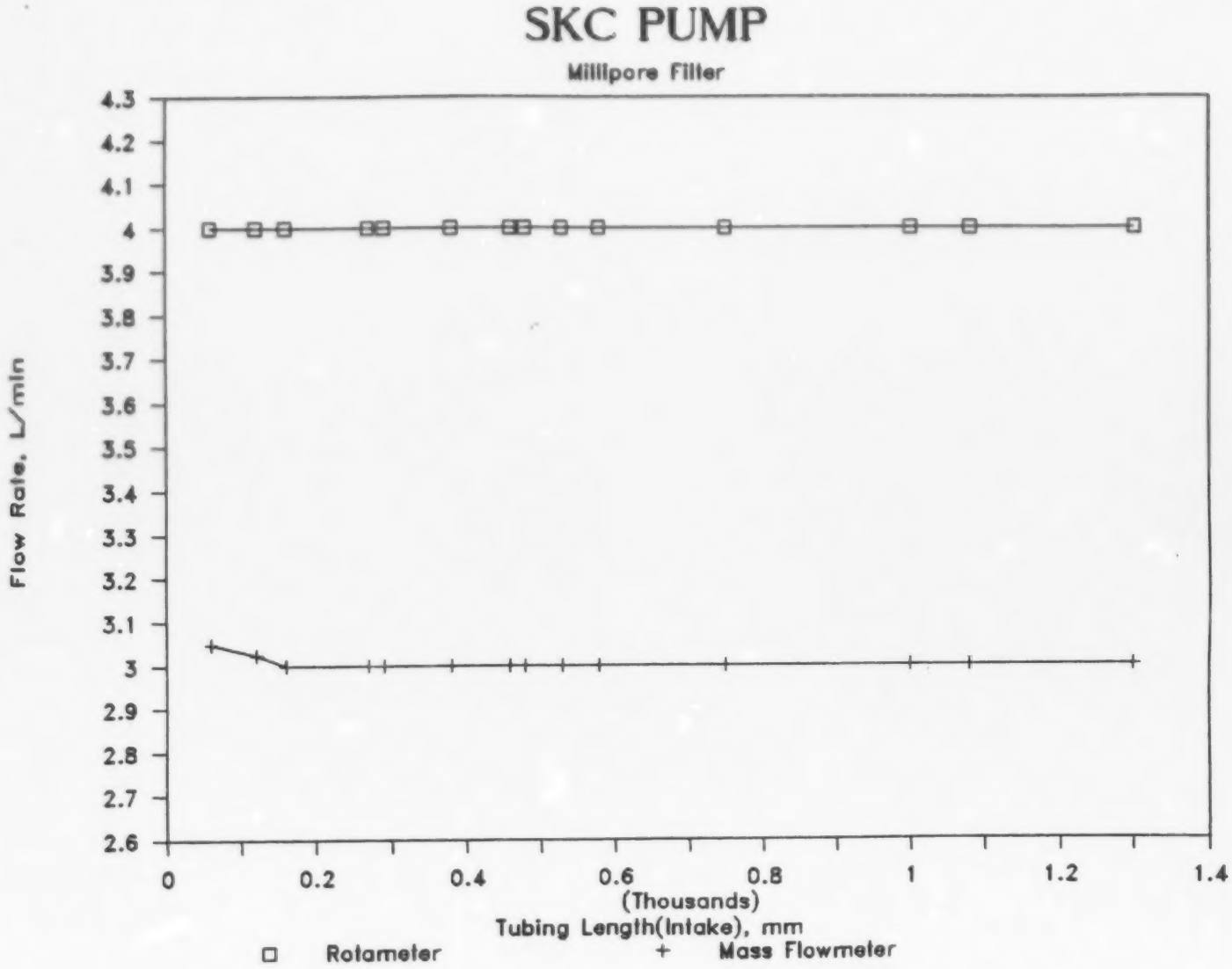

Fig. 44 - Airflow rate versus intake tubing length for the SKC pump. Millipore filter.

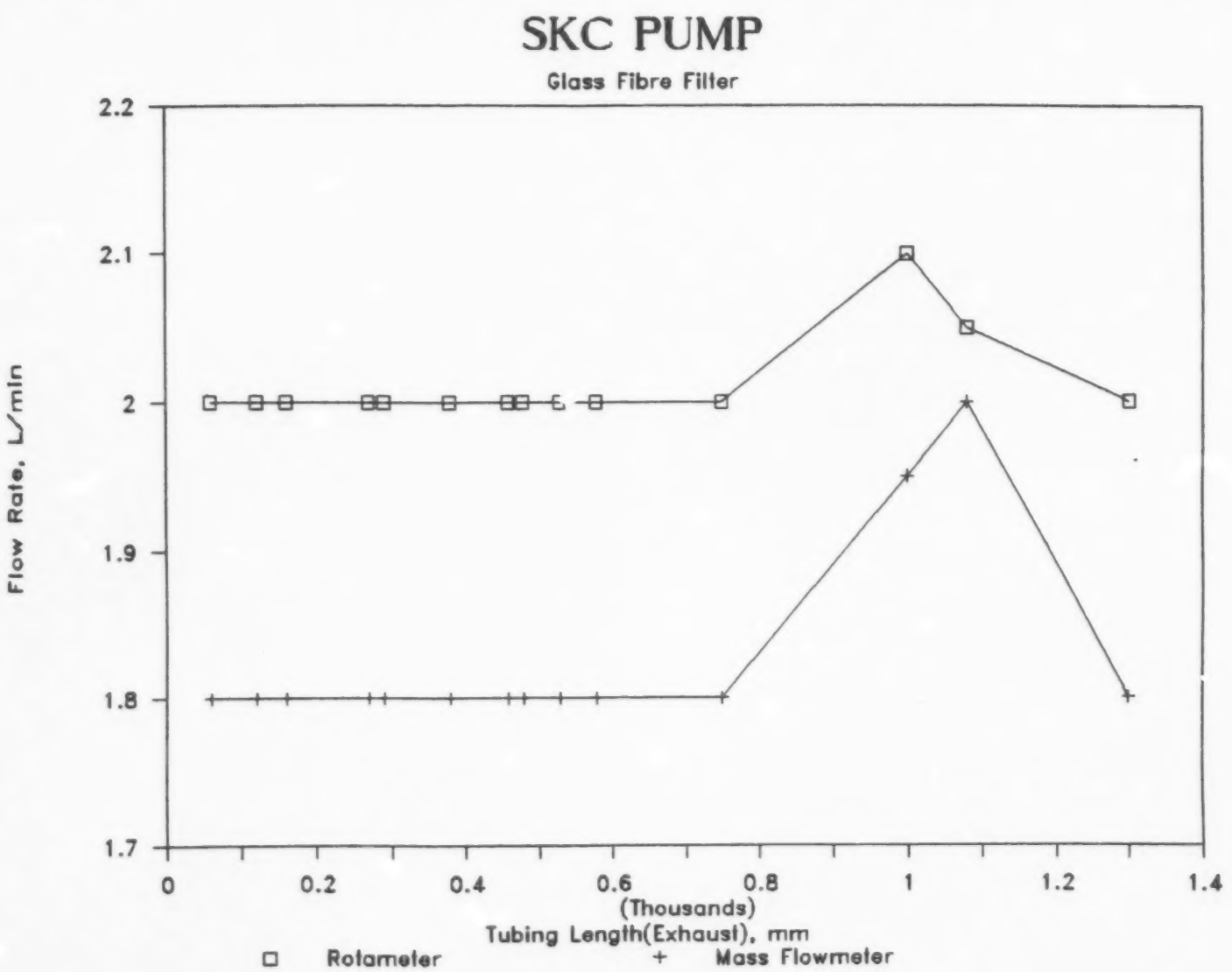

Fig. 45 - Airflow rate versus exhaust tubing length for the SKC pump. Glass fibre filter.

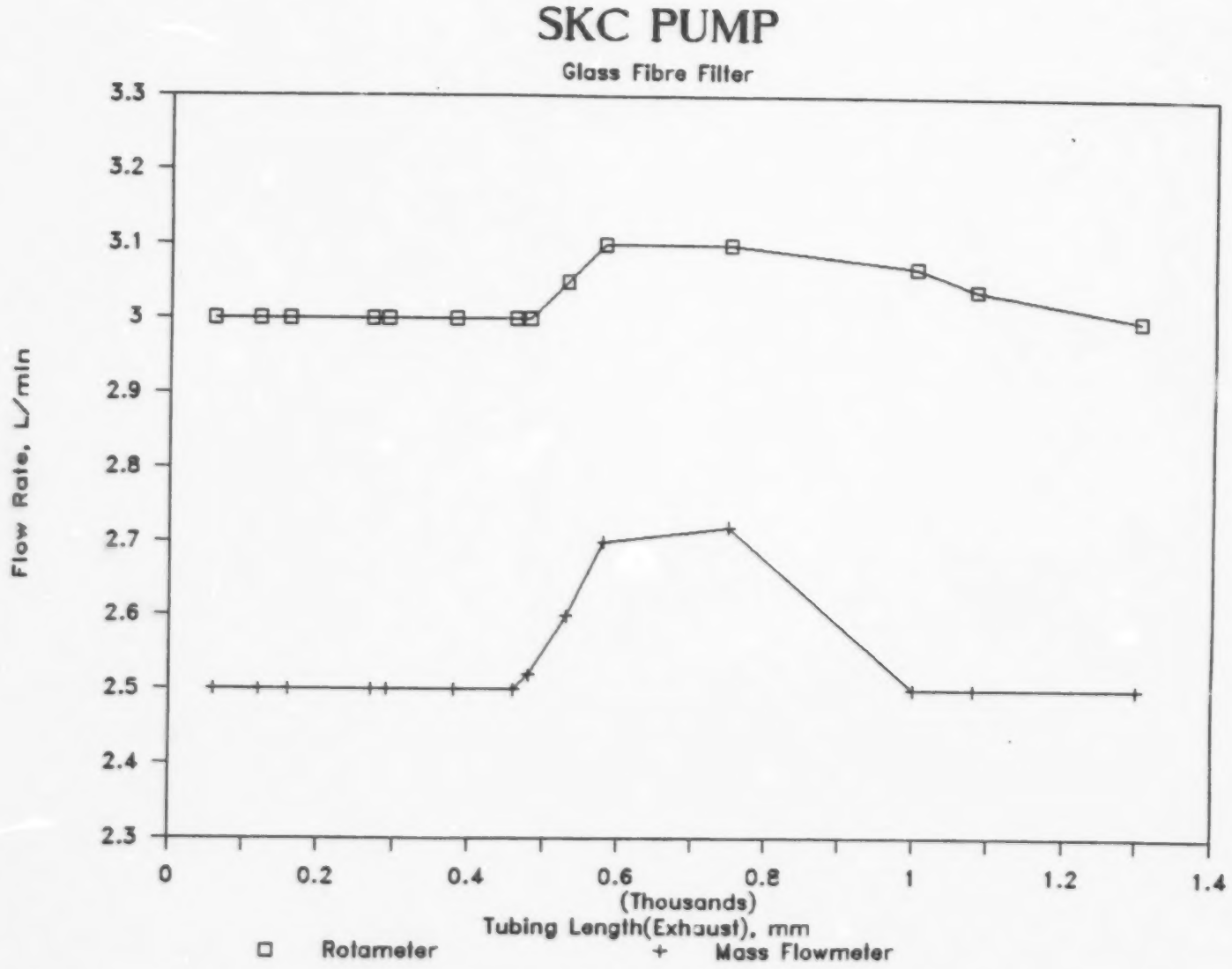

Fig. 46 - Airflow rate versus exhaust tubing length for the SKC pump. Glass fibre filter.

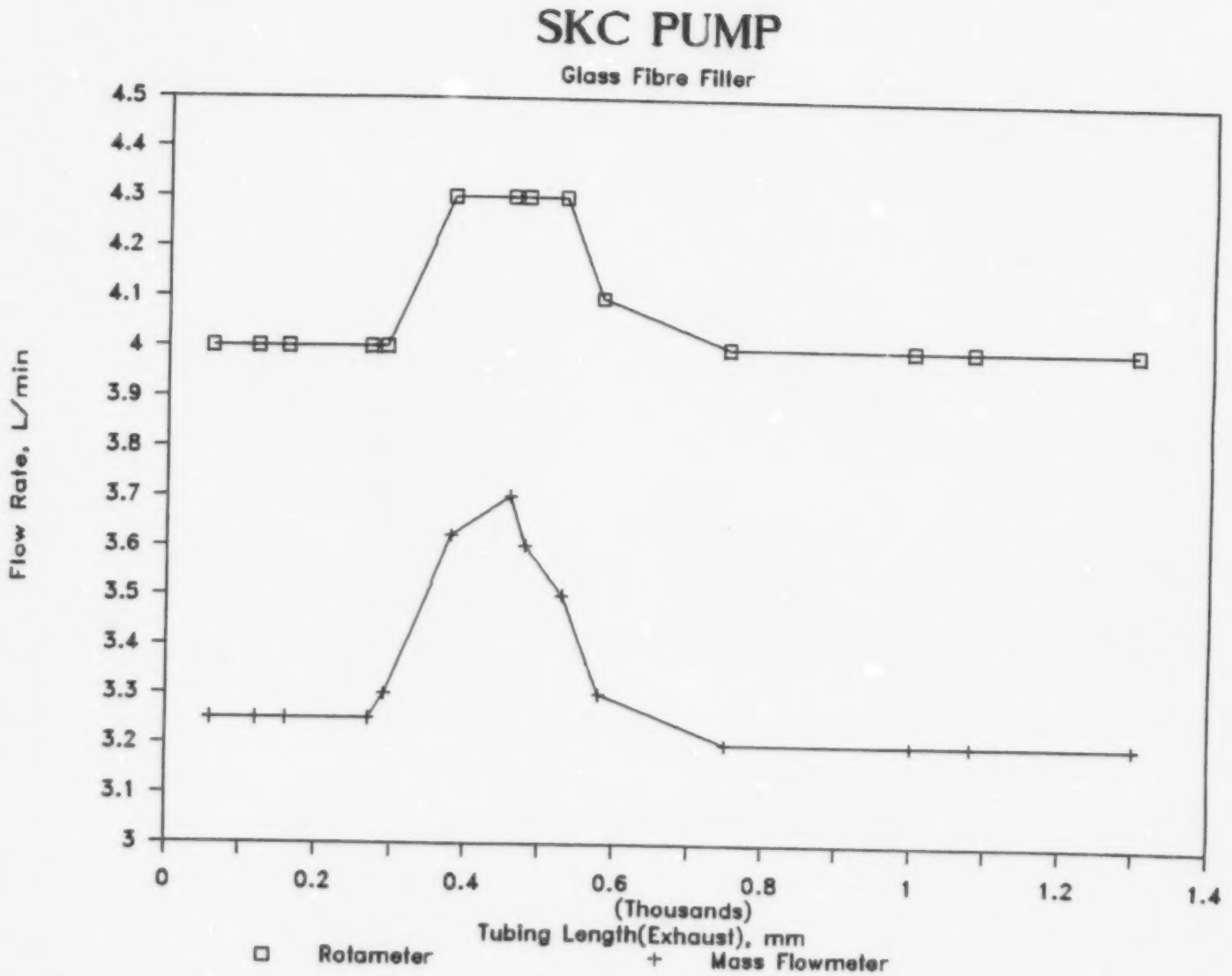

Fig. 47 - Airflow rate versus exhaust tubing length for the SKC pump. Glass fibre filter.

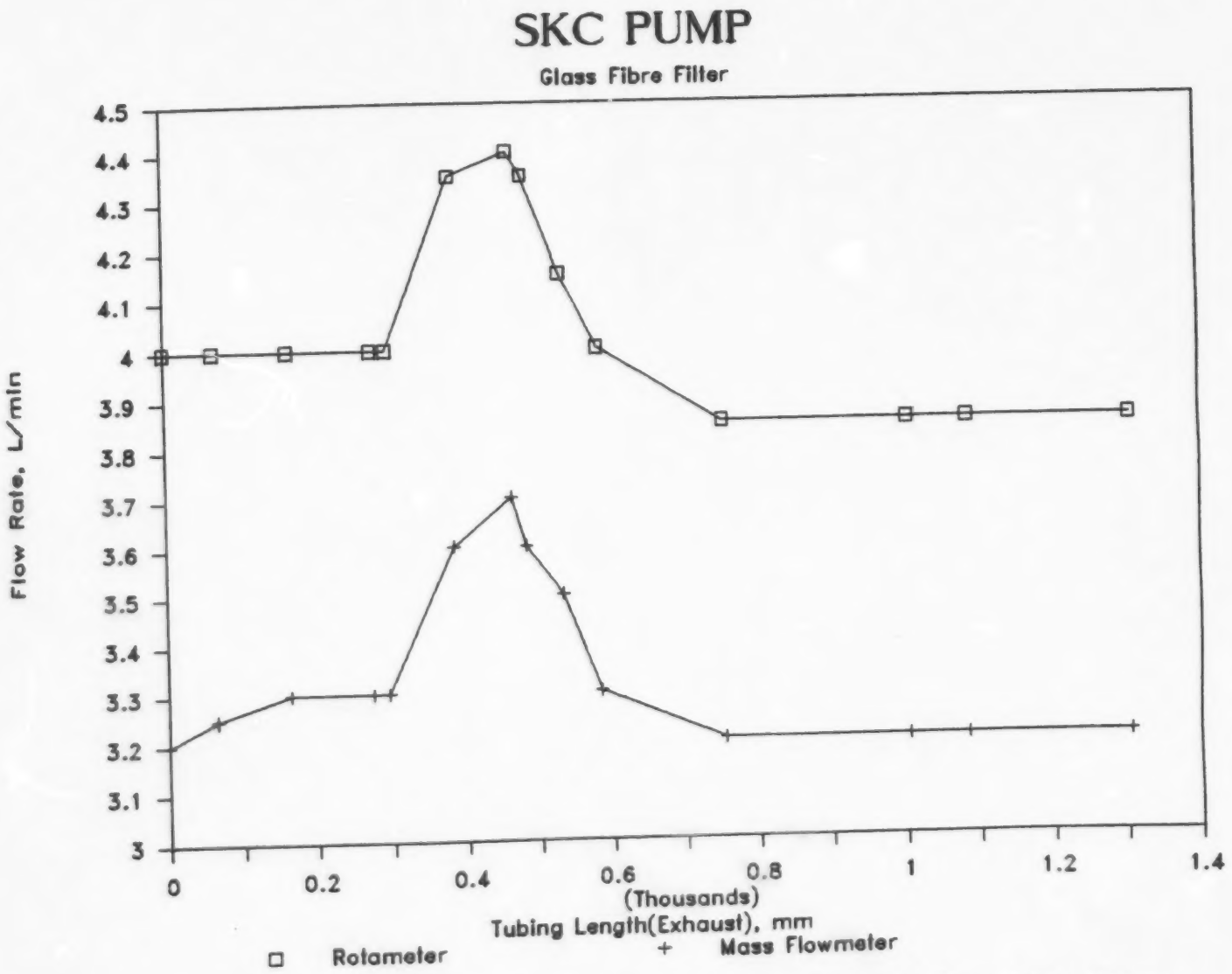

Fig. 48 - Airflow rate versus exhaust tubing length for the SKC pump. Glass fibre filter.

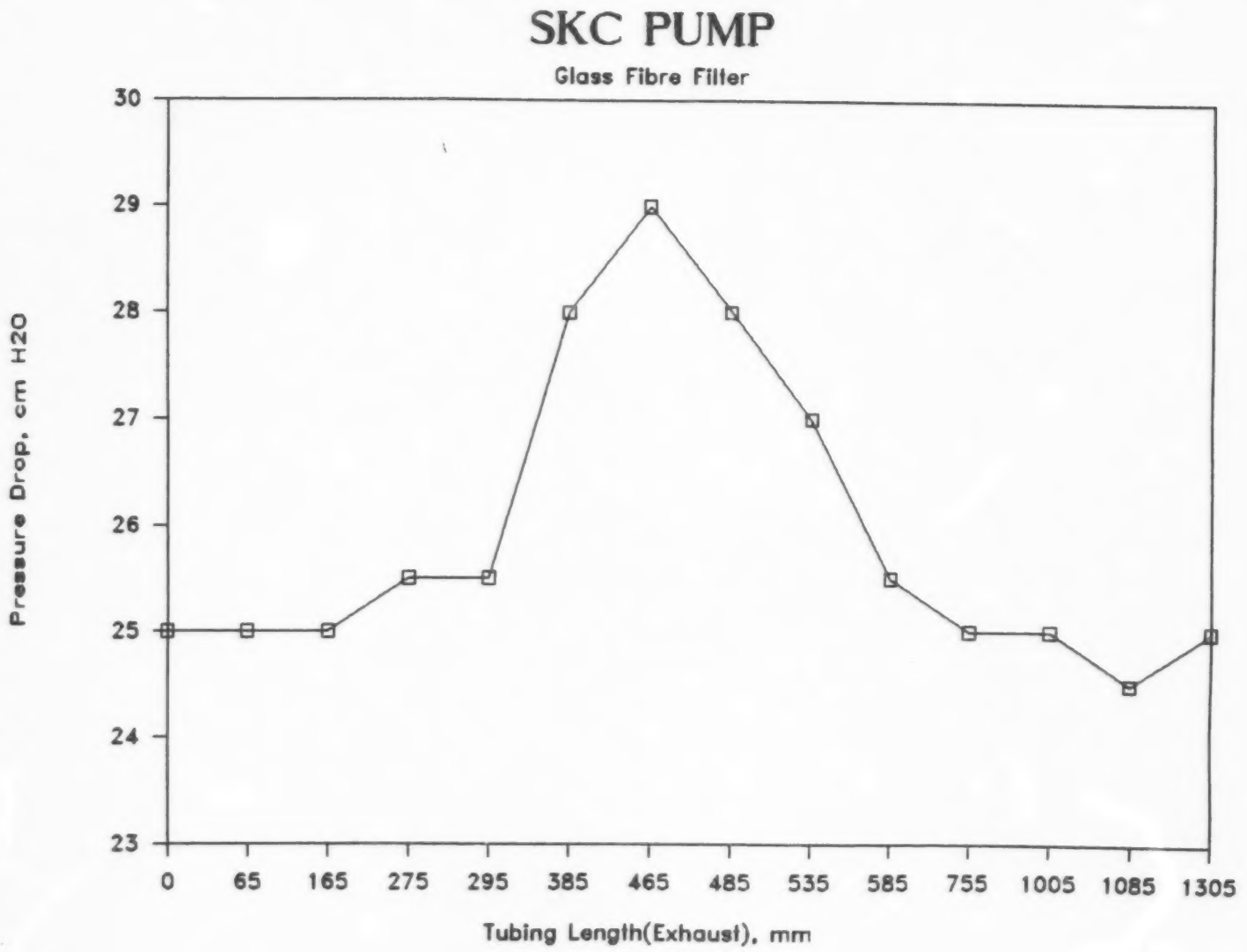

Fig. 49 - Pressure drop across the filter versus exhaust tubing length for the SKC pump. Glass fibre filter.

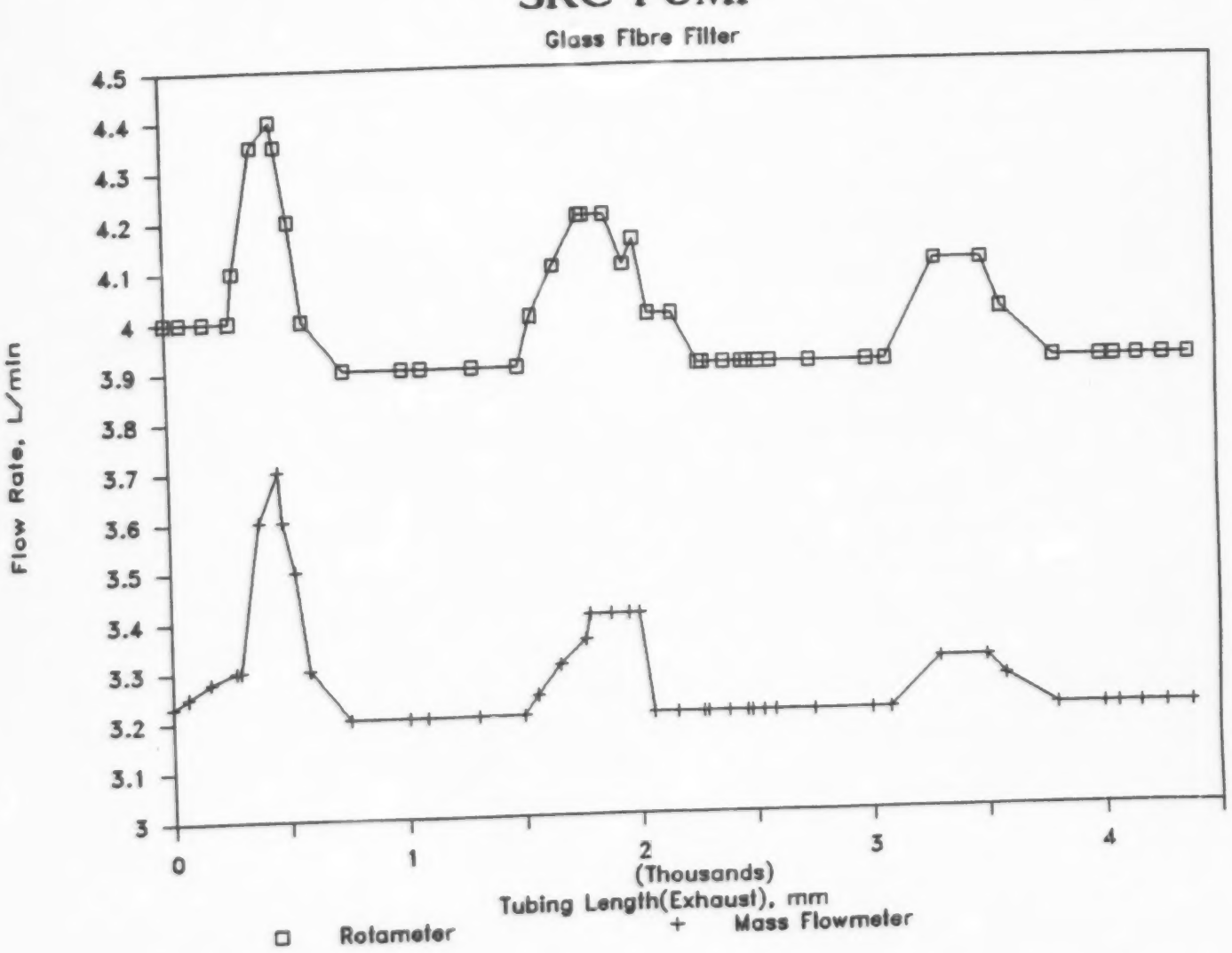

Fig. 50 - Airflow rate versus exhaust tubing length for the SKC pump. Glass fibre filter.

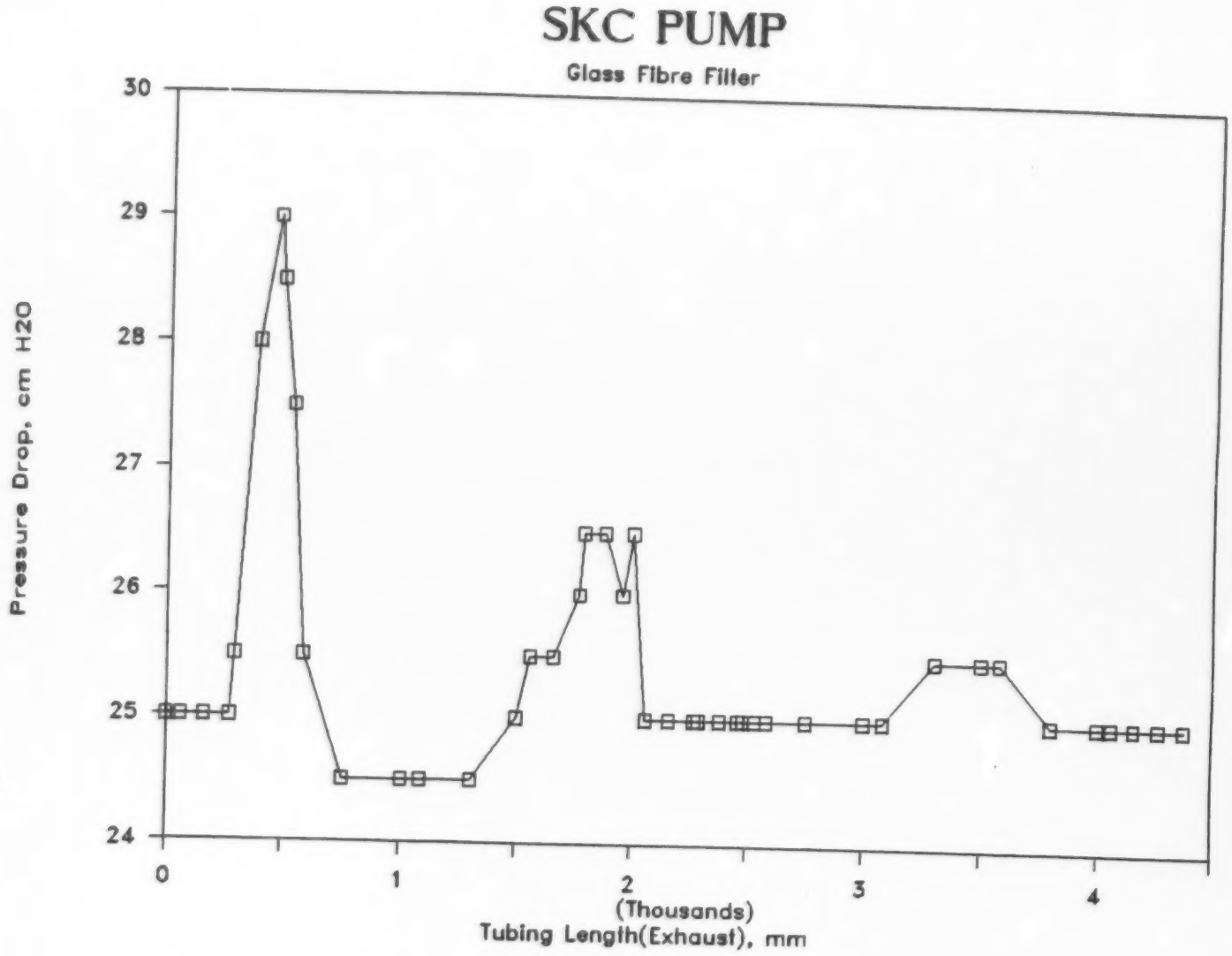

Fig. 51 - Pressure drop across the filter versus exhaust tubing length for the SKC pump. Glass fibre filter.

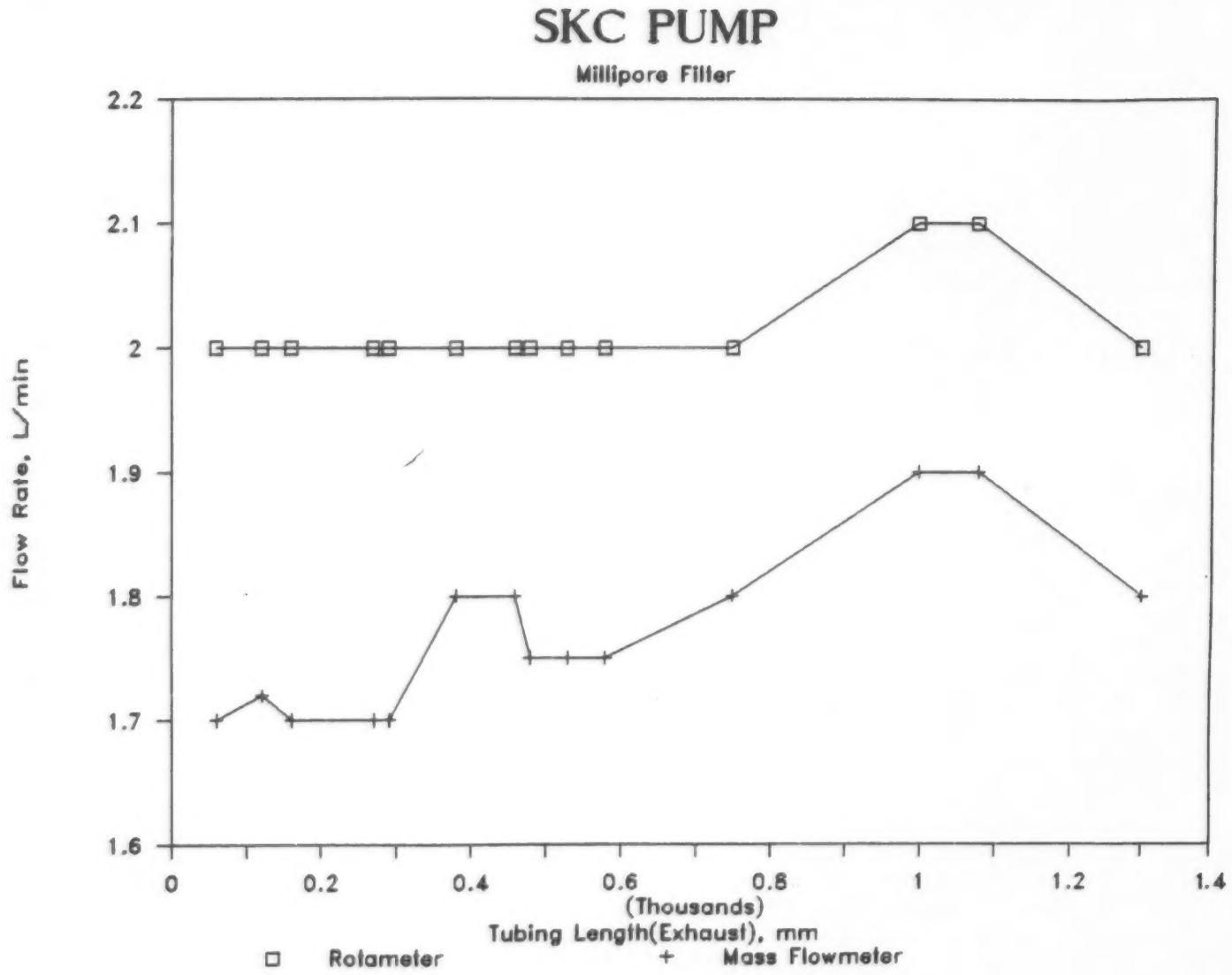

Fig. 52 - Airflow rate versus exhaust tubing length for the SKC pump. Millipore filter.

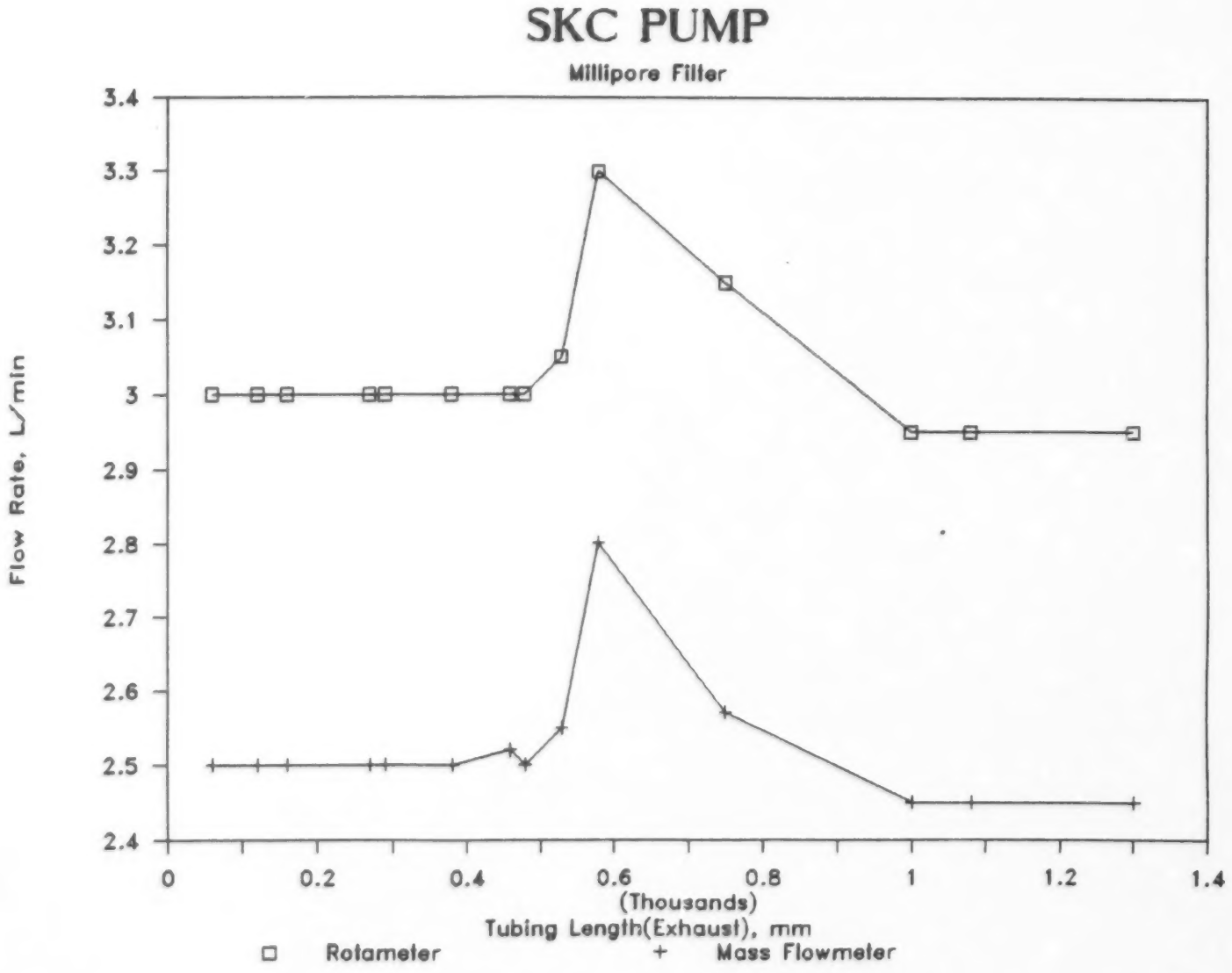

Fig. 53 - Airflow rate versus exhaust tubing length for the SKC pump. Millipore filter.

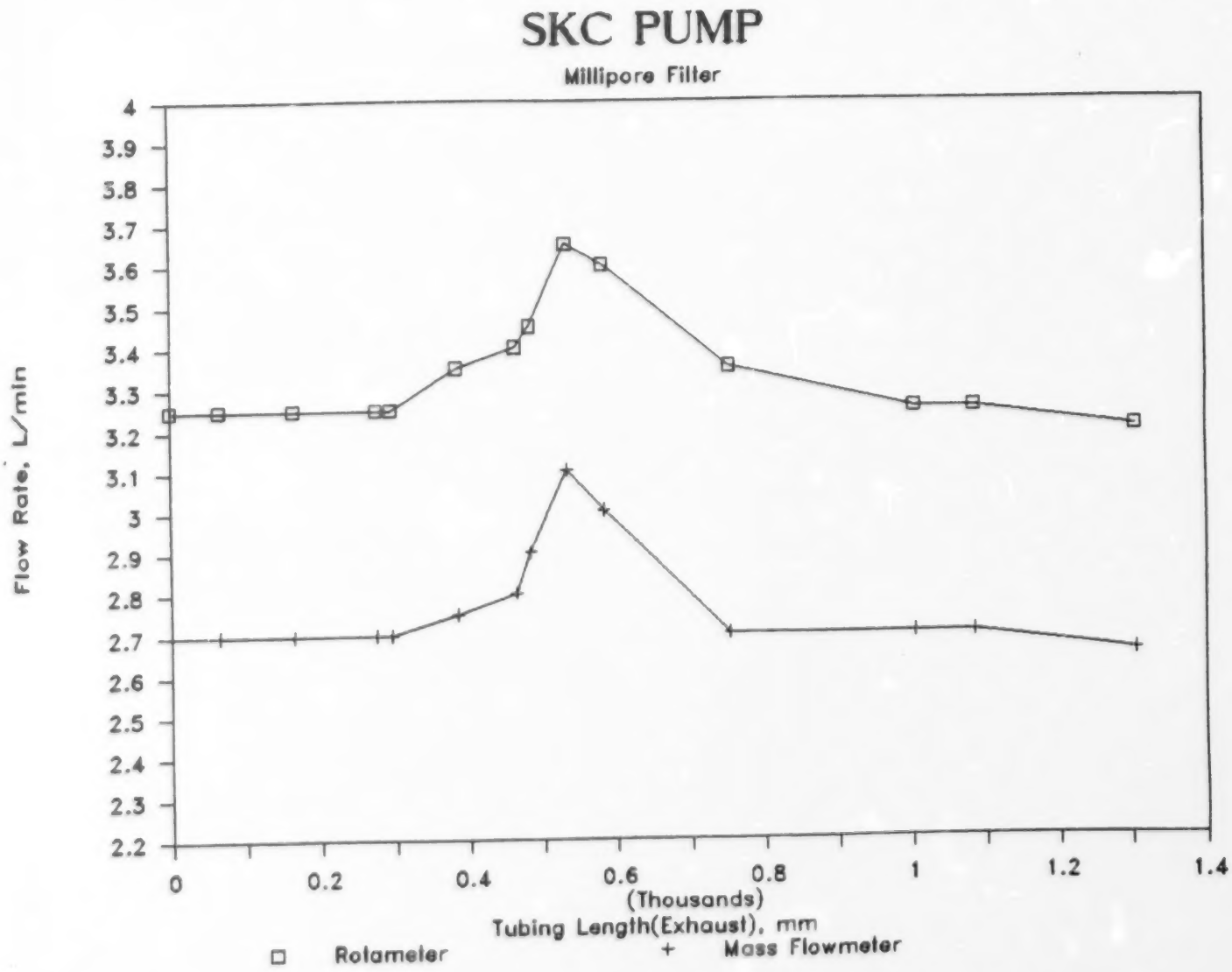

Fig. 54 - Airflow rate versus exhaust tubing length for the SKC pump. Millipore filter.

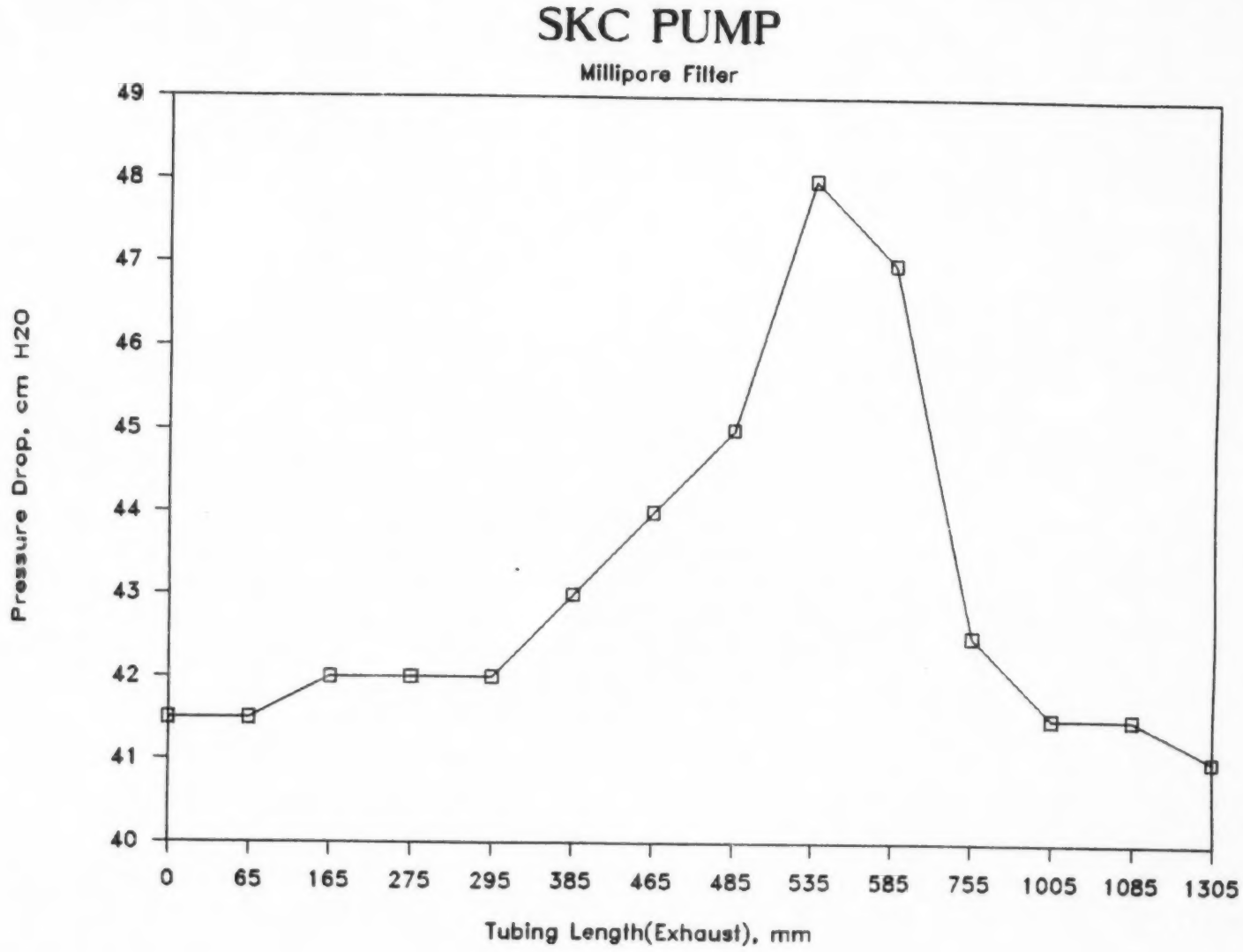

Fig. 55 - Pressure drop across the filter versus exhaust tubing length for the SKC pump. Millipore filter.

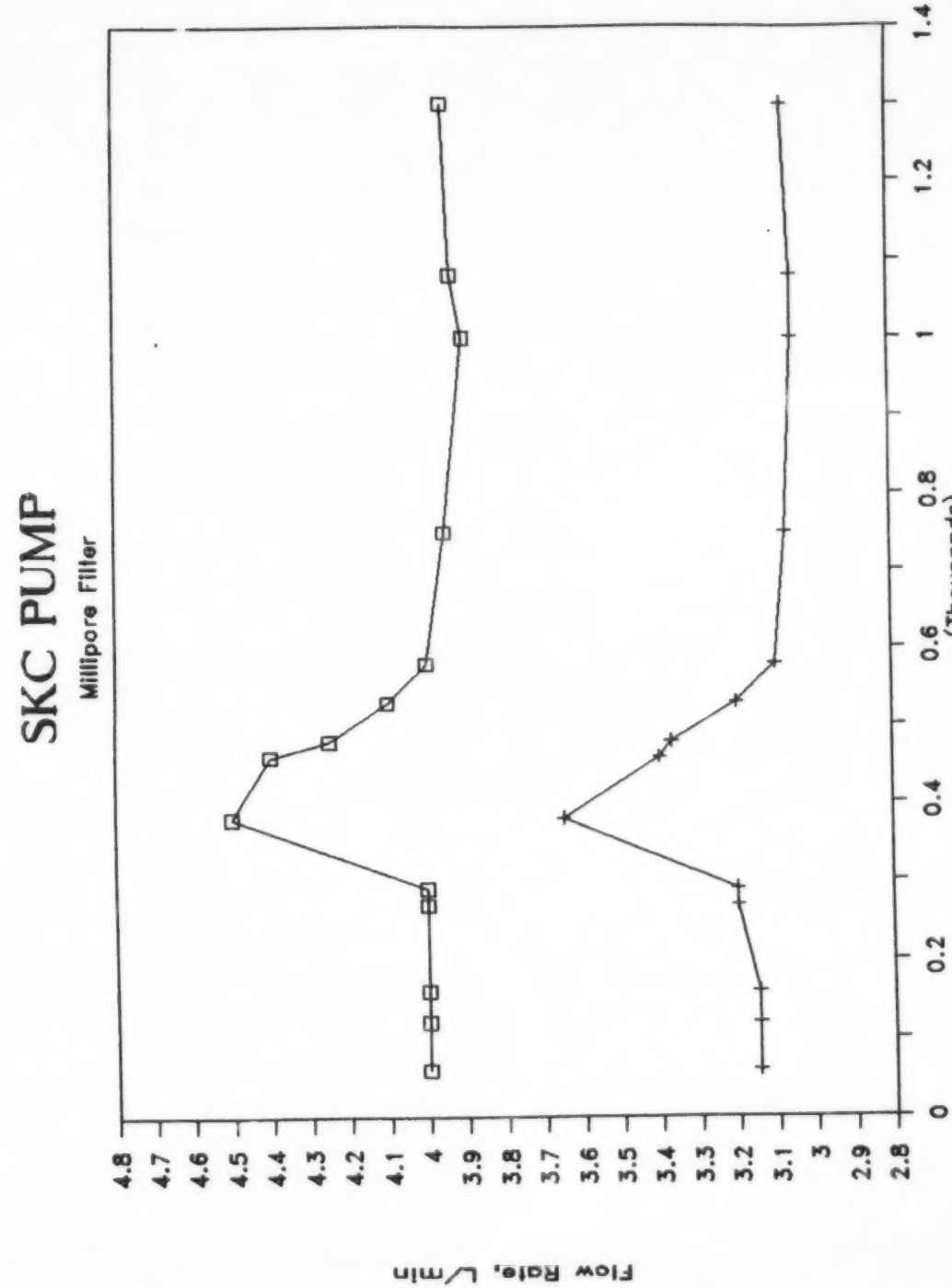

Fig. 56 - Airflow rate versus exhaust tubing length for the SKC pump. Millipore filter.

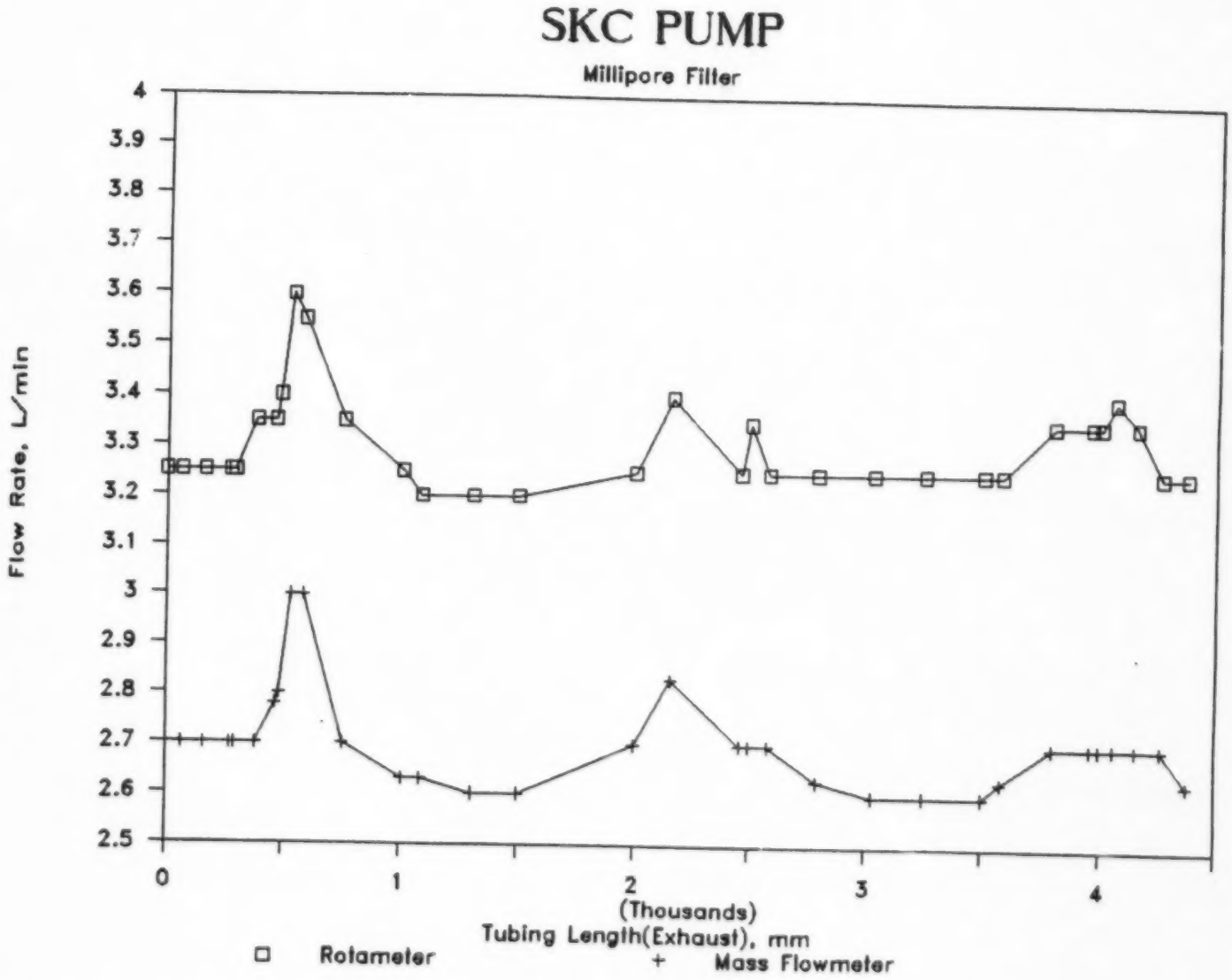

Fig. 57 - Airflow rate versus exhaust tubing length for the SKC pump. Millipore filter.

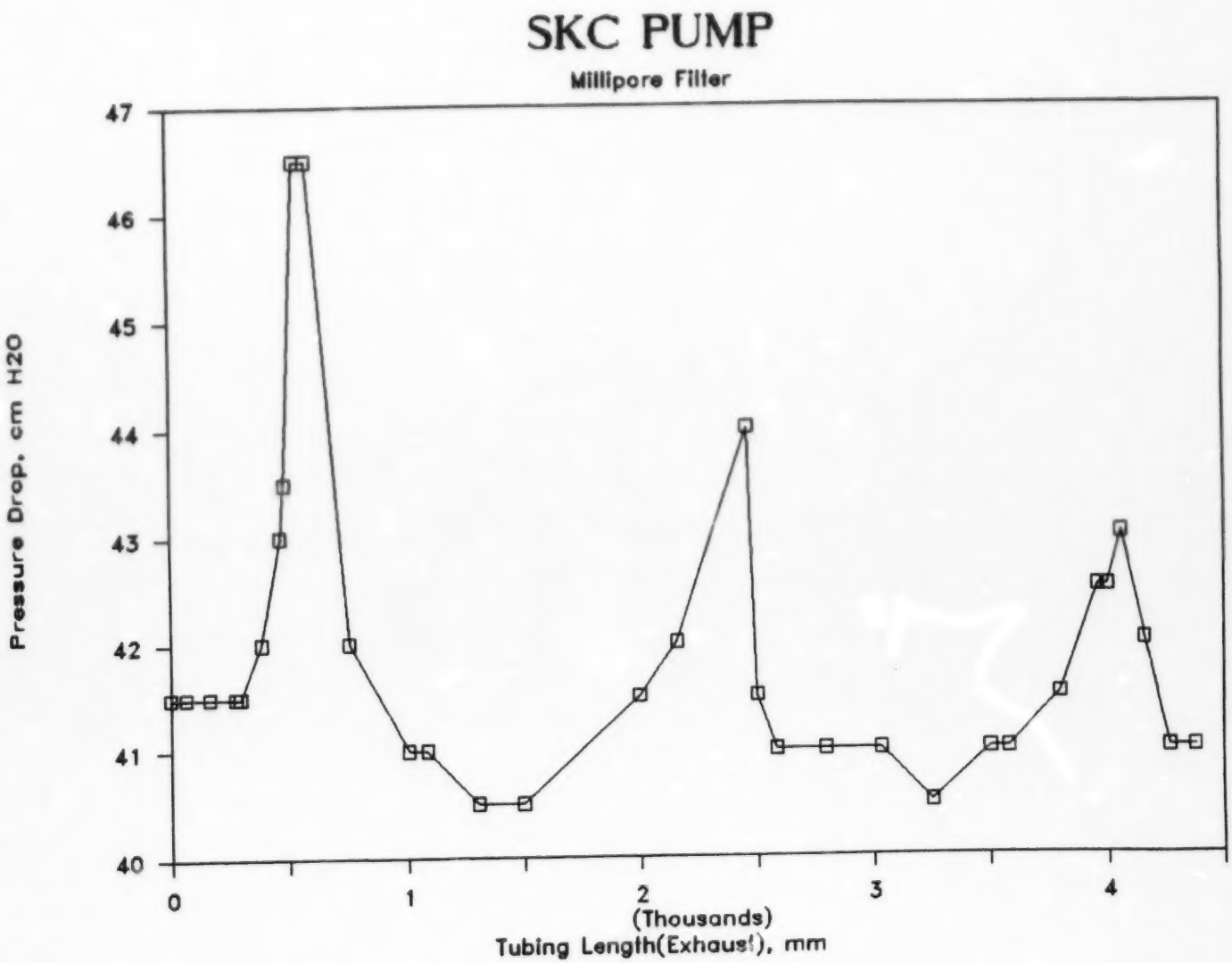

Fig. 58 - Pressure drop across the filter versus exhaust tubing length for the SKC pump. Millipore filter.

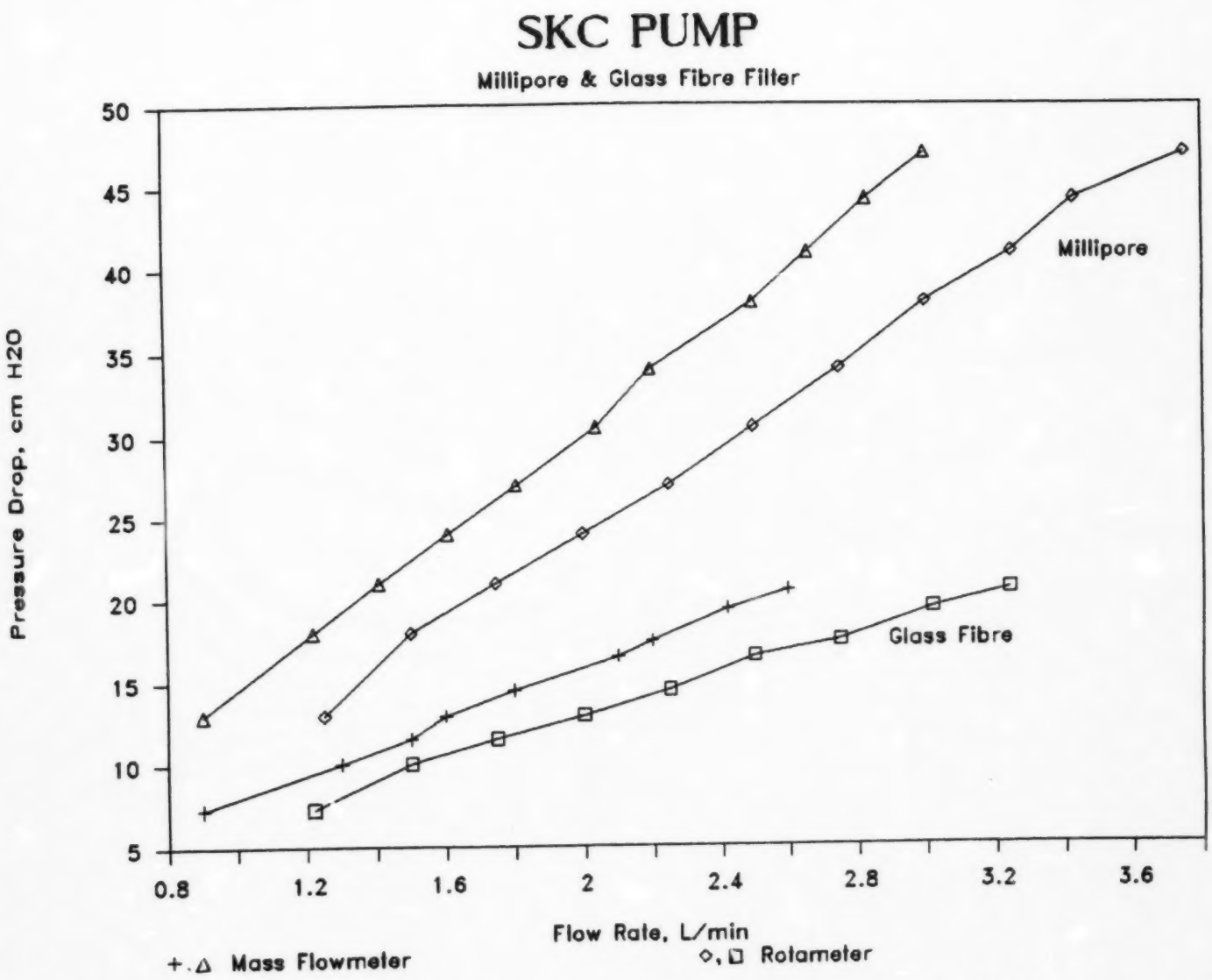

Fig. 59 - Pressure drop across the filter versus airflow rate for Millipore filters (upper graphs), and Glass fibre filters (lower graphs). SKC pump.

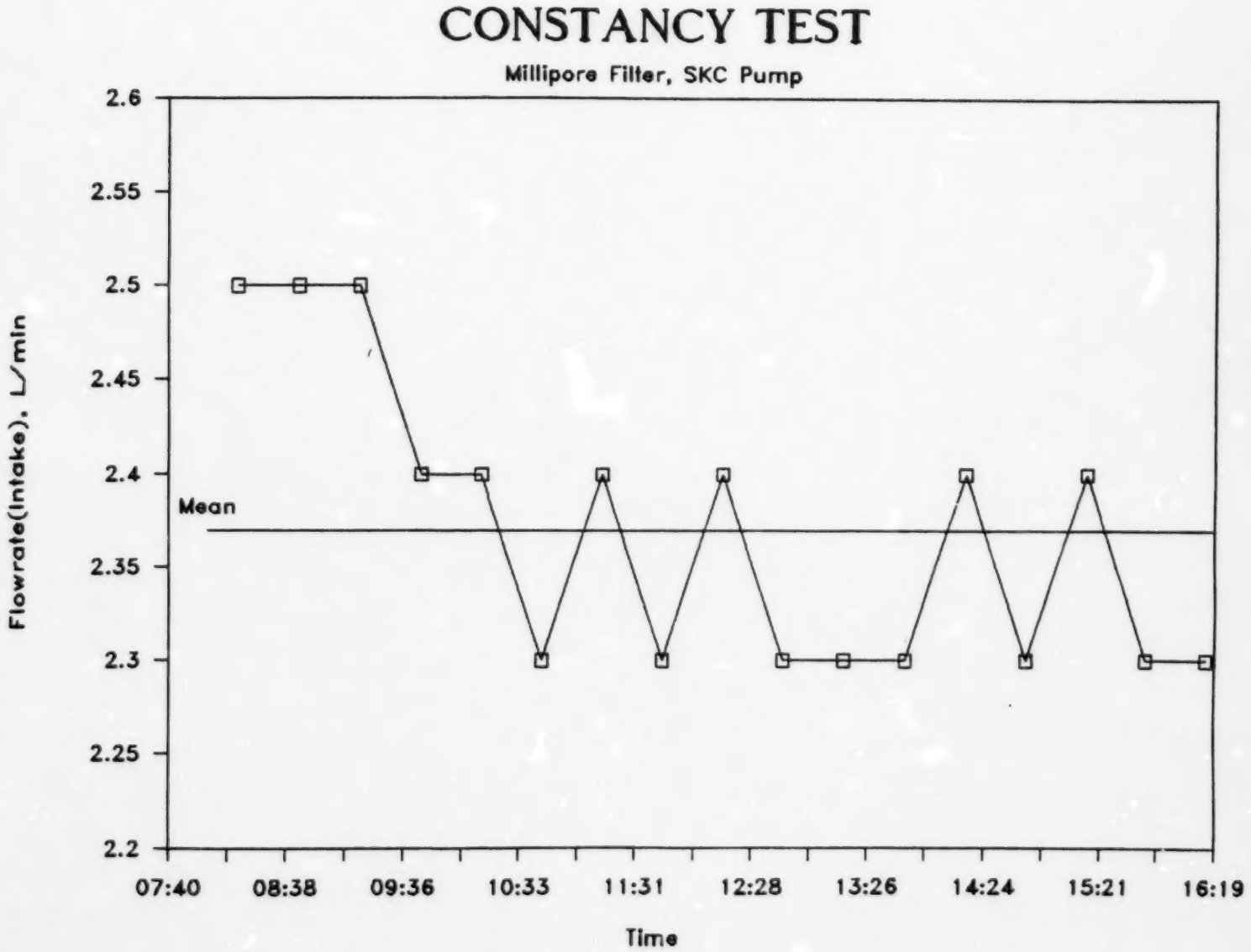

Fig. 60 - Airflow rate versus time for the SKC pump. Millipore filter.

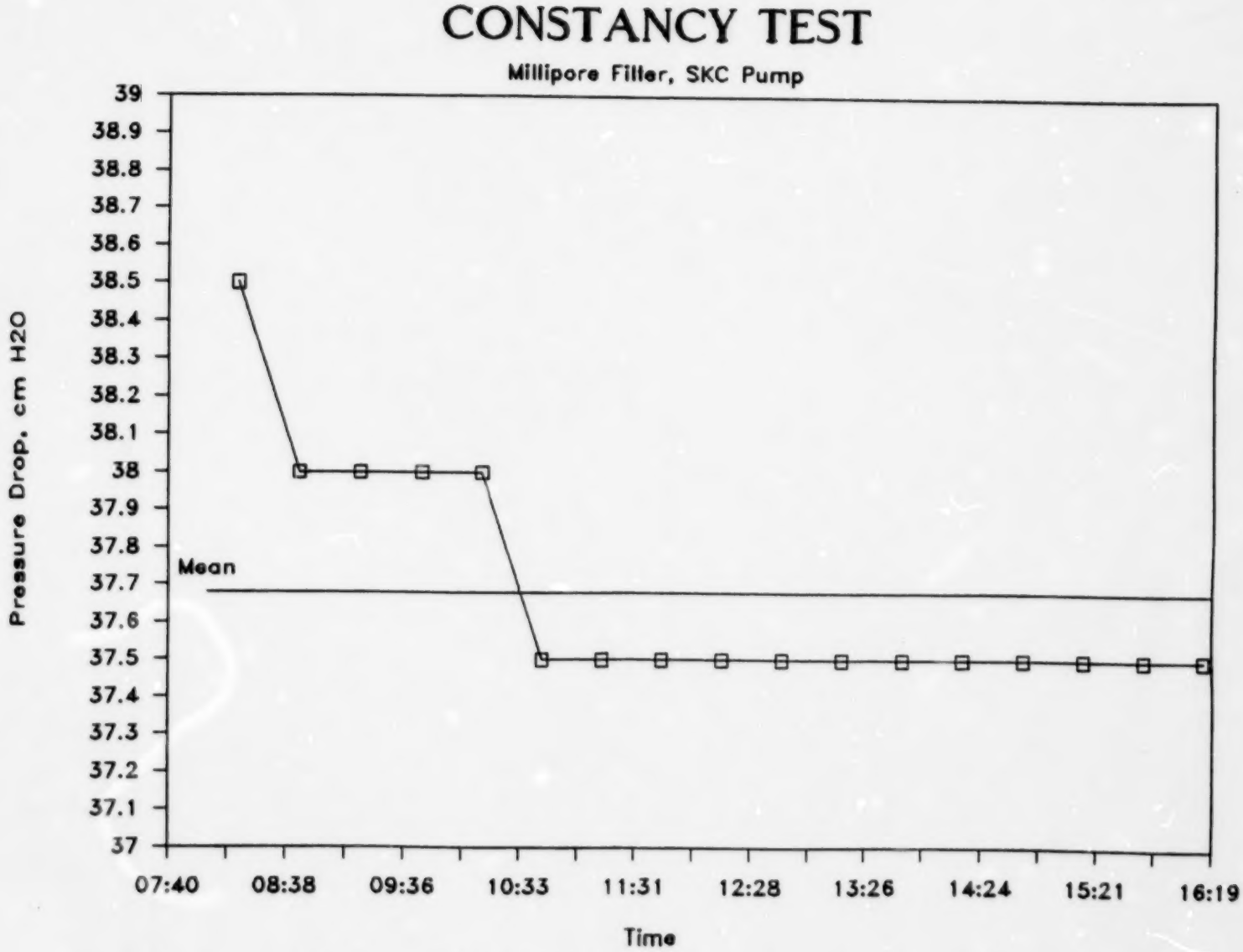

Fig. 61 - Pressure drop across the filter versus time for the SKC pump. Millipore filter.

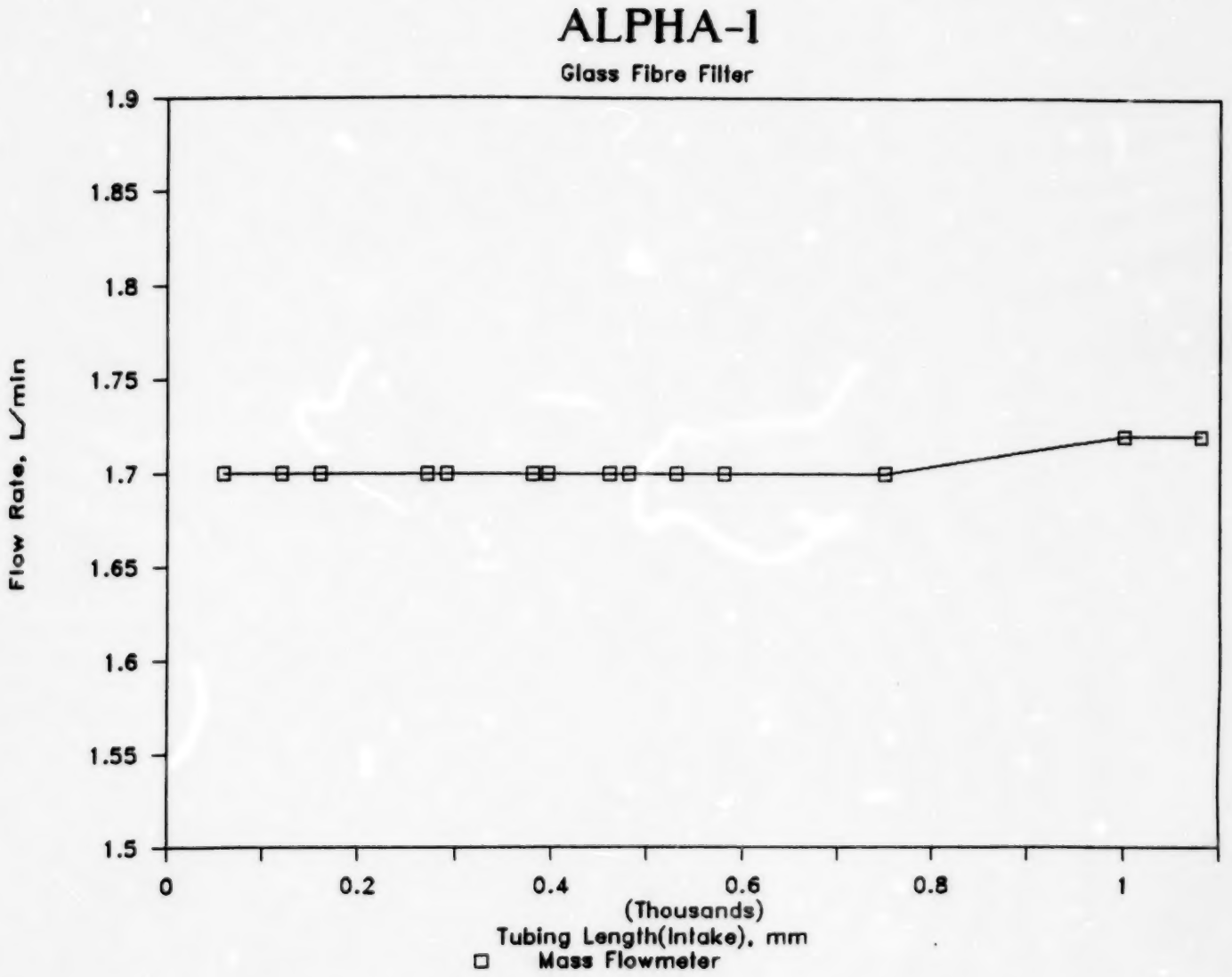

Fig. 62 - Airflow rate versus intake tubing length for the Alpha-1 pump. Glass fibre filter.

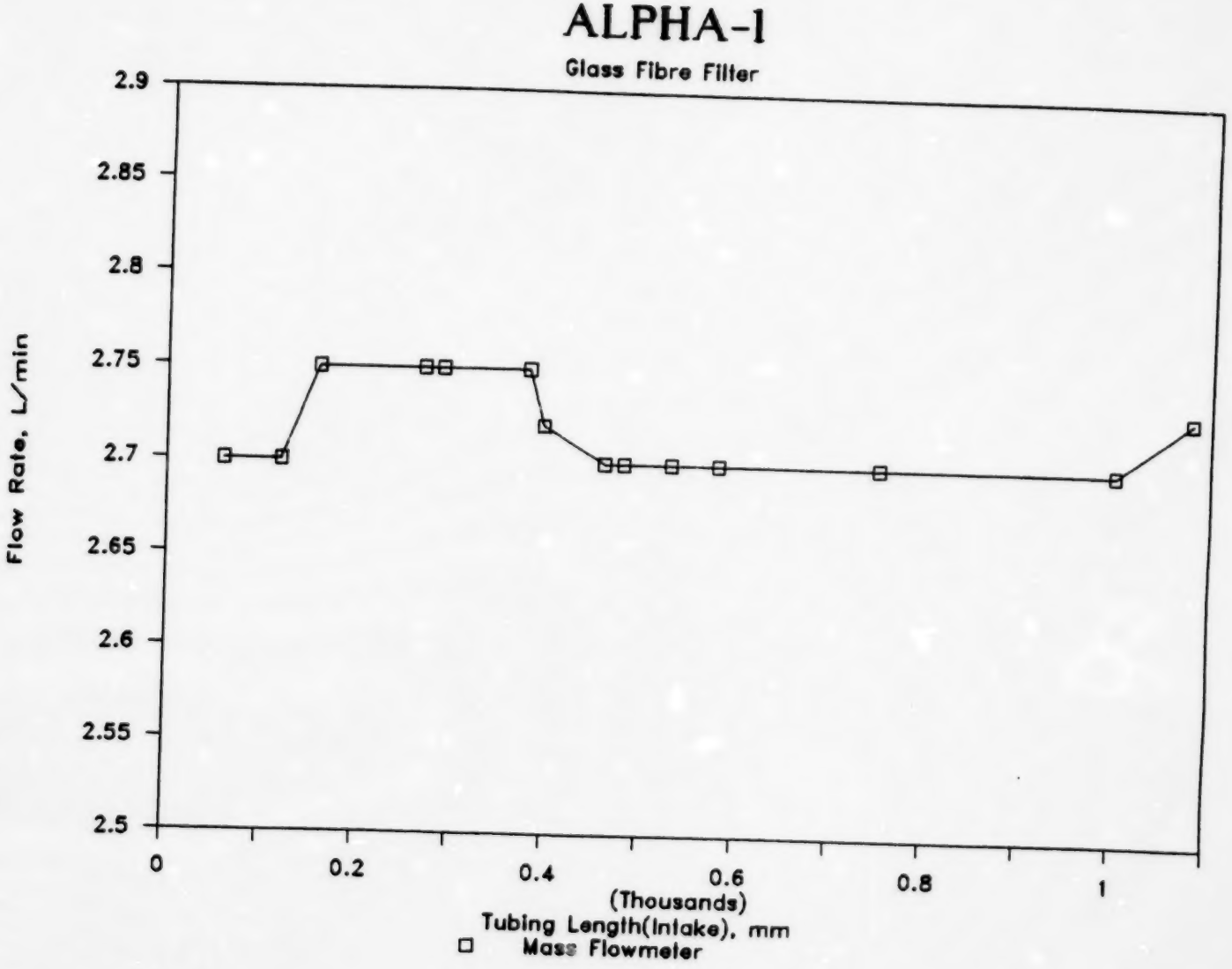

Fig. 63 - Airflow rate versus intake tubing length for the Alpha-1 pump. Glass fibre filter.

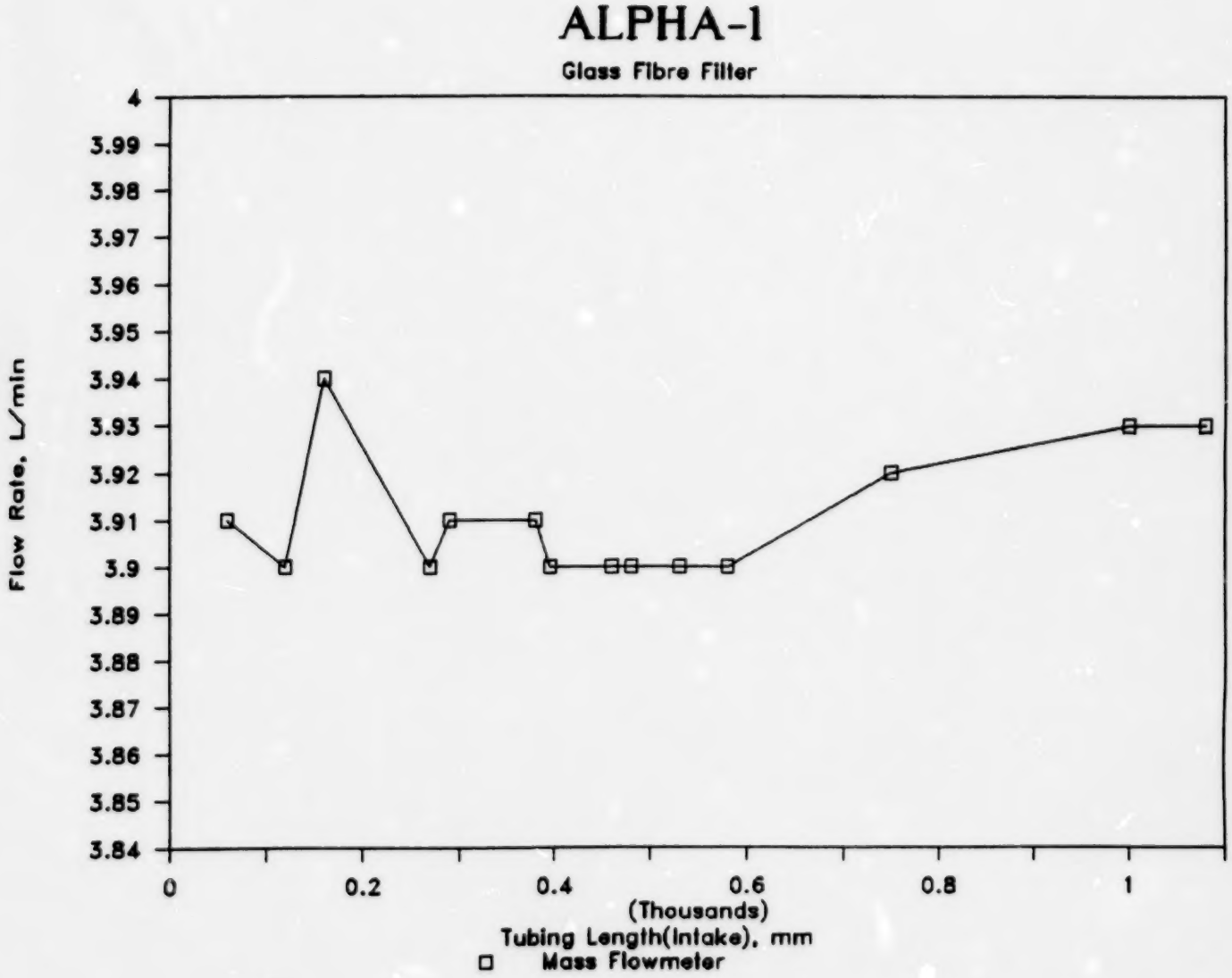

Fig. 64 - Airflow rate versus intake tubing length for the Alpha-1 pump. Glass fibre filter.

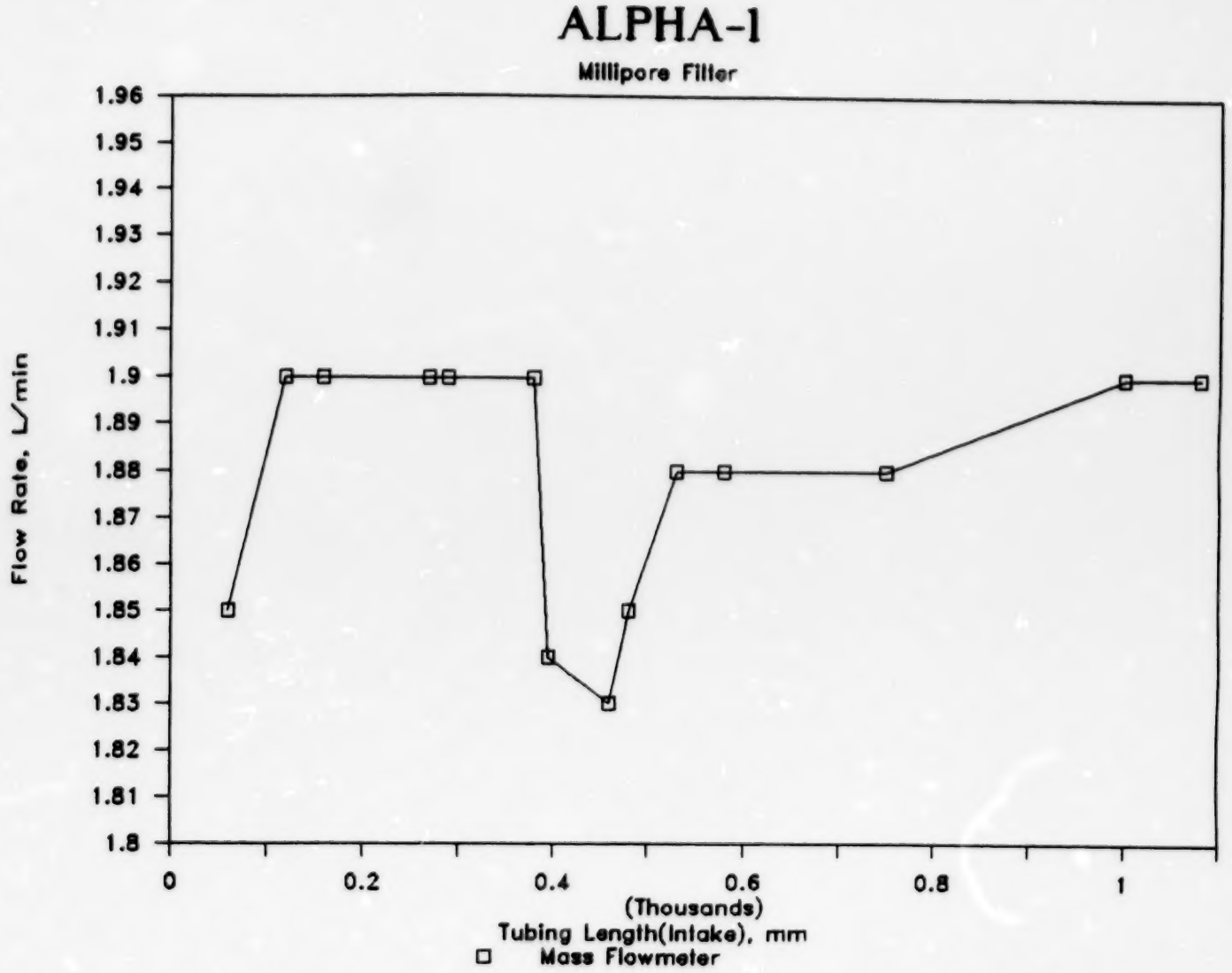

Fig. 65 - Airflow rate versus intake tubing length for the Alpha-1 pump. Millipore filter.

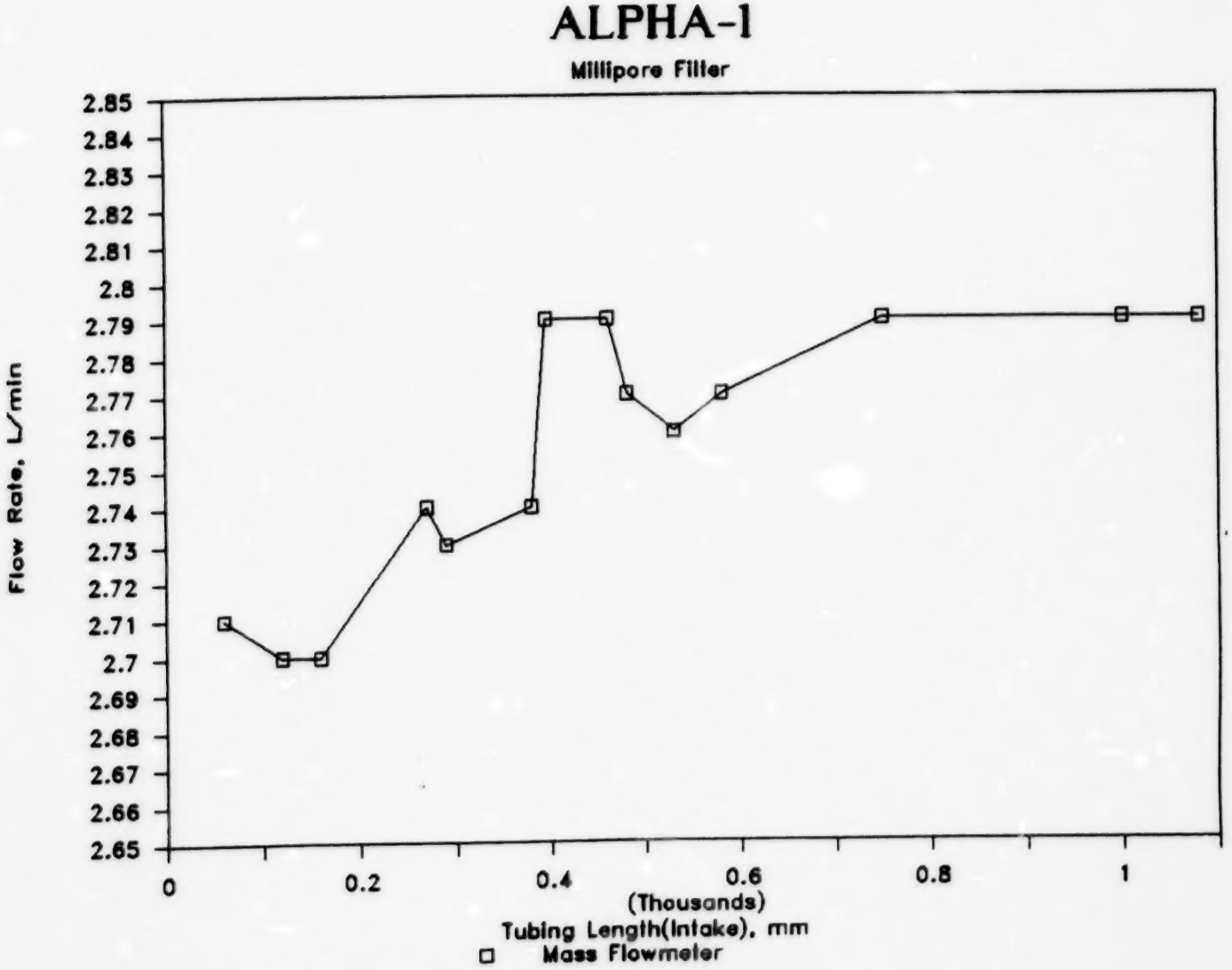

Fig. 66 - Airflow rate versus intake tubing length for the Alpha-1 pump. Millipore filter.

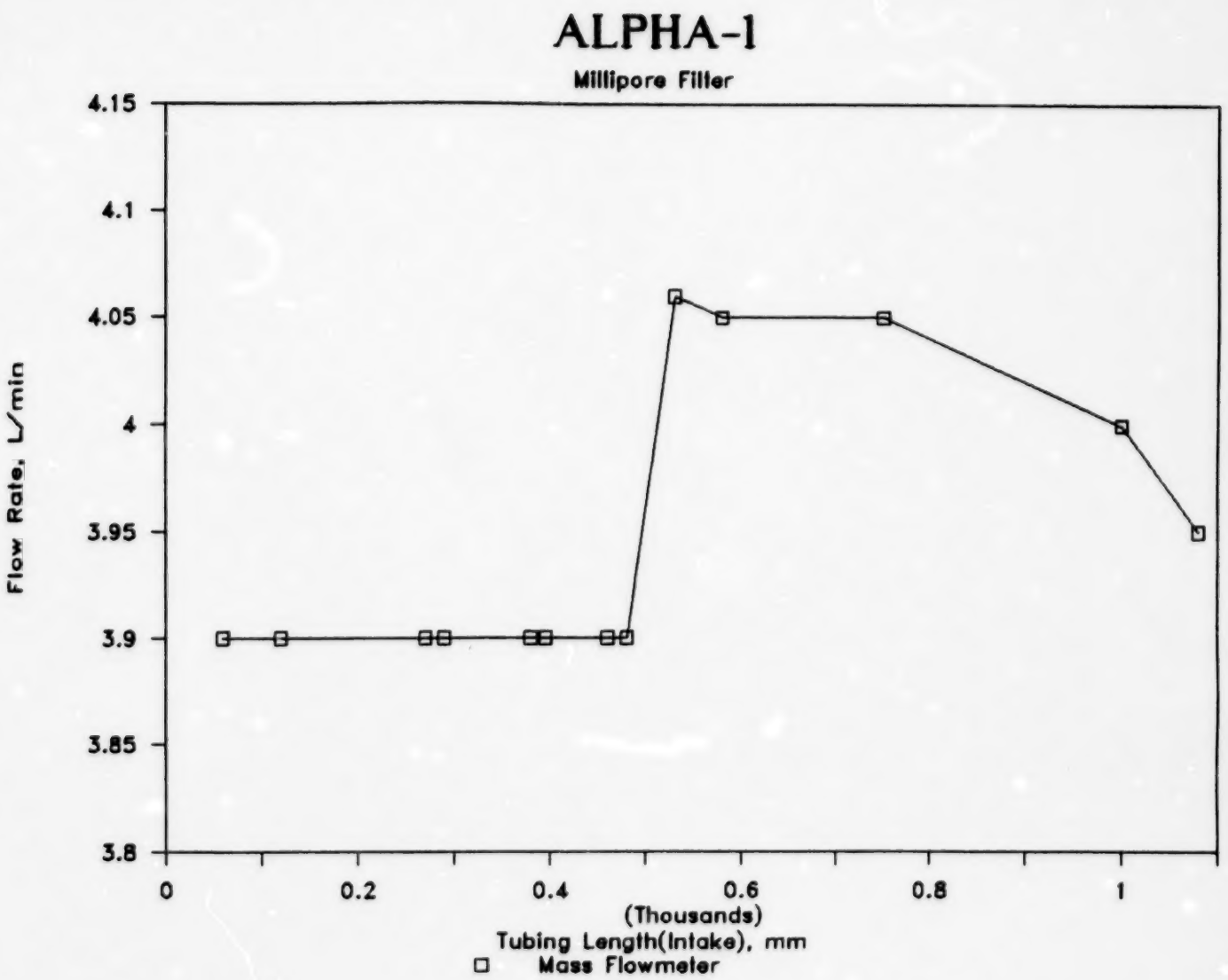

Fig. 67 - Airflow rate versus intake tubing length for the Alpha-1 pump. Millipore filter.

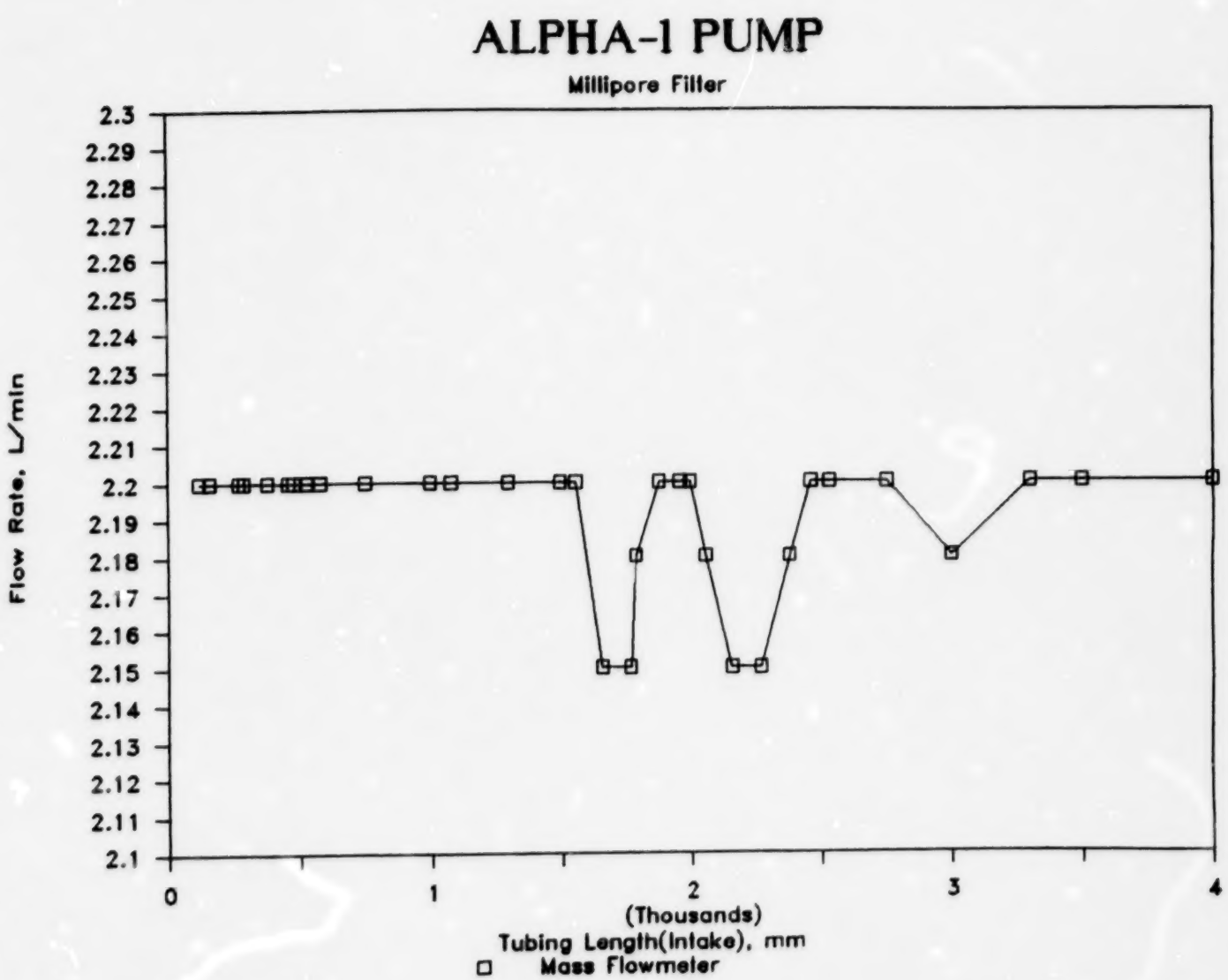

Fig. 68 - Airflow rate versus intake tubing length for the Alpha-1 pump. Millipore filter.

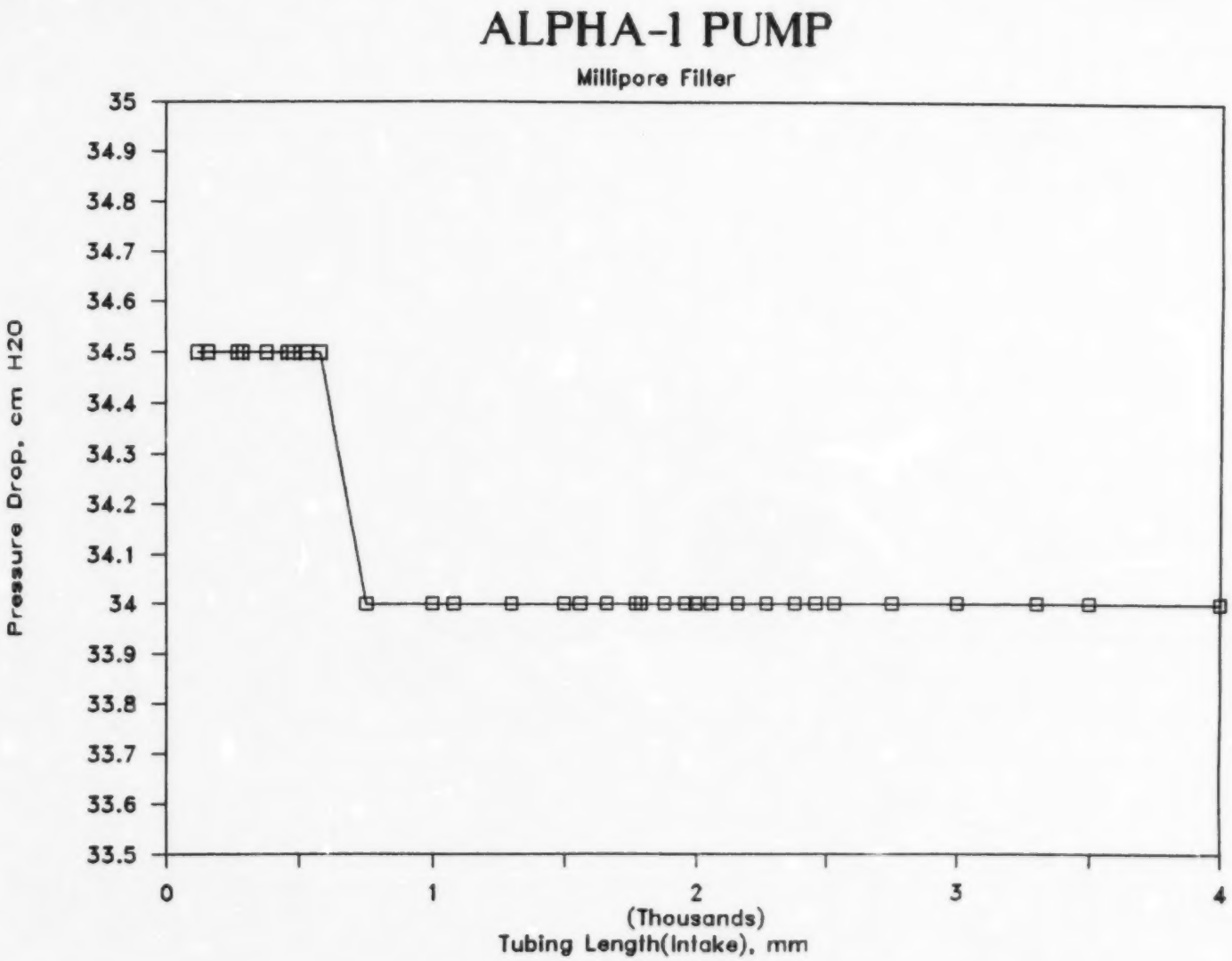

Fig. 69 - Pressure drop across the filter versus intake tubing length for the Alpha-1 pump. Millipore filter.

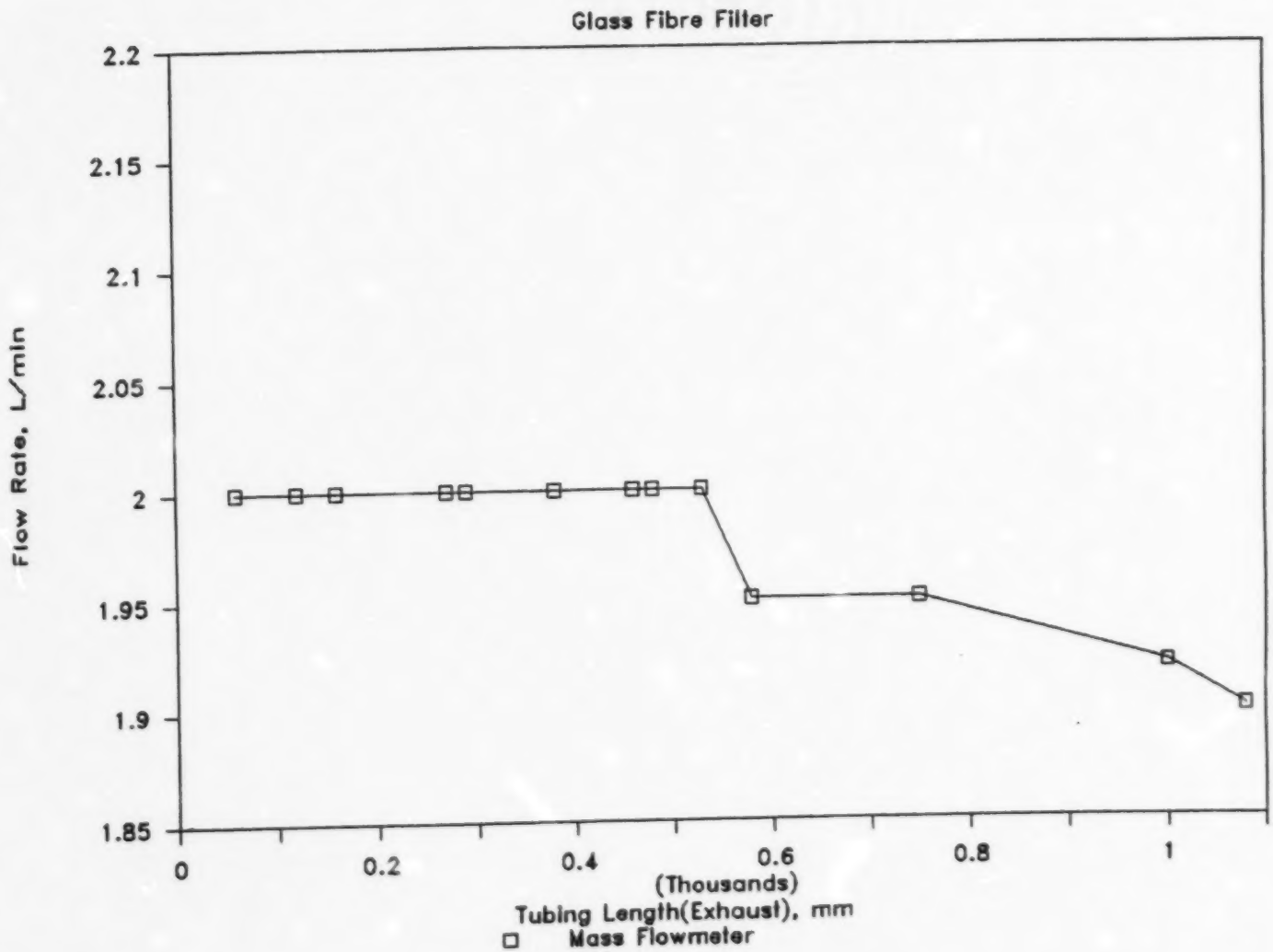

Fig. 70 - Airflow rate versus exhaust tubing length for the Alpha-1 pump. Glass fibre filter.

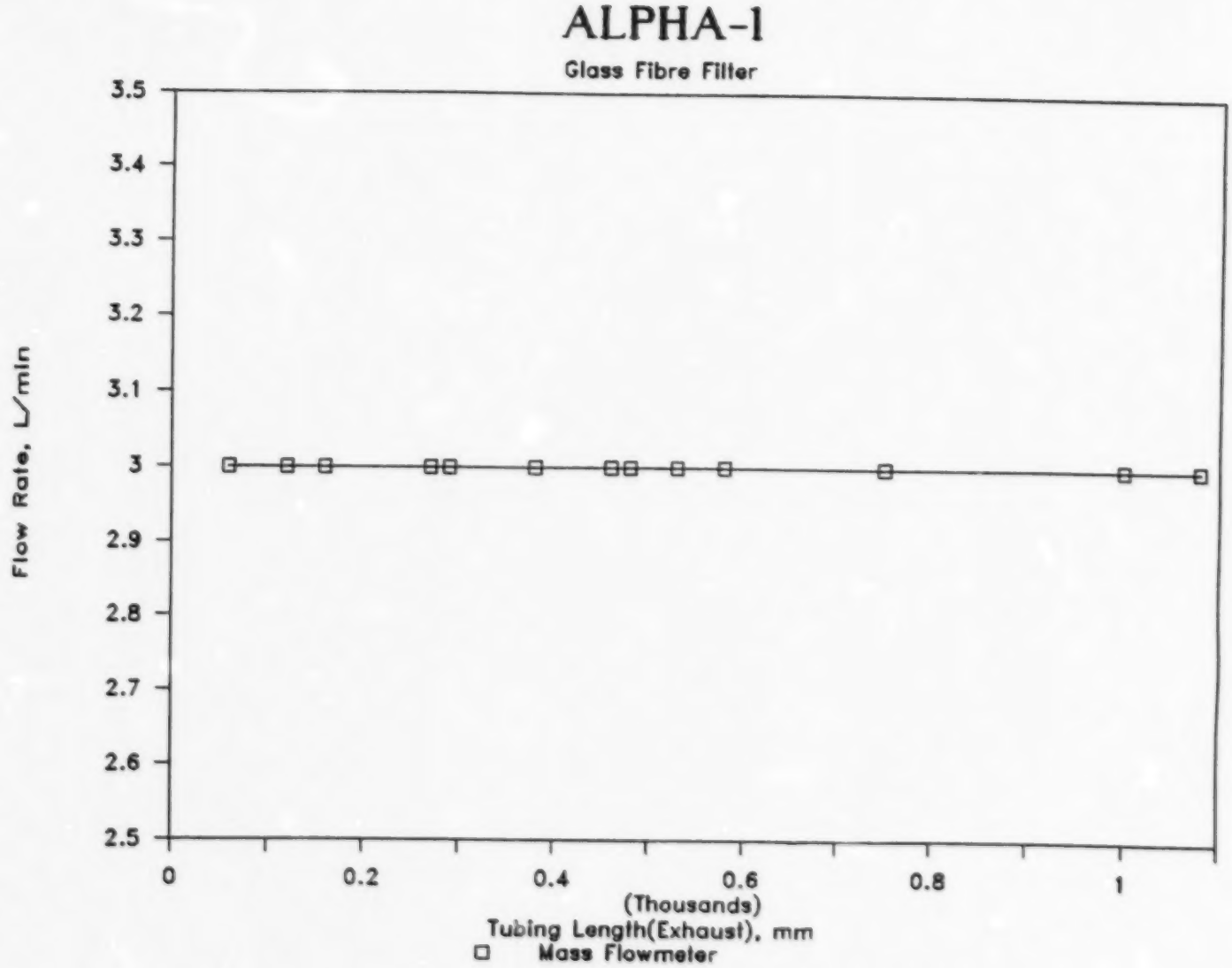

Fig. 71 - Airflow rate versus exhaust tubing length for the Alpha-1 pump. Glass fibre filter.

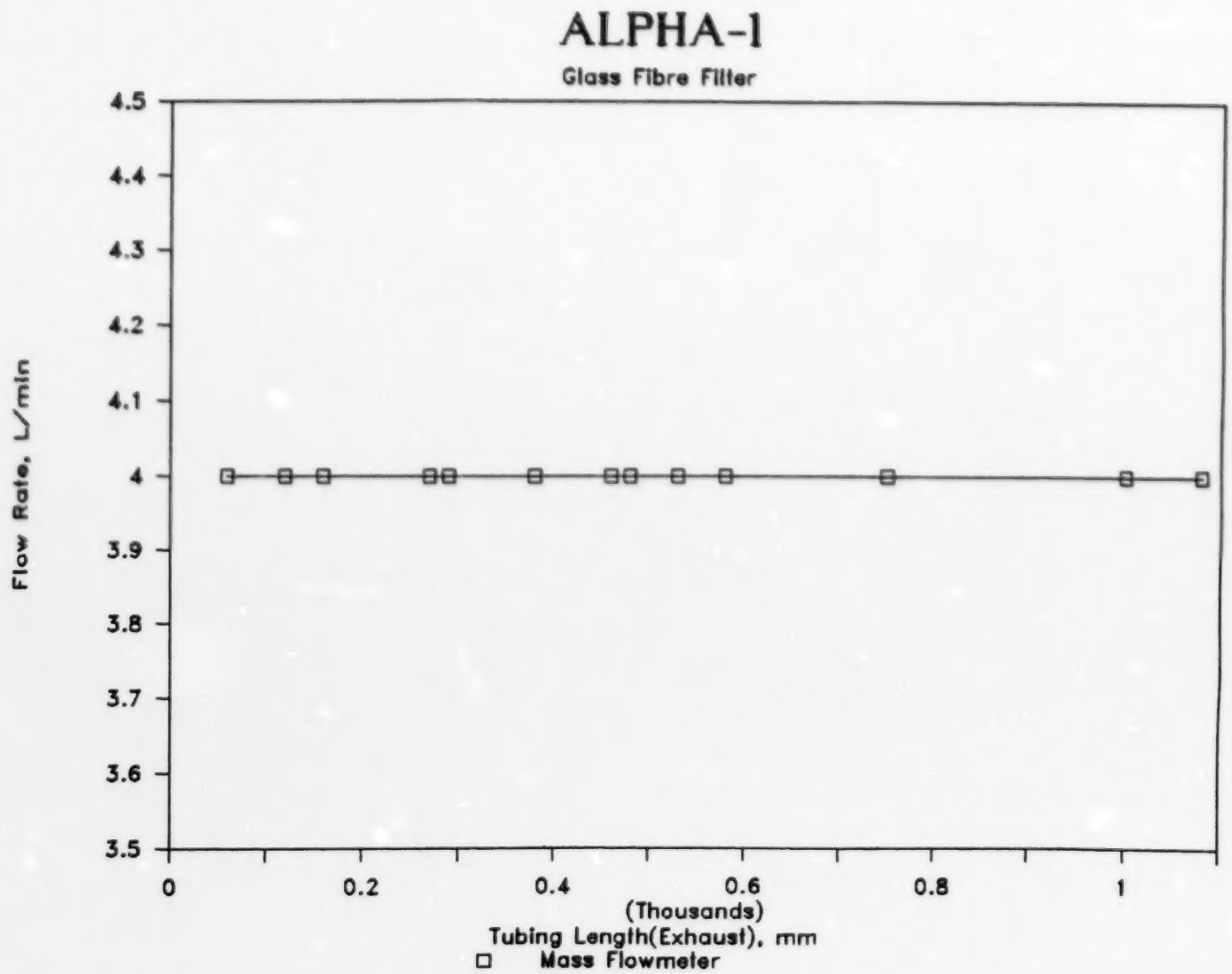

Fig. 72 - Airflow rate versus exhaust tubing length for the Alpha-1 pump. Glass fibre filter.

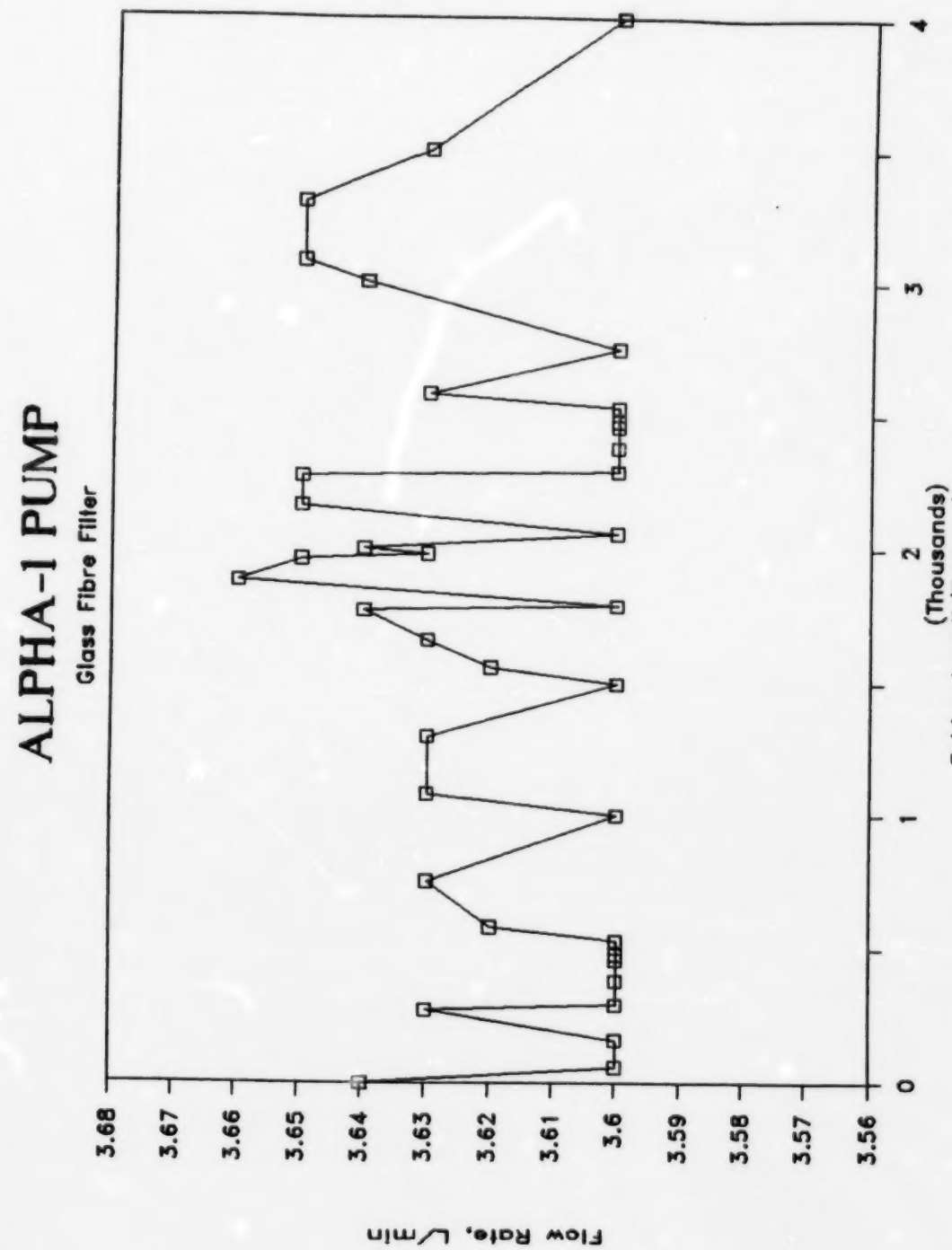

Fig. 73 - Airflow rate versus exhaust tubing length for the Alpha-1 pump. Glass fibre filter.

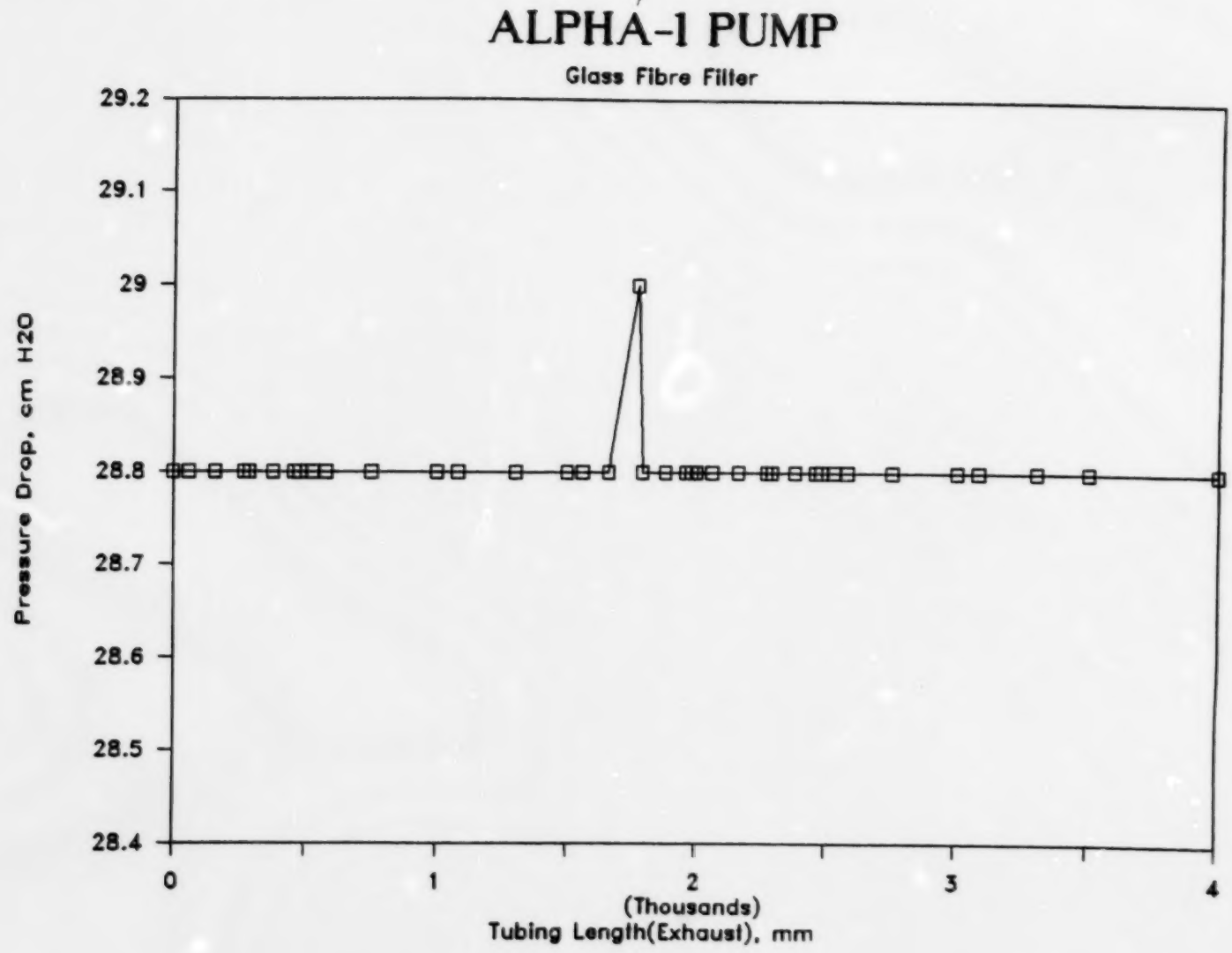

Fig. 74 - Pressure drop across the filter versus exhaust tubing length for the Alpha-1 pump. Glass fibre filter.

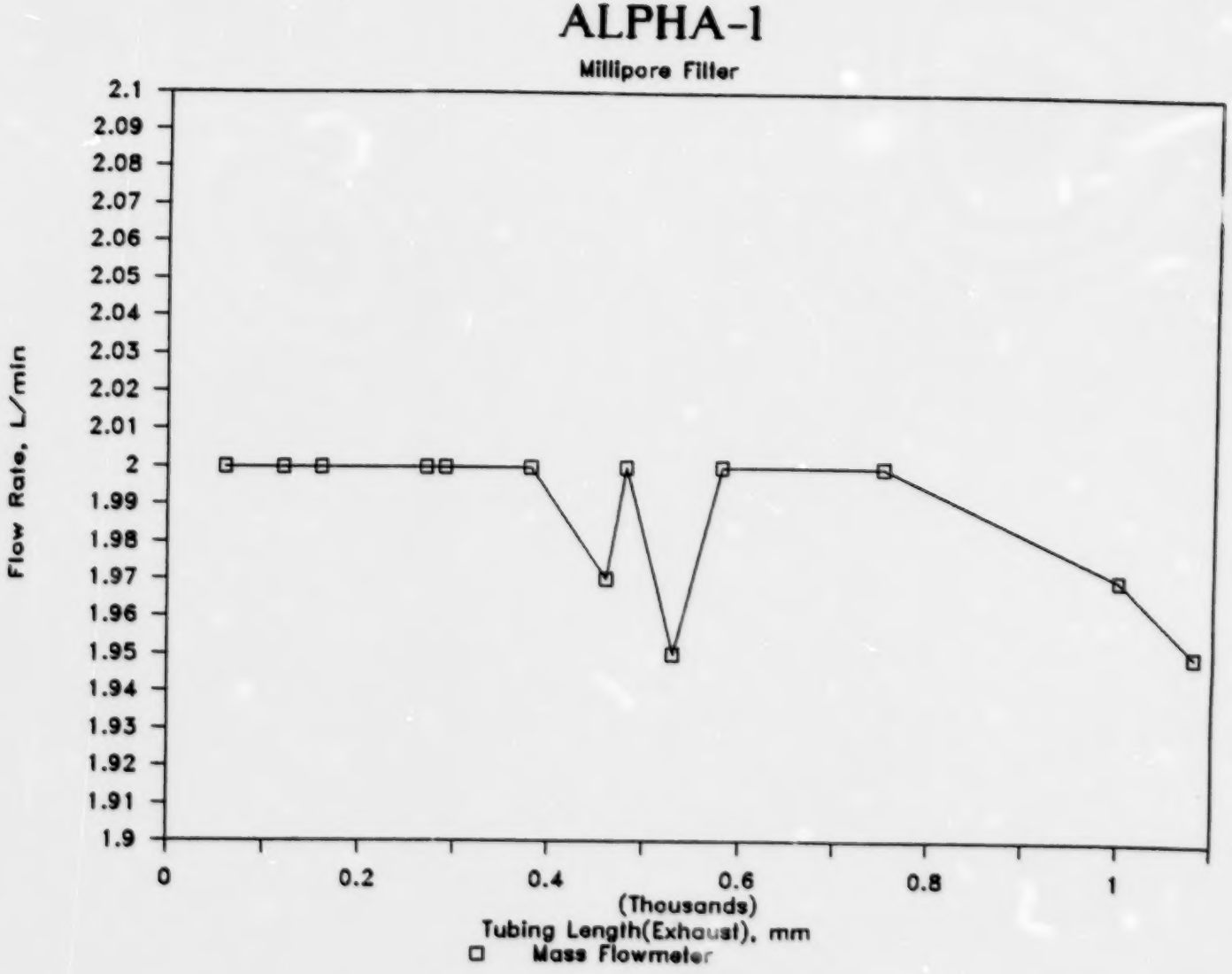

Fig. 75 - Airflow rate versus exhaust tubing length for the Alpha-1 pump. Millipore filter.

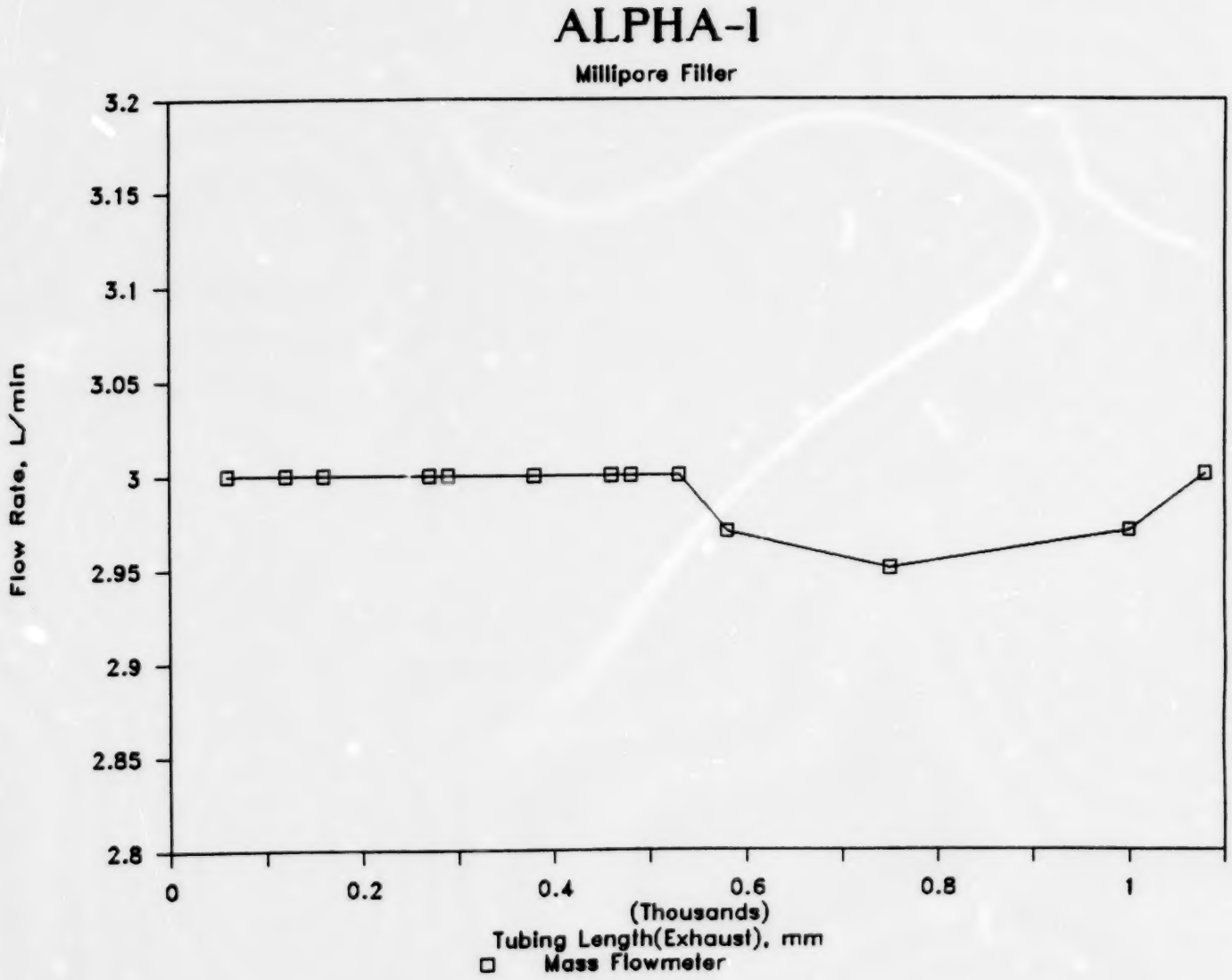

Fig. 76 - Airflow rate versus exhaust tubing length for the Alpha-1 pump. Millipore filter.

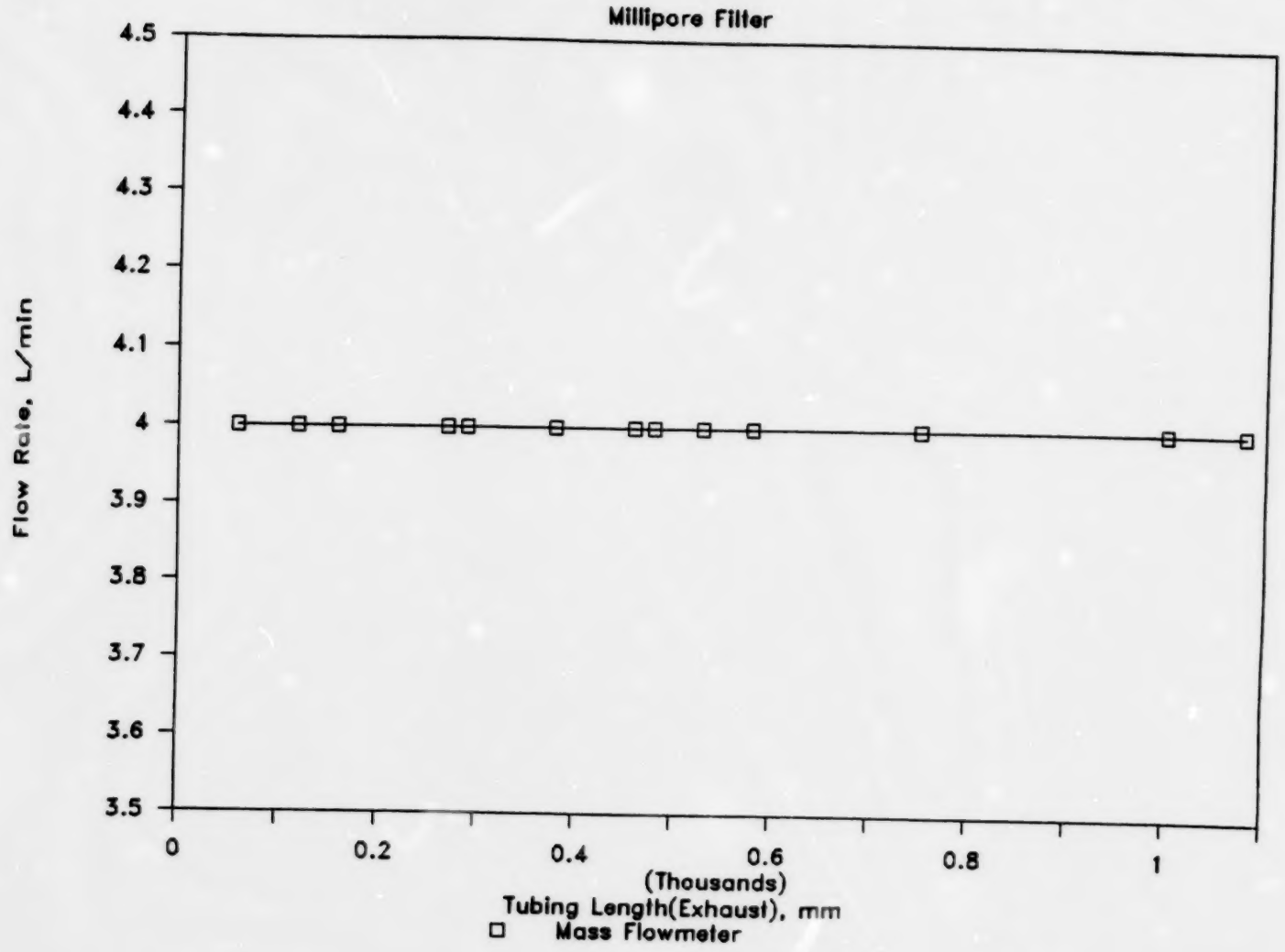

Fig. 77 - Airflow rate versus exhaust tubing length for the Alpha-1 pump. Millipore filter.

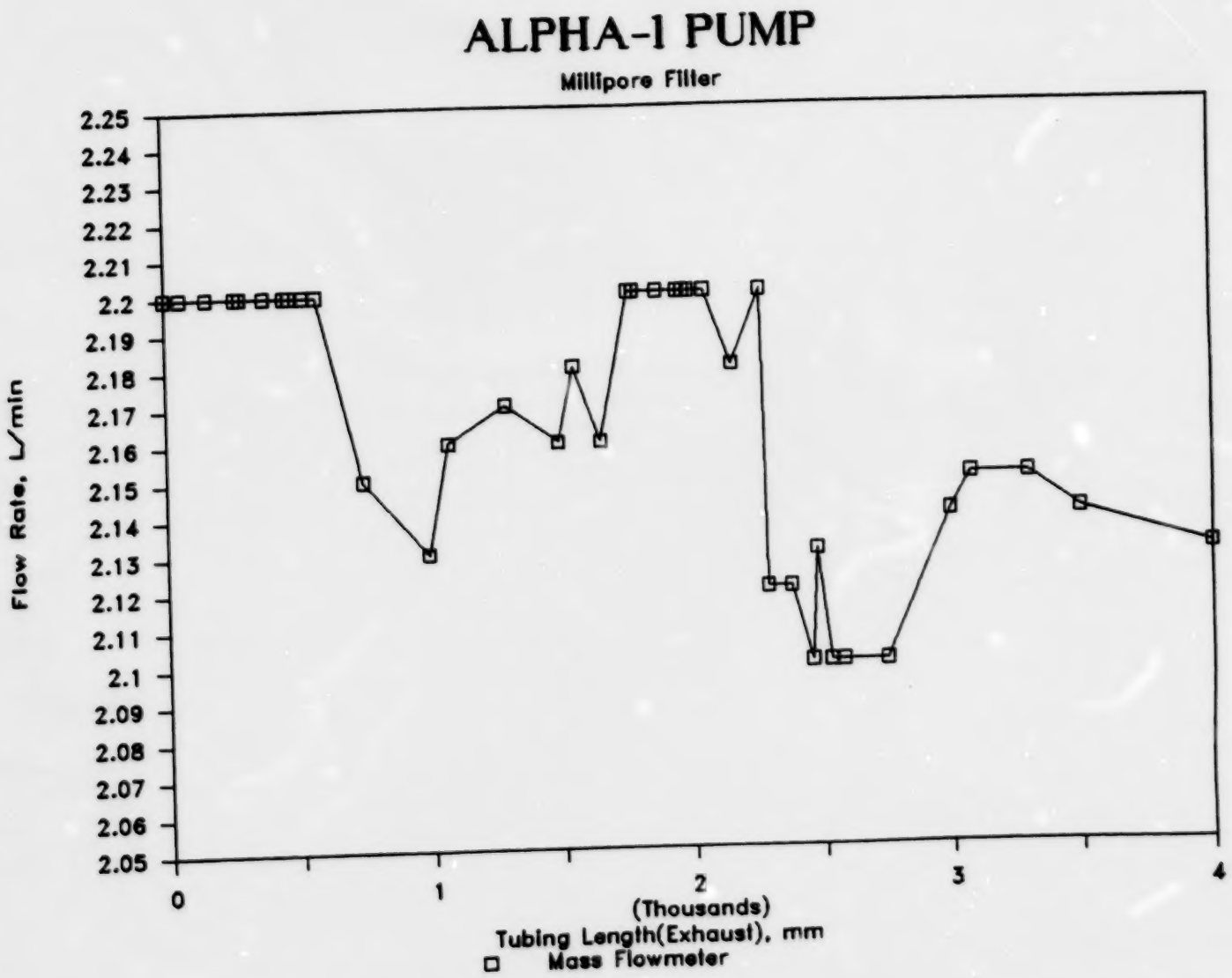

Fig. 78 - Airflow rate versus exhaust tubing length for the Alpha-1 pump. Millipore filter.

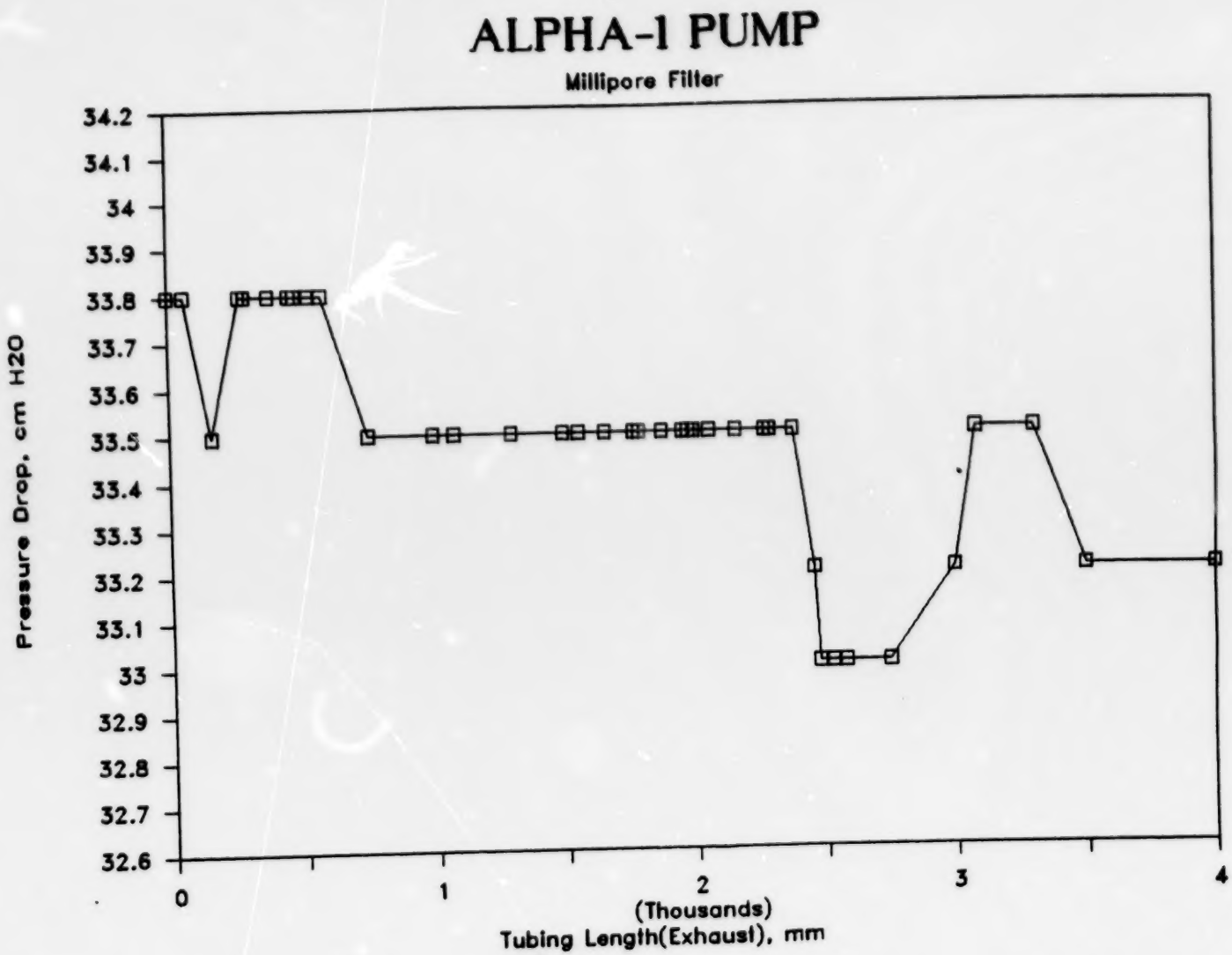

Fig. 79 - Pressure drop across the filter versus exhaust tubing length for the Alpha-1 pump. Millipore filter.

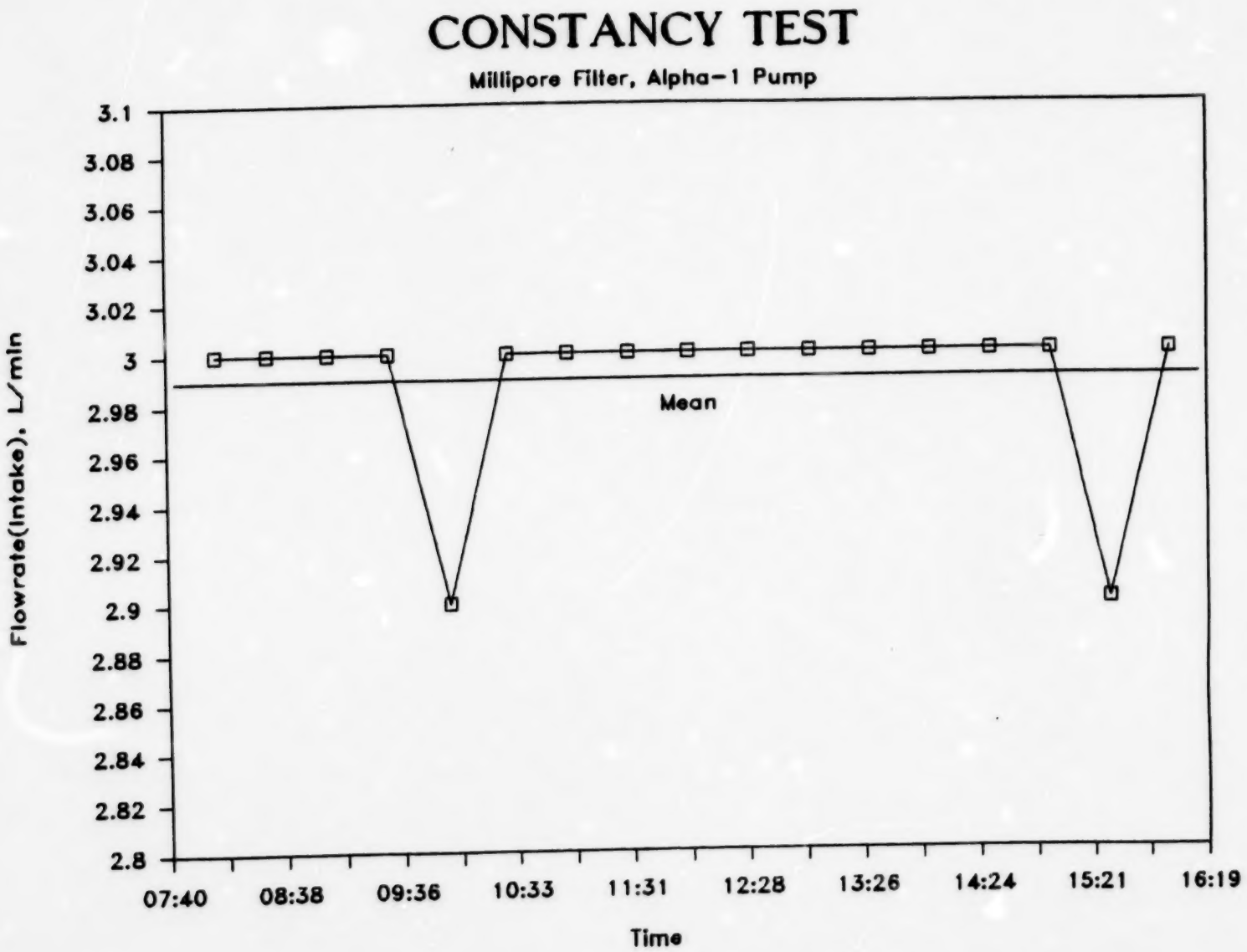

Fig. 80 - Airflow rate versus time for the Alpha-1 pump. Millipore filter.

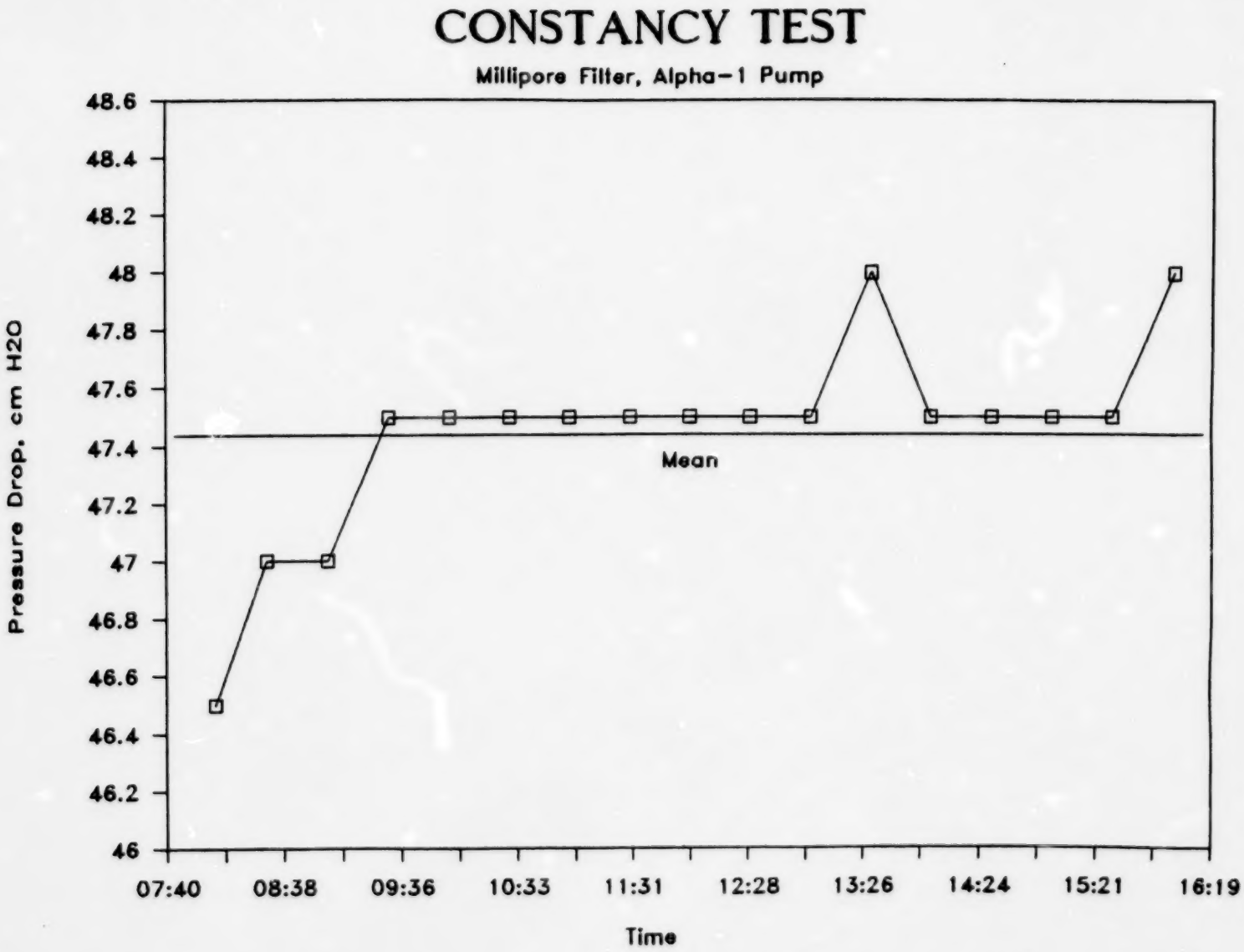

Fig. 81 - Pressure drop across the filter versus time for the Alpha-1 pump. Millipore filter.

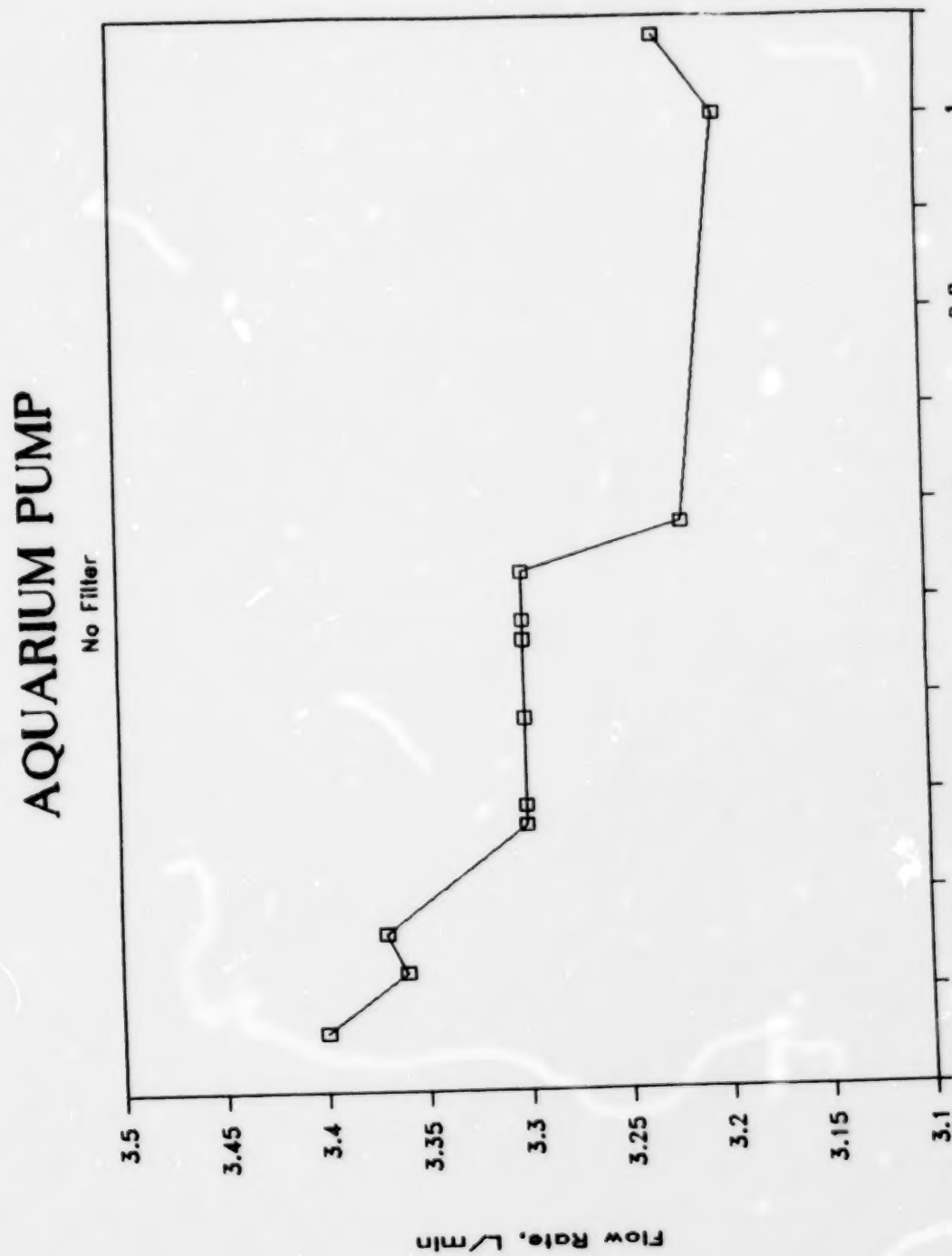

Fig. 82 - Airflow rate versus intake tubing length for the aquarium pump. No filter.

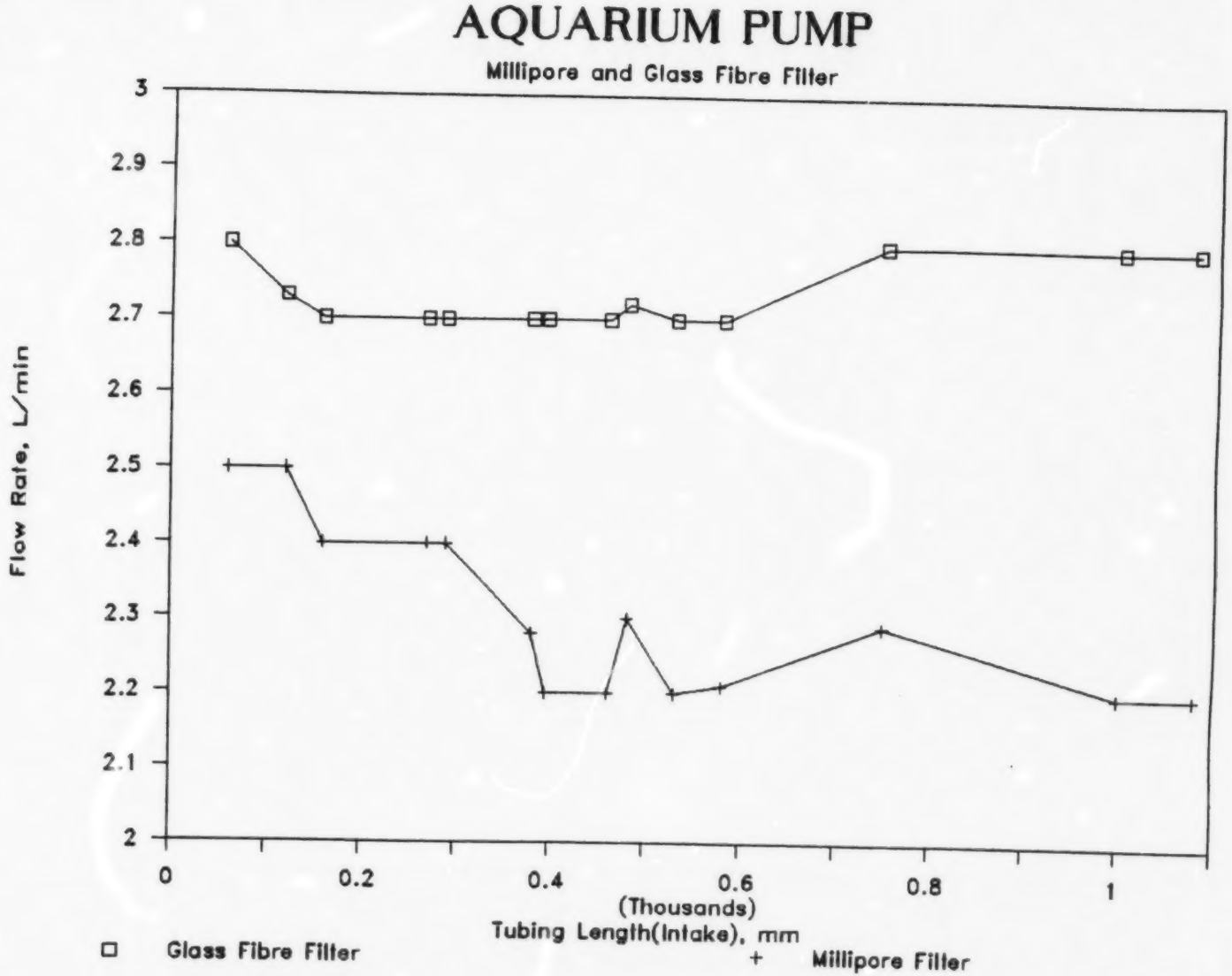

Fig. 83 - Airflow rate versus intake tubing length for the aquarium pump. Millipore filter (lower graph), and glass fibre filter (upper graph).

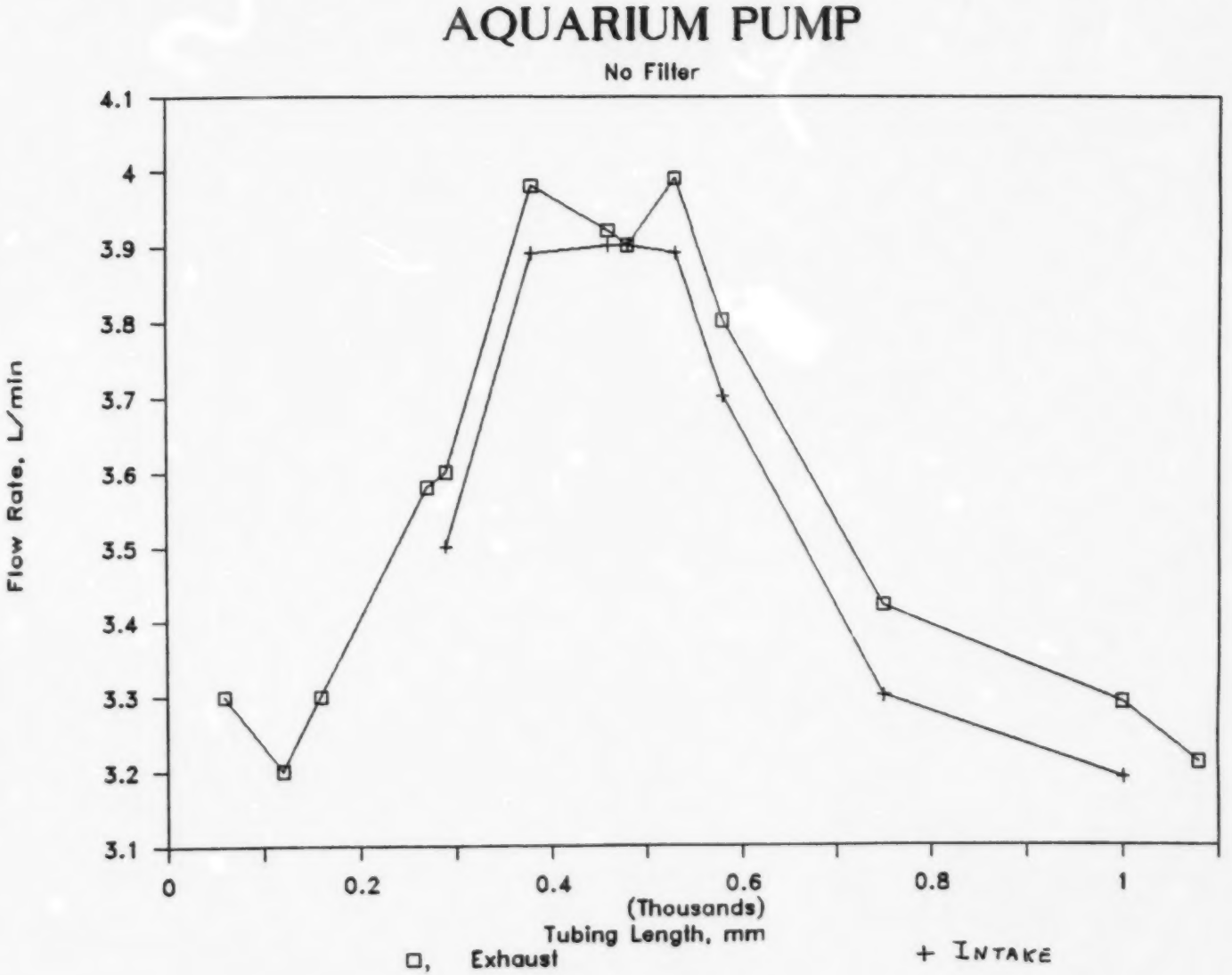

Fig. 84 - Airflow rate versus intake tubing length (lower graph), and exhaust tubing length (upper graph) for the aquarium pump. No filter.

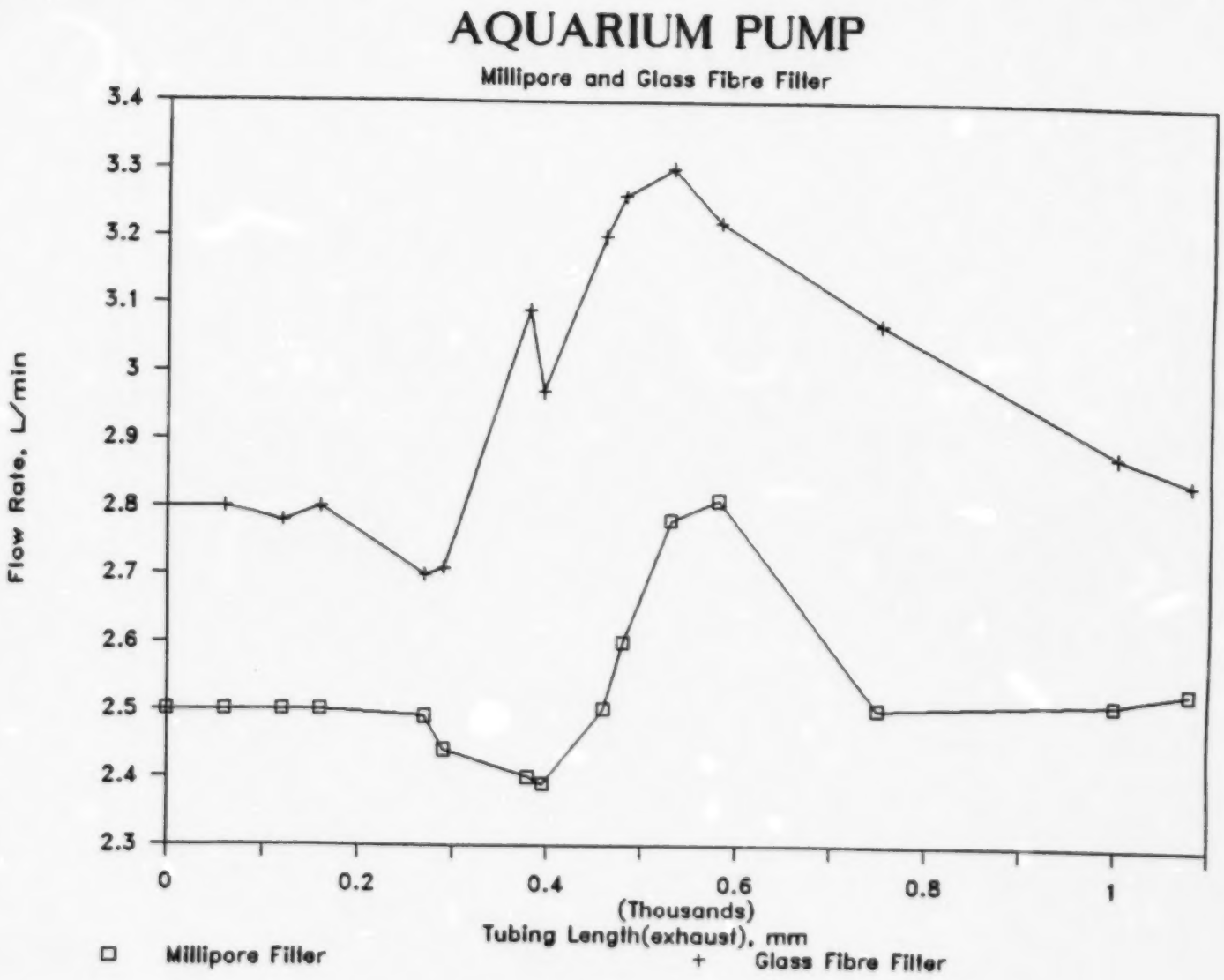

Fig. 85 - Airflow rate versus exhaust tubing length for the aquarium pump. Millipore filter (lower graph), and glass fibre filter (upper graph).

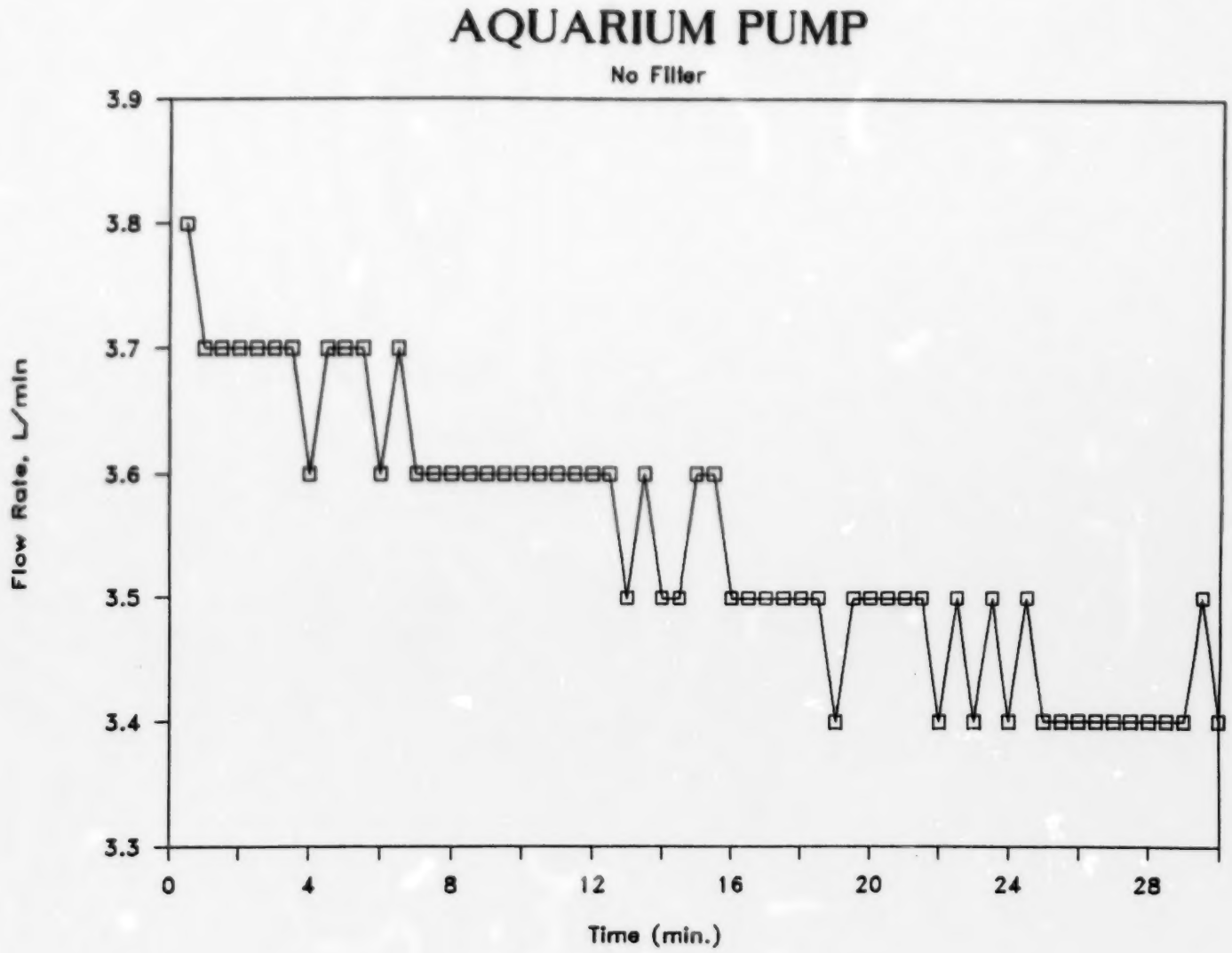

Fig. 86 - Airflow rate versus time for the aquarium pump. No filter.

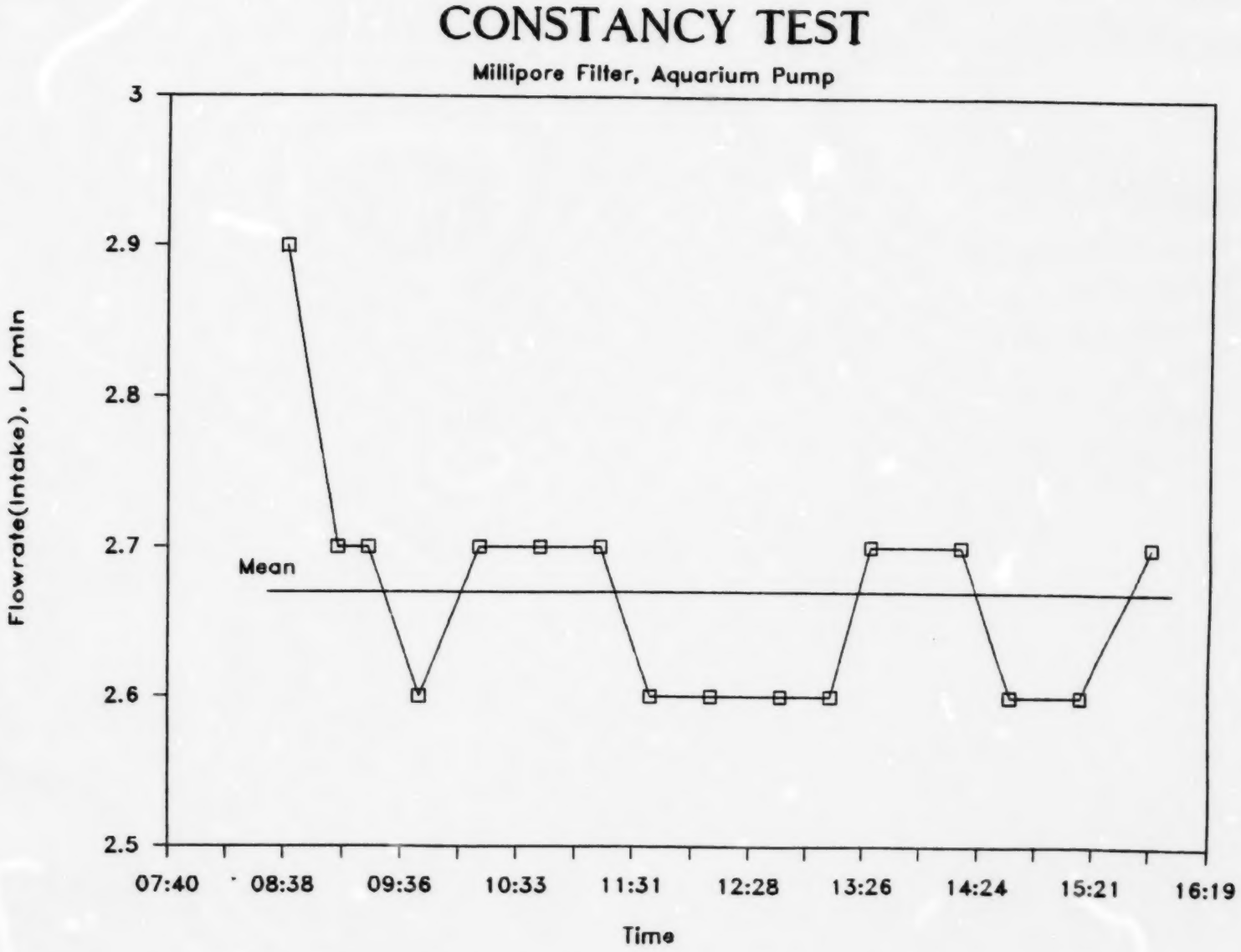

Fig. 87 - Airflow rate versus time for the aquarium pump. Millipore filter.

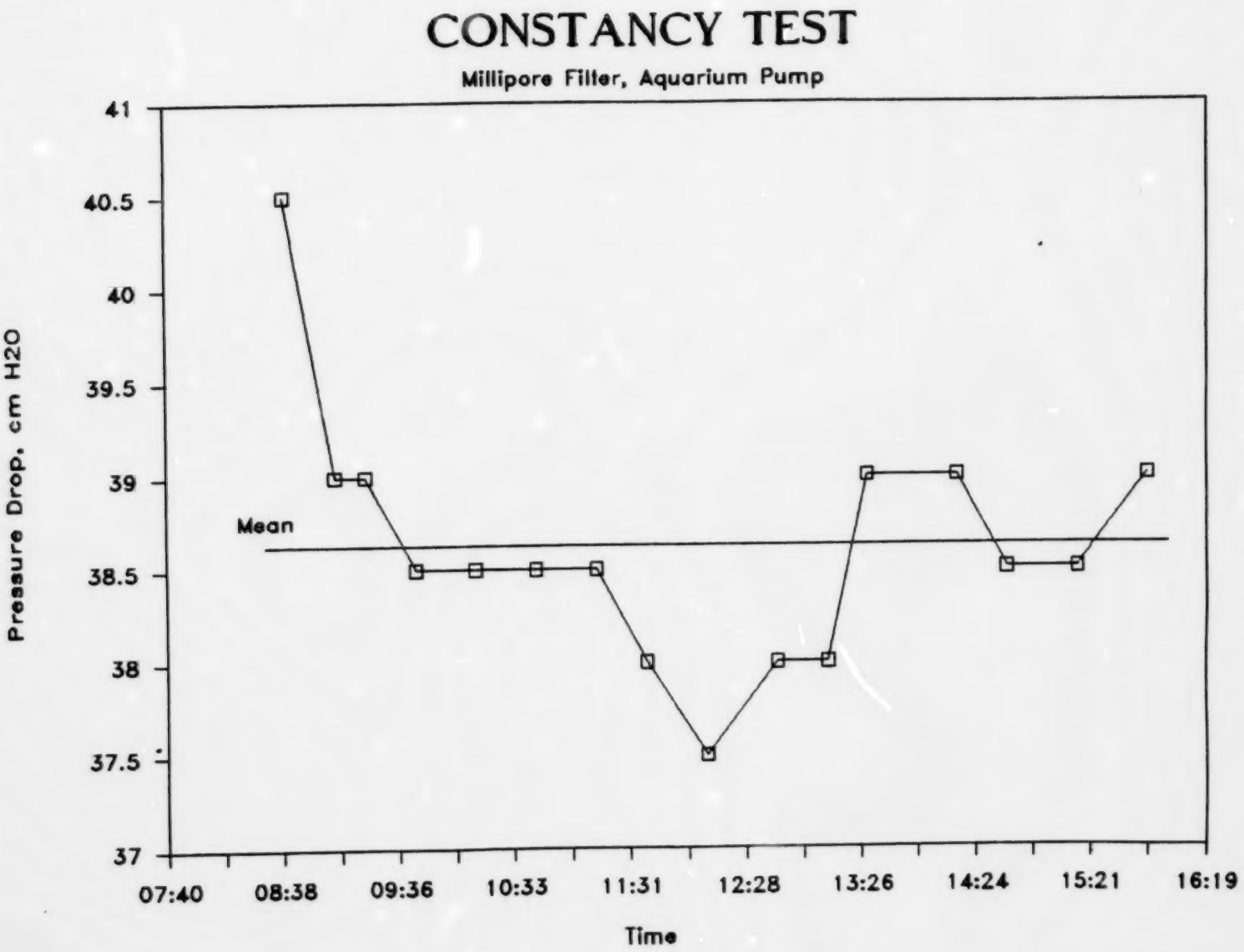

Fig. 88 - Pressure drop across the filter versus time for the aquarium pump. Millipore filter.

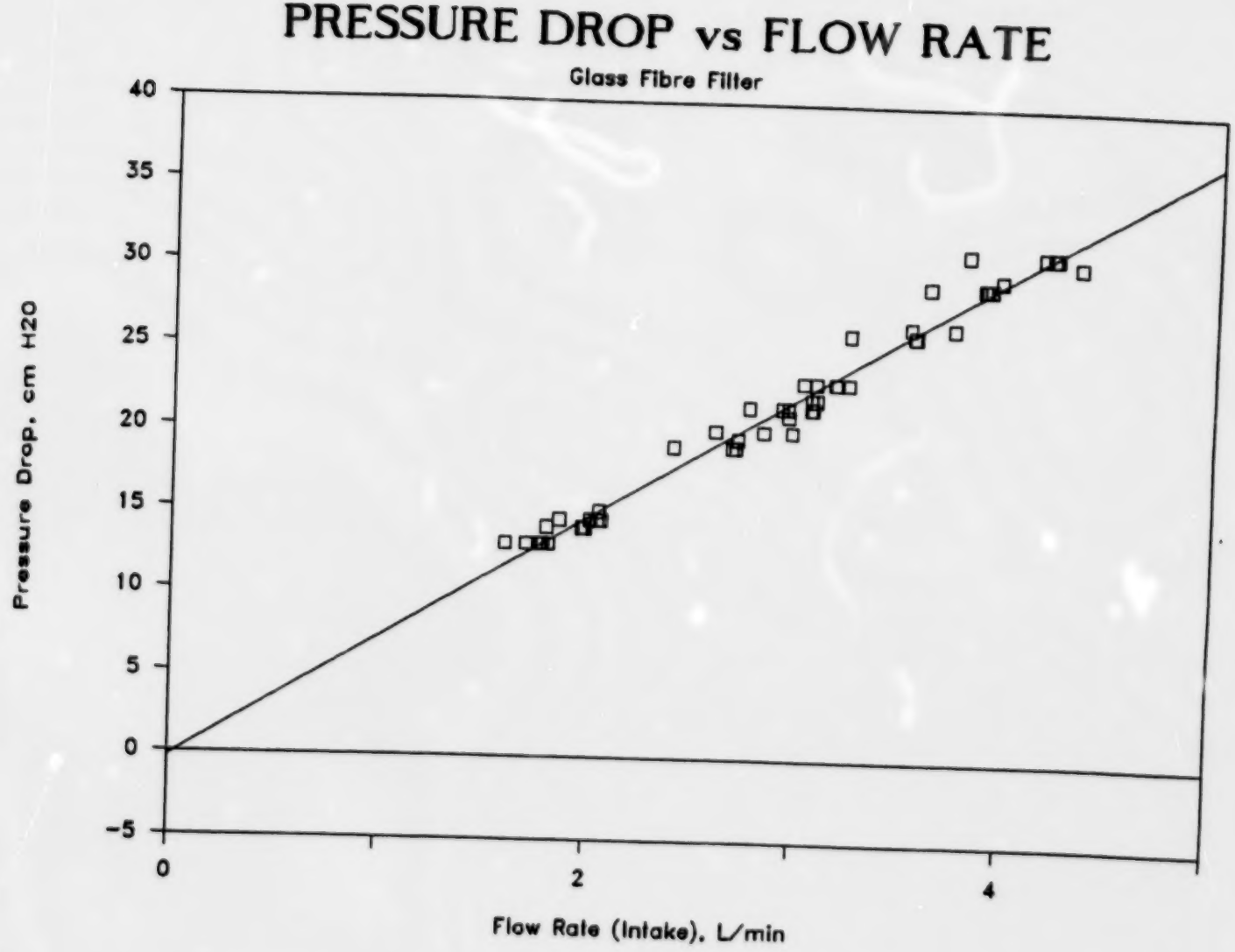

Fig. 89 - Pressure drop across the filter versus pump's intake airflow rate for all the pumps. Glass fibre filter.

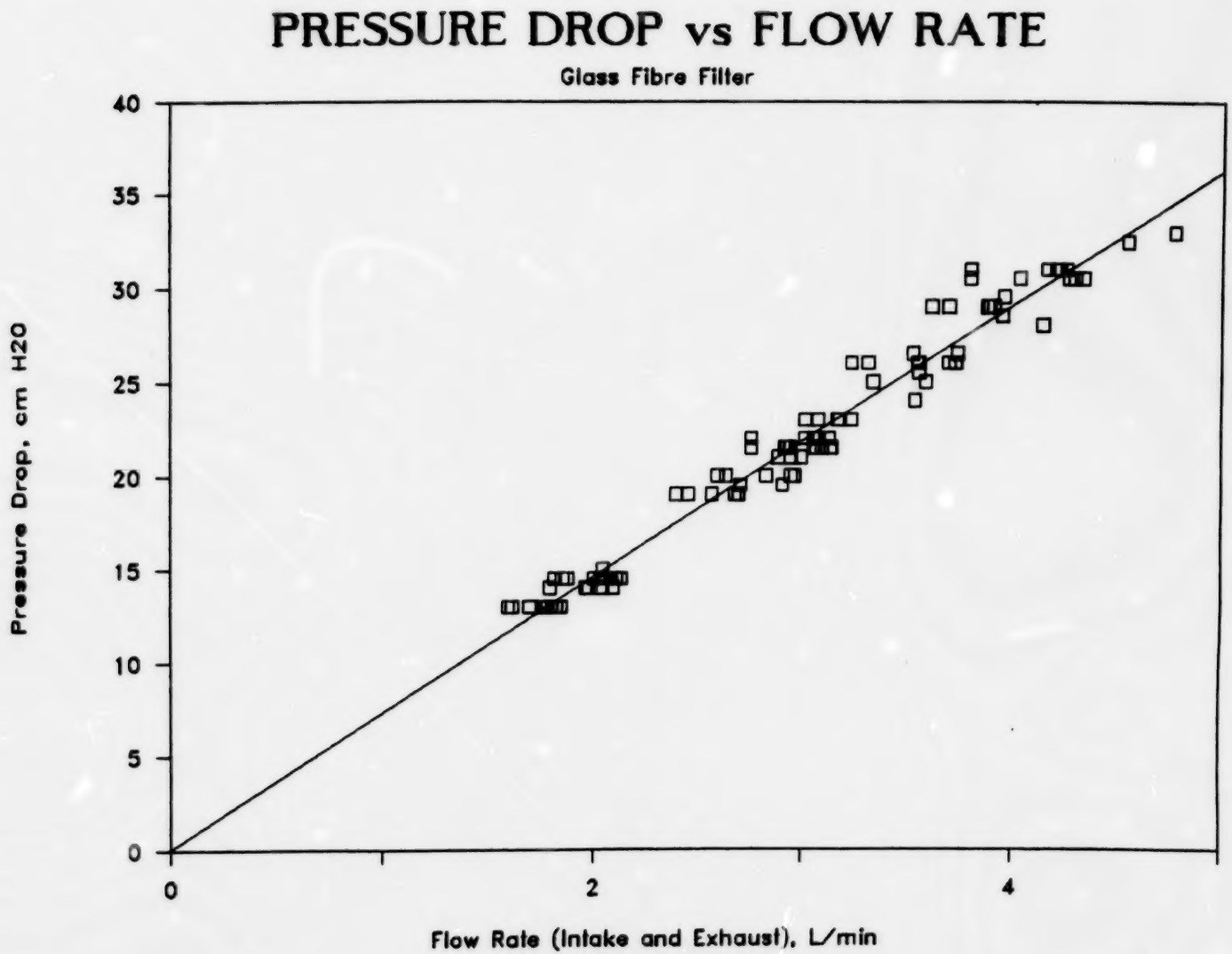

Fig. 90 - Pressure drop across the filter versus the pump's intake and exhaust airflow rates for all the pumps. Glass fibre filter.

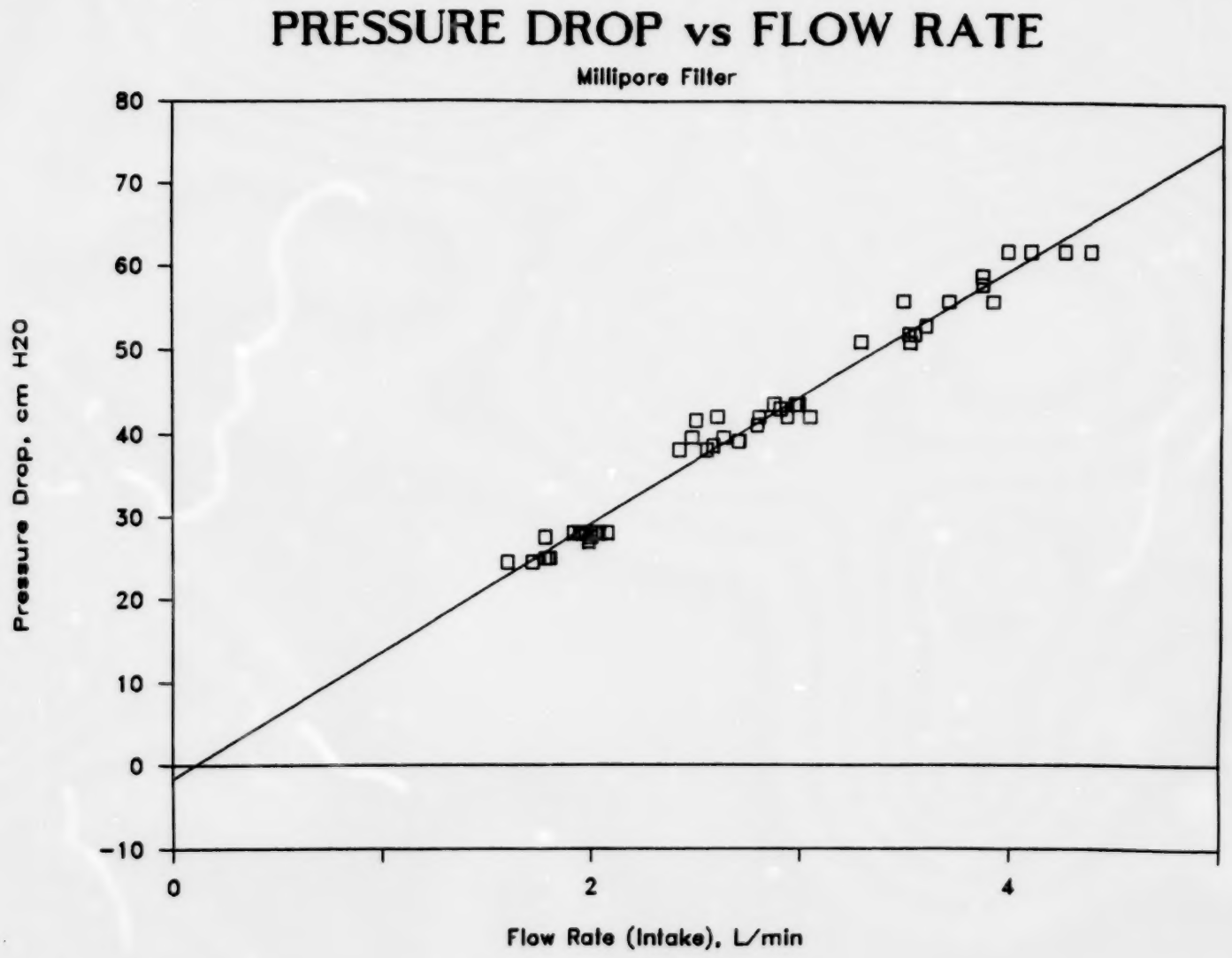

Fig. 91 - Pressure drop across the filter versus pump's intake airflow rate for all the pumps. Millipore filter.

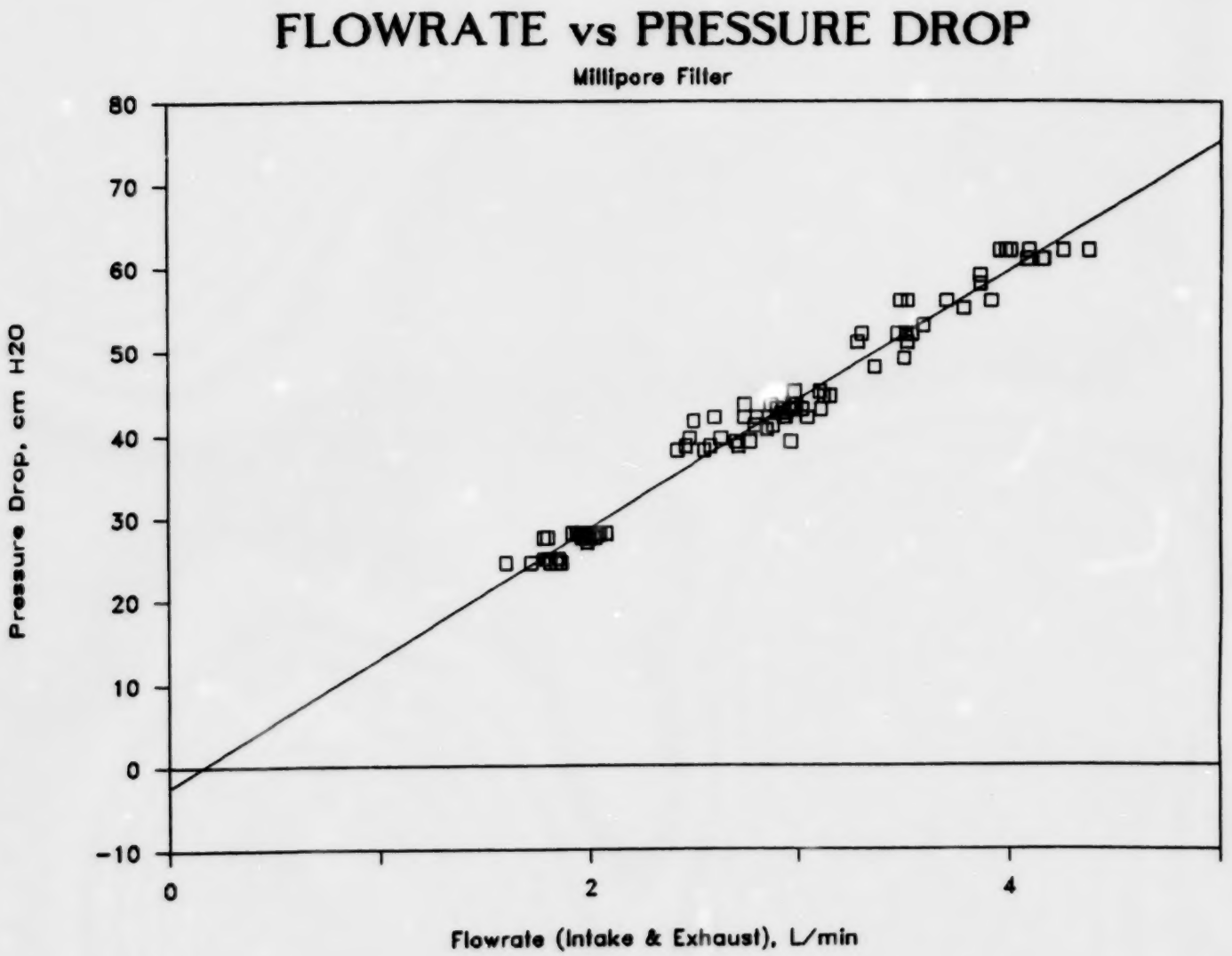

Fig. 92 - Pressure drop across the filter versus the pump's intake and exhaust airflow rates for all the pumps. Millipore filter.

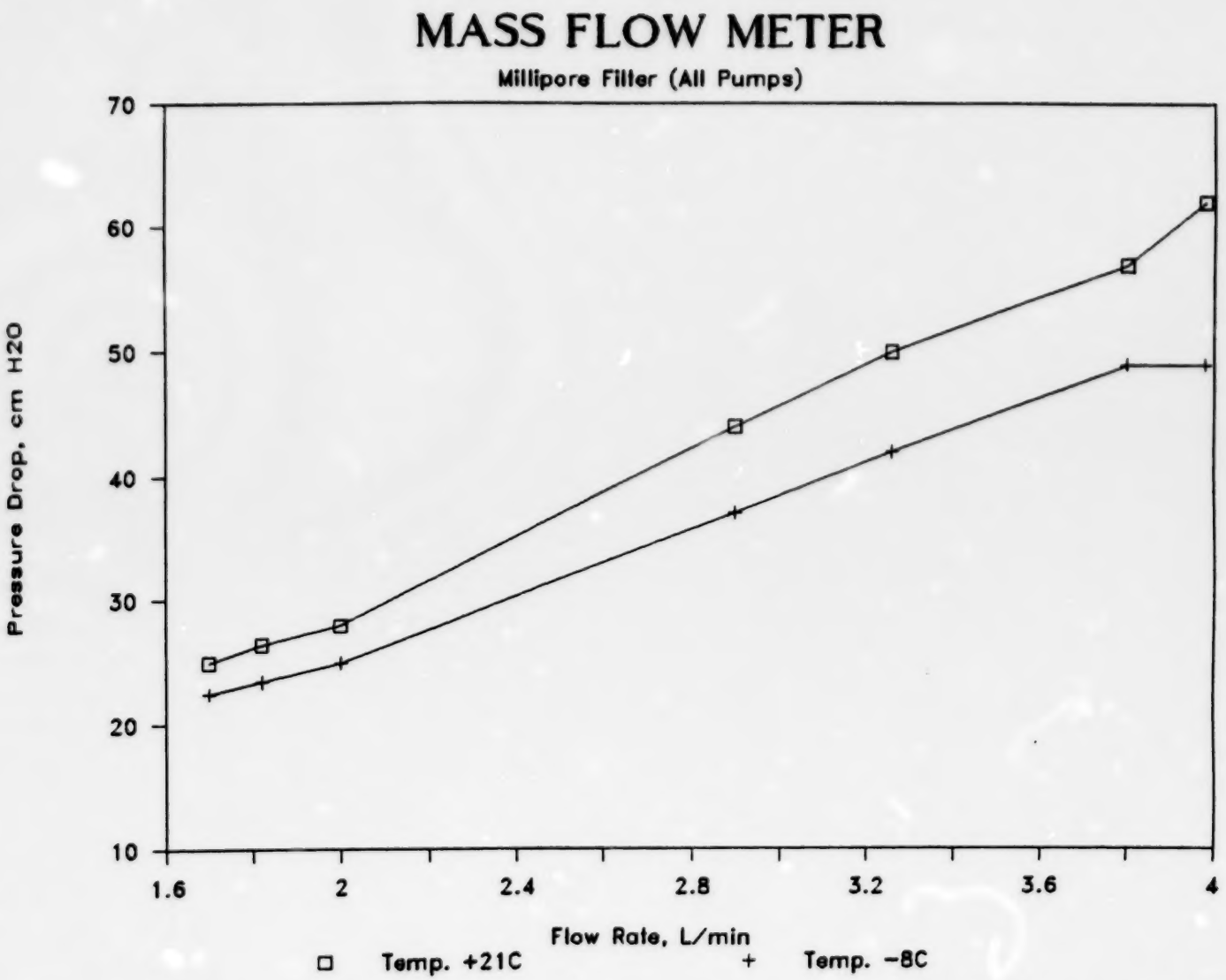

Fig. 93 - Pressure drop across the filter versus airflow rate for all the pumps at two different temperatures: 21°C (upper graph) and -8°C (lower graph). Millipore filter. Measurements carried out with a mass flow meter.

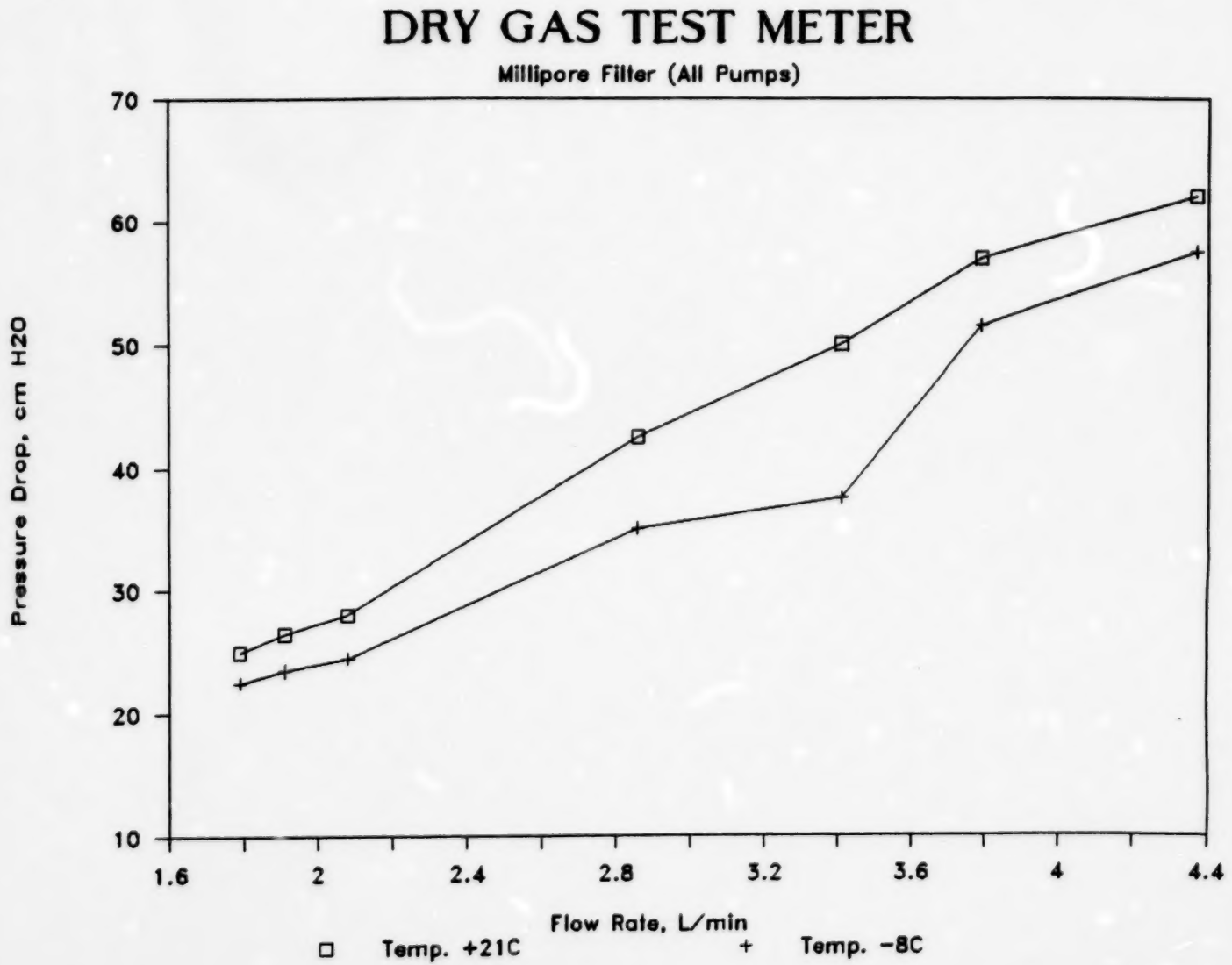

Fig. 94 - Pressure drop across the filter versus airflow rate for all the pumps at two different temperatures: 21°C (upper graph) and -8°C (lower graph). Millipore filter. Measurements conducted with a dry gas test meter.